

TABLE DES MATIÈRES

RÉSUMÉ	I
AVANT PROPOS	III
TABLE DES MATIÈRES	IV
INTRODUCTION GÉNÉRALE	1
CHAPITRE I	
VARIATIONS TEXTURALES DANS DES GOUTTELETTES SULFURÉES DE MORB CAUSÉES PAR DIFFÉRENTES HISTOIRES DE CRISTALLISATION	7
Résumé:.....	7
Contributions des auteurs :.....	8
TEXTURAL VARIATIONS IN MORB SULFIDE DROPLETS CAUSED BY DIFFERENCES IN CRYSTALLIZATION HISTORY.....	10
ABSTRACT:.....	10
INTRODUCTION	11
SAMPLING AND ANALYTICAL METHODS:	13
RESULTS:	15
The texture of sulfide droplets	16
Relationship between diameter and texture	17
Composition of the sulfide droplets	19
Occurrence of magnetite	20
DISCUSSION:.....	20
Processes of crystallization	21
Implications of crystallization rates on the textures	23
Why are the small droplets more undercooled?	24
Implication of the undercooling of sulfide droplets on solidification history	26
Pentlandite content of sulfide droplets.....	27
CONCLUSIONS:	28
ACKNOWLEDGMENTS:	28
REFERENCES	29
APPENDIX:.....	32
Appendix 1: Sulfide droplets bulk composition calculations	32

Appendix 2: Whole-rock Ni values	33
Appendix 3: Composition of oxide inclusions in sulfide droplets.....	33
FIGURE CAPTIONS.....	33
CHAPITRE II	
COEFFICIENTS DE PARTAGE LIQUIDE SILICATÉ-LIQUIDE SULFURÉ POUR DES ÉLÉMENTS CHALCOPHILES ET CRISTALLISATION DE GOUTTELETTES SULFUREÉS DE MORB	50
Résumé:.....	50
Contributions des auteurs :.....	52
SIDEROPHILE AND CHALCOPHILE ELEMENTS DISTRIBUTION IN MORB SULPHIDE DROPLETS: DETERMINATION OF NEW SULPHIDE MELT-SILICATE MELT PARTITION COEFFICIENTS AND EARLY SULPHIDE CRYSTALLISATION HISTORY.	53
ABSTRACT:.....	53
INTRODUCTION:	55
SAMPLING AND ANALYTICAL METHOD:	57
RESULTS:	60
Sulphide droplets population:	60
LA-ICP-MS results for fine-grained and coarse-grained sulphide droplets:	63
LA-ICP-MS results for the host glass:.....	64
Partition coefficients:.....	64
LA-ICP-MS analyses of zoned sulphide droplets:.....	66
DISCUSSION:.....	67
MORB differentiation:.....	67
Sulphide droplets transport to the surface:.....	69
Quenching of sulphide droplets:	69
Sulphide importance in the mantle:	71
Crystallisation of a sulphide liquid:	73
CONCLUSIONS:	75
ACKNOWLEDGMENTS:	76
REFERENCES:	77
FIGURE CAPTIONS:	83

CONCLUSIONS GÉNÉRALES	107
REMERCIEMENTS.....	112
RÉFÉRENCES	113
ANNEXES	116
Annexe A: Localisation des échantillons.....	116
Annexe B: Cartographie d'une gouttelette sulfurée au LA-ICP-MS.....	117
Annexe C: Conférence au 11th Platinum Symposium, Sudbury	118
Annexe D: Conférence au Ottawa 2011 Joint GAC-MAC-SEG-SGA meeting.....	123
Annexe E: Conférence au Goldschmidt 2011.....	125

INTRODUCTION GÉNÉRALE

Les Éléments Hautement Sidérophiles (EHS) et les éléments chalcophiles représentent un large panel d'éléments du tableau périodique et sont principalement regroupés dans le groupe des métaux de transition. Les EHS sont caractérisés par leur capacité à former des liaisons métalliques et ont tendance à former des alliages. Le groupe des EHS comprend les Éléments du Groupe du Platine (EGP : Ru, Rh, Pd, Os, Ir et Pt) ainsi que le Re et l'Au. Les éléments chalcophiles sont caractérisés par leur capacité à former des liaisons covalentes et ont tendance à former des liaisons avec le S. Ce groupe comprend de nombreux éléments et ceux auxquels nous nous intéressons dans ce projet sont le Co, Ni, Cu, Zn, As, Se, Mo, Ag, Sn, Sb, Te, Pb et Bi. Les EHS et les éléments chalcophiles ont un grand intérêt économique et scientifique. Ils sont au cœur de nos sociétés occidentales étant utilisés dans de nombreuses industries (EHS, Ni, Cu...), en joaillerie (Au, Pt, Pd) et ayant une importance financière (Au). Ils sont également utilisés en recherche fondamentale et en recherche appliquée.

En recherche fondamentale, les EHS sont utilisés dans la compréhension de processus majeurs tels que la différenciation terrestre : la formation du noyau et l'évolution du manteau terrestre. Puisque les EHS forment préférentiellement des liaisons métalliques il est généralement admis que lors de la différenciation terrestre ils ont migré dans le noyau (Chou, 1978) composé principalement de Fe et de Ni. Ainsi, le manteau primitif a été appauvri en ces éléments suite à la formation du noyau. Cependant, les études de xénolithes mantelliques ont prouvé que le manteau n'est pas appauvri en EHS (e.g. Alard *et al.*, 2000) impliquant qu'il ait subi un phénomène d'enrichissement postérieur à la formation du noyau. La théorie communément acceptée pour un tel

phénomène est un bombardement météoritique tardif qui refertilisa le manteau en EHS (Chou, 1978). Dans le manteau, où les conditions sont moins réductrices que dans le noyau, les EHS forment des liaisons covalentes à l'instar des éléments chalcophiles. Même si dans le manteau les sulfures représentent une phase mineure ($\approx 0,07\%$ poids) les EHS sont considérés comme y étant concentrés (e.g. Mitchell & Keays, 1981; Lorand 2008).

Dans le manteau les EHS et les éléments chalcophiles ne sont pas contrôlés de la même façon par les sulfures lors de la fusion partielle. Leur comportement dépend de leur coefficient de partage entre le liquide sulfuré et le liquide silicaté (D_{sulf} _{sil}) qui définit leur attirance pour l'un ou pour l'autre. Les éléments ayant des coefficients de partage élevés sont fortement contrôlés par les sulfures alors que ceux avec de faibles coefficients de partage sont faiblement contrôlés par les sulfures et davantage contrôlés par les silicates. Ainsi pendant la fusion du manteau, un fractionnement entre tous ces éléments s'opère en fonction de leur coefficient de partage : les éléments avec des coefficients de partage faibles auront tendance à migrer dans le magma silicaté tandis que ceux avec des coefficients de partage élevés auront tendance à rester dans les sulfures mantelliques résiduels.

Même si de manière générale le comportement des EHS dans le manteau est relativement bien compris, ce n'est pas le cas pour les éléments chalcophiles. Les EHS ont des D_{sulf} _{sil} élevés (de l'ordre du dizaine de milliers, e.g. Peach *et al.*, 1990; Fleet *et al.*, 1999), alors que les éléments chalcophiles ont des coefficients de partage de plusieurs ordres de magnitude plus bas. Dans le manteau, puisque les sulfures sont présents en

faible quantité il n'est pas clair si tous les éléments chalcophiles sont contrôlés par les sulfures et aussi quelle est l'importance de ce contrôle. Selon leur coefficient de partage, ils peuvent se comporter comme des éléments chalcophiles ou lithophiles. Ces comportements ne sont pas bien compris principalement à cause du manque de données précises des coefficients de partage. Dans le manteau, le Ni et le Co sont contrôlés par l'olivine (Irving, 1978) alors que le Zn, Sn, Cd, Ag et Bi sont considérés comme des éléments plutôt lithophiles (e.g. Hertogen *et al.*, 1980; Yi *et al.*, 2000) et finalement le Cu, Te et le Pb sont considérés comme étant contrôlés par les sulfures (e.g. Yi *et al.*, 2000; Hart & Gaetani, 2006). De nouvelles données de coefficients de partages permettraient de mieux contraindre et de préciser le comportement de ces éléments.

L'étude du comportement des EHS et des éléments chalcophiles est également essentielle en géologie économique pour avoir une meilleure compréhension de la formation des gisements magmatiques. La majorité des modèles de formation des gisements magmatiques à Ni-Cu-EGP suggère qu'un liquide sulfuré immiscible ségrégue d'un liquide silicaté en y collectant les EHS et les éléments chalcophiles (e.g. Naldrett, 1980; Barnes & Lightfoot, 2005). Ce liquide sulfuré coule à la base du réservoir magmatique à cause de la différence de densité entre les deux liquides puis cristallise et se différencie en différents minéraux sulfurés à mesure que l'intrusion se refroidit. Dans de nombreux gisements magmatiques à Ni-Cu-EGP, les Minéraux du Groupe du Platine (MGP) constituent les phases concentrant la majorité des EGP. Ils sont formés d'EGP combinés avec de l'As, ou du Bi et du Te, ou du Sn (Cabri, 2002) et sont associés avec les sulfures de métaux communs (SMC) (e.g. Sudbury, Dare *et al.*, 2010). Cependant, le comportement des EGP et le mode de formation des MGP durant les premières étapes de

la cristallisation des sulfures ne sont pas bien compris. Certains modèles suggèrent que des grappes (clusters) de EGP se forment dans le liquide silicaté puis sont incorporées par les sulfures (Tredoux *et al.*, 1995; Ballhaus & Sylvester, 2000). Les MGP peuvent aussi cristalliser directement depuis le liquide sulfuré à haute température (e.g. Dare *et al.*, 2010), ou à partir d'un liquide sulfuré résiduel riche en EGP et en semi-métaux (e.g. Prichard *et al.*, 2004; Holwell & McDonald, 2010), ou éxsolver des différentes phases sulfurées à température sub-solidus (Prichard *et al.*, 2004, Barnes *et al.*, 2008; Dare *et al.*, 2010). Ils peuvent également se former pendant des événements postérieurs à la mise en place et à la cristallisation de l'intrusion tels que pendant l'action de fluides deutériques (Peregoedova *et al.*, 2004; Godel & Barnes, 2007) ou du métamorphisme (Barnes *et al.*, 2008). De plus, dans le gisement de Noril'sk (Russie), Barnes *et al.* (2006) observèrent que les EHS étaient intégrés en solution solide dans les sulfures à l'exception de l'Au et du Pt. Ces auteurs suggèrent que ces sulfures, présents dans des sills, refroidissent relativement rapidement, abaissant les taux de diffusion dans les sulfures et inhibant les processus d'exsolution de MGP. Cela suggère que l'exsolution est l'un des processus majeurs pour la formation des MGP et que ce processus est contrôlé par le taux de refroidissement des sulfures.

Les verres frais de MORB (Mid-Ocean Ridge Basalt) contiennent des sulfures qui ont été trempés depuis une température initiale de ~1200°C à seulement quelques degrés en quelques minutes (Moore, 1975). Les occurrences de sulfures dans les MORB sont variables (Moore & Calk, 1971; Moore & Schilling, 1973; Yeats & Mathez 1976; Czamanske & Moore, 1977). Cependant, ces sulfures sont généralement sous la forme de gouttelettes sphériques et sont supposés avoir été formés avant l'éruption; d'ailleurs

Mathez & Yeats (1976) estiment qu'ils ont eu le temps de s'équilibrer avec le magma. La taille des gouttelettes varie de quelques micromètres jusqu'à une centaine de micromètres de diamètre, pour un diamètre moyen de $27\mu\text{m}$. Les gouttelettes sulfurées présentent des textures variant de finement trempées à différencier. Les gouttelettes ayant des textures trempées présentent une sphéricité parfaite et sont composées d'intercroissances micrométriques de Solution Solide Monosulfurée (SSM) et de Solution Solide Intermédiaire (SSI) avec présence mineure de pentlandite et d'oxydes xénomorphes. Les gouttelettes différencieront, présentant une sphéricité crénelée, ont quant à elles des textures zonées avec de la SSM et de la SSI massives ainsi que des exsolutions de pentlandite, et des oxydes automorphes (*e.g.* Mathez, 1976; Czamanske & Moore, 1977). Mathez & Yeats (1976) et Czamanske & Moore (1977) établissent que les parties les plus externes des coussins basaltiques ont été trempées de 1200°C à $700\text{-}600^\circ\text{C}$ en quelques dizaines de secondes. Avec un refroidissement si brutal, toutes les gouttelettes sulfurées devraient montrer les mêmes textures. Et cependant, ce n'est pas le cas.

Les avancées techniques de l'Ablation Laser couplée à un Spectromètre de Masse (LA-ICP-MS) permettent d'analyser une large gamme d'éléments et d'atteindre une résolution spatiale et des limites de détection qui n'étaient pas accessibles auparavant. L'analyse des gouttelettes sulfurées de MORB, par LA-ICP-MS ainsi que par Microsonde Électronique (EPMA), par Microscope Électronique à Balayage (MEB) et par Dilution Isotopique à Haute Pression (HPA-ID) offre une opportunité unique d'étudier le comportement des EHS et des éléments chalcophiles dans un liquide sulfuré en équilibre avec un liquide silicaté. Dans le cadre de cette maîtrise, 24 échantillons provenant de dragages le long de la dorsale océanique de l'Atlantique Sud et de la dorsale

Est Pacifique ont été étudiés. Parmi ces 24 échantillons, seuls 11 contiennent des gouttelettes sulfurées pouvant être analysées (Annexe A). Nos données obtenues par LA-ICP-MS ont été effectuées au LabMaTer à l'Université du Québec à Chicoutimi. Des analyses par EPMA et par MEB ont été faites à l'Université Laval à Québec.

Le but de ce projet de maîtrise est d'apporter des éléments de réponse aux thèmes développés précédemment et pouvant être résumés succinctement par :

- 1) Quels paramètres contrôlent les textures des gouttelettes sulfurées présentent dans les verres frais de MORB?
- 2) En calculant de nouveaux coefficients de partage, est-il possible de prédire le comportement des éléments chalcophiles dans le manteau?
- 3) Comment se comportent les EHS et les éléments chalcophiles dans les premières étapes de la cristallisation des sulfures?
- 4) S'il y a présence ou non de MGP dans les gouttelettes sulfurées de MORB, quelles sont les implications sur les modes de formation des MGP?

Le premier chapitre de ce mémoire aborde l'aspect textural des gouttelettes sulfurées dans les verres frais de MORB par une approche thermodynamique et se base sur des analyses pétrographiques et des analyses faites par EPMA. Il a pour but de répondre à la première question exposée précédemment. Ce chapitre correspond à un article accepté par le *Canadian Mineralogist* afin d'être publié. Le second chapitre du mémoire aborde l'aspect géochimique des gouttelettes sulfurées et se base sur des données obtenues par LA-ICP-MS et MEB en plus des analyses précédentes. Il a pour but de répondre aux trois autres questions exposées. Ce chapitre correspond à un article qui sera prochainement soumis au *Journal of Petrology*.

CHAPITRE I

VARIATIONS TEXTURALES DANS DES GOUTTELETTES SULFURÉES DE MORB CAUSÉES PAR DIFFÉRENTES HISTOIRES DE CRISTALLISATION.

Titre du Manuscrit:

Textural variations in MORB sulfide droplets caused by differences in crystallization history.

Auteurs:

Clifford Patten, Sarah-Jane Barnes, Edmond A. Mathez.

Journal :

The Canadian Mineralogist

Résumé:

Les gouttelettes sulfurées provenant de verres frais de MORB (Mid-Ocean-Ridge Basalts) présentent différentes textures. Certaines gouttelettes sont constituées d'intercroissances micrométriques à grains fins de Solution Solide Monosulfurée (SSM) et de Solution Solide Intermédiaire (SSI), avec de la pentlandite à l'interface SSM-SSI et des oxydes micrométriques xénomorphes disséminés de manière homogène. D'autres présentent des textures zonées avec la SSM et la SSI massives et individualisées, la pentlandite est sous forme de grains et d'exsolutions en flammes; il y a également présence d'oxydes automorphes pluri-micrométriques. Ces variations texturales impliquent des différences dans l'histoire de cristallisation des gouttelettes sulfurées. Ces différences sont surprenantes car dans certains échantillons des gouttelettes présentant des textures à grains fins et zonées sont distantes de seulement quelques millimètres

impliquant que les conditions de cristallisation sont identiques pour les deux types de texture. Ainsi, d'autres processus contrôlent les textures. Nous avons remarqué qu'il existe une relation entre la taille et les textures: les gouttelettes les plus grandes ont tendance à avoir une texture plus zonée alors que les gouttelettes les plus petites ont tendance à avoir une texture trempée. Nous proposons que ces dernières aient subi un sur-refroidissement plus important avant la cristallisation. La cause pour le délai de la cristallisation pourrait être que, dans les petites gouttelettes sulfurées, de larges grains de SSM avec un ratio surface sur volume faible ne peuvent pas se former; ce qui se traduit par une solubilité effective de la SSM plus élevée. À cause du haut degré de sur-refroidissement au moment de la cristallisation, il y a moins de sites de nucléation et les taux de diffusion des composants du cristal dans le liquide sont plus faibles. À l'opposé, dans les grosses gouttelettes avec une solubilité effective plus faible, la SSM commence à cristalliser à plus haute température, et donc a moins de sites de nucléation, des taux de diffusion plus élevés et plus de temps pour la différenciation des sulfures.

Mots-clés: gouttelettes sulfurées, Mid-Ocean-Ridge Basalt, solution solide monosulfurée, solution solide intermédiaire, énergie interne, cristallisation.

Contributions des auteurs :

1^{er} auteur : Clifford Patten :

- Échantillonnage.
- Analyses pétrographiques, analyses EMPA et traitement des données.
- Rédaction du manuscrit.

2^{ième} auteur : Sarah-Jane Barnes :

- Planification et direction du projet.
- Aide à la rédaction du manuscrit.
- Correction du manuscrit.

3^{ième} auteur : Edmond A. Mathez :

- Mise à disposition des échantillons.
- Aide au développement de la discussion.
- Correction du manuscrit.

TEXTURAL VARIATIONS IN MORB SULFIDE DROPLETS CAUSED BY DIFFERENCES IN CRYSTALLIZATION HISTORY.

CLIFFORD PATTEN

*Module des Sciences de la Terre, Université du Québec à Chicoutimi, Chicoutimi,
Québec, G7H 2B1, Canada. clifford.patten@uqac.ca*

SARAH-JANE BARNES

*Module des Sciences de la Terre, Université du Québec à Chicoutimi, Chicoutimi,
Québec, G7H 2B1, Canada. sjbarnes@uqac.ca*

EDMOND A. MATHEZ

*Department of Earth & Planetary Sciences, American Museum of Natural History, New
York, NY 1002, United States of America. mathez@amnh.org*

ABSTRACT:

Sulfide droplets from fresh Mid-Ocean-Ridge Basalts (MORB) glasses show different textures. Some are fine-grained droplets consist of Monosulfide Solid Solution (Mss) and Intermediate Solid Solution (Iss) micrometric intergrowths with pentlandite at the Mss-Iss interface and disseminated Fe-oxide grains; other droplets display a characteristic “zoned” texture consisting of segregated massive grains of Mss and Iss, with euhedral Fe-oxides and pentlandite occurring as equant grains and as flame-shaped domains in the Mss formed by exsolutions. The difference in the textures implies a difference in the crystallization history of the sulfide droplets. These different textures are observed in droplets that are only millimeters apart in the same sample and thus, had identical cooling

history. Thus, some other factors controlled the textural development. There is relationship between the size and the texture of the droplets. The larger sulfide droplets tend to have zoned textures and the smaller ones fine-grained textures. We propose that the latter have experienced greater undercooling before crystallization. The reason for the delay in crystallization could be that, in the small sulfide droplets, large stable grains with low surface to volume ratio cannot form which results into higher effective solubility of the *Mss*. Due to the high degree of undercooling in the small droplets, there were numerous nucleation sites and diffusion rates of the crystal components in the liquid were lower, leading to fine-grained *Mss*-*Iss* intergrowths. In contrast larger droplets with lower effective solubility of *Mss* began to crystallize at higher temperature, and thus had fewer nucleation sites, higher diffusion rates and more time for sulfide differentiation.

Keywords: sulfide droplet, mid-ocean-ridge basalt, monosulfide solid solution, intermediate solid solution, effective solubility, crystallization.

INTRODUCTION

Fresh Mid-Ocean-Ridge Basalt (MORB) glasses contain sulfide droplets with a wide range of textures, for which few explanations exist (*e.g.* Mathez & Yeats, 1976; Czamanske & Moore, 1977). Upon eruption, MORB quench from ~1200°C to seawater temperature in less than a few minutes (Moore, 1975). In addition, because the quenching occurs under pressures of the deep ocean, MORBs typically do not undergo substantial degassing (Mathez, 1976). Sulfides occur as micrometric spherules embedded in the walls of vesicles (Moore & Calk, 1971; Moore & Schilling, 1973; Yeats & Mathez 1976), as small angular interstitial grains in microcrystalline aggregates of plagioclase and olivine (Mathez & Yeats, 1976) and as well-developed spherical globules mostly in the

glass or in some cases in phenocrysts (Mathez & Yeats, 1976; Czamanske & Moore, 1977). The well developed droplets represent frozen immiscible sulfide melt believed to have equilibrated with the silicate melt before eruption (Mathez & Yeats, 1976).

The globules in the glass have different textures. The textures vary from fine-grained intergrowth of Monosulfide Solid Solution (Mss), Intermediate Solid Solution (Iss) to coarser-grained intergrowth of MSS and Iss, pentlandite and oxide (Mathez, 1976; Czamanske & Moore, 1977). Mathez & Yeats (1976) and Czamanske & Moore (1977) suggested that such samples quenched from ~1200°C to 700-600°C in tens of seconds. With such rapid cooling one might expect the texture of droplets to be similar. Yet this is not the case.

The textures displayed by sulfide droplets are controlled by component nucleation and the diffusion rates which, in turn, are controlled by factors that remain unknown. Czamanske & Moore (1977) speculated that droplets displaying fine-grained textures may have undergone more rapid cooling than coarse-grained droplets. They did not speculate on cause of the textural variability but did note that it is not linked to the distance of the droplet from the lava surface, *i.e.* not linked to cooling rate.

In this study, 24 samples of fresh glass of MORB pillow margins from various locations were examined for sulfide droplets. Eighty-five droplets were found in 11 samples. Twenty-five were analyzed by Electron-Probe-Micro Analyses (EPMA) and show a rather constant bulk composition while displaying a wide variation of texture. In some samples, sulfide droplets have different textures, although the droplets segregated from the same magma, have the same composition, and were subjected to the same

quench event. Therefore, neither sulfide droplet composition nor cooling rate are the main factors controlling the textures of the droplets. Instead we observe a correlation between the droplet textures and the size.

The aims of this study are 1) to describe in detail the textures of the sulfide droplets, and 2) to understand how droplet size can influence the texture.

SAMPLING AND ANALYTICAL METHODS:

Samples come from the repository at Lamont Doherty Earth Observatory of Columbia University, New York. Twenty-four samples, mainly from the South Atlantic Ridge and the East Pacific Rise, were investigated of which 11 were found to contain sulfide droplets large enough to study. Six of them are from the South Atlantic Ridge, located between 25°41'S and 26°32'S along the ridge; on the East Pacific Rise, two samples are from the Hotu seamount chain and, three close to the Garrett fracture zone. All samples were dredged from depths ranging from 2579 to 3999 m. Fragments of fresh glass were hand-picked from the most external parts of pillow lavas, with care being taken to avoid Mn-coated parts.

The sulfide droplets were observed optically in reflected light with an Olympus DP 71 microscope at 100X magnification coupled with the Image Pro Plus Analysis 6.2 image analysis package. Modes were calculated from pictures based on pixel colors representative of each phase. To gain a sense of the precision of the measurements, modes were measured five times on an individual sulfide droplet yielding a sample standard deviation of 1.9, 1.3, 1.2, and 0.6%, respectively for MSS, ISS, Ni-rich phase and oxide. The variation reflects the ability of the observer to choose the right pixel colors for

each phase. On one small droplet with a diameter of 10 μm sample standard variations of 6.5, 6.8 and 5.2% for MSS, ISS and Ni-rich phase were recorded owing to the difficulty of observing such small objects. Therefore, the minimum size of analyzed sulfide droplets was set at 10 μm .

Electron-microprobe analyses were carried out with a CAMECA SX-100 instrument at Laval University, Québec city. Both sulfide droplets and the surrounding glass were analyzed. For sulfide minerals, an accelerating voltage of 15 kV, a beam diameter of 5 μm and a beam current of 20 nA were used, as advocated by Czamanske & Moore (1977) and with counting time of 20 sec. The same settings were used for the analysis of silicate glass. They are similar to those used by Liu *et al.* (2007) and Wallace & Carmichael (1992). Astimex standards were used for sulfide calibration: pyrite for S, hematite for Fe, chalcopyrite for Cu and pentlandite for Ni. For major elements in the glass chromite from P&H Development was used for Cr, nickeline from P&H Development for Ni, rutile from P&H Development for Ti, bustamite from Astimex for Mn, pyrite from Astimex for S, orthoclase from P&H Development for K, diopside from P&H Development for Ca, albite from P&H Development for Na, plagioclase from P&H Development for Al, quartz from Astimex for Si and olivine from Astimex for Mg.

For droplets having a fine-grained texture, three points were taken randomly and the averages were used for the bulk-composition calculation as the beam was too broad to analyze each phase separately. For droplets having coarser textures, analyses were obtained for each individual sulfide phases, and the droplet bulk composition was determined from the relative areas occupied by each phase on the analytical surface.

For each sulfide droplet analyzed, three points on the glass surrounding were also analyzed. The analytical points were 100 μm away from the droplet border in order to avoid a possible contamination due to dispersion of elements from the droplets to the glass or X-ray fluorescence in the sample (Dalton & Lane, 1996). The quenched sulfide droplets and fresh MORB glass are believed to reflect an equilibrium established at magmatic conditions (Mathez, 1976).

RESULTS:

All samples have a glass composition typical of low-K tholeiitic basalt and are N-MORB except for two samples from the seamounts that might be E-MORB (Table 1). Sulfur concentrations, which ranges from 782 to 1530 ppm (Table 1) are similar to those found by Mathez (1979) and Czamanske & Moore (1977) and correlate with FeO concentration in the glass (Fig. 1).

Among the 15 polished sections containing sulfide droplets, we observed 85 sulfide droplets with diameters $\geq 10 \mu\text{m}$. The majority is spherical and the remainders are elliptical. Sulfide droplets vary from 10 to more than 100 μm in diameter (average of 27 μm). This size range is similar to that observed by Moore & Calk (1971), Mathez & Yeats (1976), Mathez (1976), in their samples. Larger droplets, up to 600 μm , have been found in MORB (Czamanske & Moore 1977, Peach *et al.*, 1990), but were not encountered in our samples. The number of sulfide droplets and their sizes vary from sample to sample; some contain numerous small droplets, whereas others have fewer but larger droplets. For example, RC 28 02 22rd contains 39 droplets varying in diameter

from 5 μm up to 40 μm (average of 18 μm), whereas RC 28 02 18rd has only three droplets ranging from 56 to 111 μm .

The formation of sulfide droplet from the silicate liquid has been considered in Mungall (2002). He suggested that sulfide nucleation density in the silicate liquid depends on the degree of saturation of the principal solute species FeS, in the magma. Recently, Holzeid (2010) showed that the sulfide droplets size distribution is controlled by the degree of polymerization of the silicate liquid.

The texture of sulfide droplets

Sulfide droplets can be classified into three groups based on texture. The first includes droplets with perfectly spherical shapes and composed of fine-grained micrometric intergrowths of Fe-Ni-rich and Cu-Fe-rich sulfide phases which can be interpreted as quenched MSS and ISS (Fig. 2). In some droplets, the MSS-ISS interfaces are partially rimmed by a Ni-rich phase, presumably pentlandite or Ni-rich MSS.

A second group of droplets has a quasi-perfect spherical shape, but with some sub-micrometric irregularities giving them a rough surface. They also contain intergrown Fe-Ni-rich and Cu-Fe-rich phases interpreted as quenched MSS and ISS. However, the sizes of the phases are larger than in fine-grained textures (Fig. 3). Accordingly, these droplets will be referred to as having a coarse-grained texture. The Ni-rich grains present at the MSS-ISS interfaces are larger than the Ni-rich grains in fine-grained droplets. In some droplets, Ni-rich inclusions in the form of flame are present within the MSS. These are interpreted as exsolution-induced domains (Kelly & Vaughan, 1983; Etschmann *et al.*,

2004; Czamanske & Moore, 1977). Droplets also contain dark opaque phases interpreted as oxides.

A third texture will be referred to as zoned because it consists of two distinct, massive, and completely separate grains of MSS and ISS (Fig. 4). Droplets with this texture are spherical and have crenulated contacts with the silicate glass (Figs. 4a, b, c), in contrast to the smooth and regular interfaces of other droplet types and their host glasses. These droplets have not been described in previous studies of MORB sulfide droplets. The MSS is massive whereas the ISS reveals two different textures. The most common is one in which the ISS and oxide form a fishbone texture (Figs. 4a, b). This microassemblage can be interpreted as the residual Cu-rich sulfide-oxide liquid that remained after the MSS crystallization. Alternatively, the ISS is massive and may contain euhedral oxide grains (Fig. 4c). Pentlandite occurs in zoned droplets at the MSS and ISS interface and as flame inclusions in the MSS. Flame-shaped domains are more common than in the coarse-grained droplets. Because the MSS and ISS are not homogeneously distributed within the zoned droplet, the exposed proportions of minerals may not be representative of the whole droplet, and there is a higher variability in the modal percentage of each phase and their distribution inside the droplets. The zoned droplets are similar in texture to centimeters-size pyrrhotite-chalcopyrite-pentlandite magmatic sulfide blebs found in dykes and subvolcanic sills (e.g. Prichard *et al.*, 2004; and Barnes *et al.*, 2006).

Relationship between diameter and texture

Sulfide droplets with different textures may coexist in the same sample. For example, of the 8 droplets of the sample RC 28 02 13rd, four are fine-grained, three are coarse-

grained and one is zoned. Of the 15 polished sections, 5 contain droplets with different textures. Czamanske & Moore (1977) observed no relationship between the distance from the surface pillow and the texture of droplets. In the samples of this study, droplets exhibiting different textures are separated by only a few millimeters within homogeneous fresh glass, confirming Czamanske's & Moore's (1977) observations.

Most of the droplets (75%) show a fine-grained texture. Coarse-grained texture droplets are the next most common (15%), and zoned droplets are the least common (10%). There appears to be a relationship between the size of the droplets and their texture (Fig. 5). Over 90% of the fine-grained droplets have diameters less than 30 μm . In contrast, in the 30-50 μm range 60% of sulfide droplets are coarse-grained. Of the droplets greater than 50 μm all are zoned. It appears, therefore, that there is a positive correlation between the increase in droplet diameter and the degree of segregation of the phases. It could be argued that this is based on observations of random sections through droplets that do not reflect their real droplet diameters. This must be partly true; however, the fine-grained droplets do not represent outer portion of larger zoned droplets because the margins of the latter are uniquely crenulated, while those of the former are smooth. In addition, a section through the margin of a zoned droplet would consist predominantly of either MSS or ISS and not show a fine intergrowth of MSS and ISS. Hence, the relations observed in Figure 5 are qualitatively valid. We conclude that the internal texture of the droplets is related to its size.

Composition of the sulfide droplets

Sulfide phase relation in the system Fe-Ni-Cu-S has been widely studied for the understanding of ore deposit formation (Craig & Kullerud, 1969; Naldrett, 1969; Fleet & Pan, 1994; Ebel & Naldrett, 1997; Mungall, 2005, 2007). The bulk compositions of sulfide droplets were calculated to 100% sulfide in order to estimate liquidus temperature of the MSS using the results of Ebel & Naldrett (1997), which pertain to O-free system. Results are listed in Table 2. Calculations are documented in Appendix 1. Calculated compositions display low variability in S content ($34.9 \pm 0.96\%$), moderate variability in Fe content ($46.8 \pm 3.44\%$), and high variability in Ni ($7.8 \pm 3.61\%$) and Cu contents ($8.4 \pm 3.62\%$). Concentrations of Ni and Cu in the sulfide droplets are dependent on the degree of fractionation of the magma (Czamanske & Moore, 1977).

Figure 6 presents bulk composition of our sulfide droplets in terms of the system Fe-Ni-Cu. The results show a range in bulk compositions and are in agreement with previous work (Mathez 1976; Czamanske & Moore, 1977). One coarse grained droplet of $48 \mu\text{m}$ from sample RC 28 02 07rd contains up to 24.7% Ni. This droplet contains a large proportion of the Ni-rich phase (28.8%), which can be attributed to the 226 ppm Ni contained in the whole rock (Appendix 2). Dashed lines on Figure 6 represent the composition of the sulfide liquid at crystallization of the MSS for 1100°C , 1050°C and 1000°C from Ebel & Naldrett (1997, Fig. 5), which gives approximations of the liquidus temperature of the sulfide droplets. The liquidus temperatures range from slightly above 1100 to 1050°C , and droplets are randomly spread over this interval regardless to their texture. Hence, there appears to be no relation between texture and composition.

Occurrence of magnetite

Oxide occurs either inside MSS, inside ISS or at their interface (Figs. 2, 3 and 4) and varies from nil to 7 modal% of the droplet. In zoned droplets, where the oxide grains are best developed, electron microprobe analyses reveal that they are magnetite free of Ti (Appendix 3) indicating that magnetite crystallizes from the sulfide liquid and did not equilibrate with the silicate liquid. Magnetite is also present at the edges of the sulfide droplets (Fig. 4) but in grains too small to be analyzed and in a fishbone texture in the Cu-rich quenched residual sulfide liquid found of some zoned droplets (Figs. 4a,b) (*c.f.* Naldrett, 1969, Skinner & Peck, 1969). In a few fine-grained droplets oxides were not observed; however, Czamanske & Moore (1977) suggested that a few percent of magnetite is ubiquitous in droplets.

DISCUSSION:

To explain textural differences among sulfide droplets, one could argue that they are related to the time they started to crystallize. In such model, large sulfide droplets grew and begin to crystallize before eruption and thus also had time to develop zoned texture and small ones formed during eruption at lower temperature.

Using the PELE 7.3 database (Boudreau, 1999) and glass data from Table 1, the liquidus temperatures of the silicate glass are calculated to be in the 1250-1170°C range. Figure 6 indicates that MSS starts to crystallize in sulfide droplets at ~1100°C. Hence, large sulfide droplets could not have started crystallizing before eruption. Moreover, analysis of fine-grained, coarse-grained sulfide droplets and surrounding glass (Patten *et al.*, in prep.) show that the concentration in chalcophile and siderophile elements in these droplets are

similar to the zoned ones and that there is no depletion in those elements in the surrounding glass, implying they had time to equilibrate with the silicate melt. Hence, small sulfide droplets are likely to have formed before the eruption and, like their larger brethren, did not start to crystallize before the eruption.

Processes of crystallization

The formation of the sulfide droplets in silicate melts is considered in Mungall (2002). The textures observed into the sulfide droplets indicate variations in their crystallization histories. The development of crystals involves three processes: nucleation, diffusion and growth, all of which are characterized by rates that vary according to undercooling (Shelley, 1993). The Mss is the first phase to crystallize from Fe-Ni-Cu sulfide liquid (e.g. Fleet & Pan, 1994; Ebel & Naldrett, 1997; Mungall, 2007). Nucleation can either be homogeneous or heterogeneous. In the case of homogeneous nucleation the total energy of a spherical nucleus (ΔG) of Mss in a sulfide liquid is the sum of its internal energy and its surface energy (Mungall & Su, 2005):

$$\Delta G = \frac{4\Delta G_c}{3\pi r^3 V_m} + 4\pi r^2 \gamma \quad [1]$$

with ΔG_c the free energy per mole of the Mss crystal, r the radius of the nucleus, V_m the molar volume of the Mss , and γ the interfacial tension between Mss and sulfide liquid. At formation, the nucleus has a very large ratio of surface area to volume, implying that the surface energy is relatively high owing to the large number of atoms not electrostatically balanced (Shelley, 1993). This energy makes the nucleus unstable and leads it shrinkage (Dowty, 1980). A certain amount of energy is needed to overcome the force of the surface energy in order to reach a critical radius from which the nuclei will

grow spontaneously. This energy is called the free energy of activation (Dowty, 1980) or nucleation energy barrier (Shelley, 1983). The critical radius (r_c) is defined as (e.g. Dowty, 1980):

$$r_c = -2 \gamma V_m / \Delta G_c \quad [2]$$

The nucleation rate is dependent on the degree of undercooling: as the latter increases, the nucleation rate reaches a maximum, and then declines to zero at high degrees of undercooling (Shelley, 1983). The undercooling is the extra amount of cooling sustain by the droplet from its freezing point before it starts to crystallize. The undercooling delays crystallization and leads it to occur at lower temperature. Much work has been done on silicate nucleation rates using crystal-size distributions (CSD) (e.g. Gibb, 1974; Dowty, 1980; Cashman & Marsh, 1988; Higgins, 2006), but none on sulfides are known to the authors.

Heterogeneous nucleation can occur on preexisting interfaces. The surface energy of heterogeneous nucleation is lower than that of homogeneous nucleation in equation [2] and thus, the size needed for nucleus stability is also lower (Mungall & Su, 2005). Heterogeneous nucleation thus also needs less undercooling to occur.

Once nuclei are created and stable, diffusion to the nuclei occurs by volume diffusion (the diffusion of elements in a liquid), and the nuclei grow by interface diffusion (across the crystal-liquid interface) and surface diffusion (parallel to the surface) (Dowty, 1980). Diffusion rates decrease with the undercooling (Shelley, 1983) and systems with high undercooling will not contain fully grown crystals.

Implications of crystallization rates on the textures

As described above, the fine-grained droplets contain numerous small intergrowths of MSS and ISS. During crystallization, numerous nucleation sites were created randomly inside the droplet and diffusion was slow, preventing crystal growth from occurring. Thus, fine-grained droplets have experienced substantial undercooling followed by rapid crystallization. This process could be interpreted as homogeneous nucleation.

Coarse-grained droplets have the same textural features as fine-grained droplets, but the grains are larger and less numerous. They developed because there were fewer nucleation sites and more rapid diffusion, suggesting a lower degree of undercooling. These features could also suggest homogeneous nucleation. As can be seen in Figure 6, the bulk compositions of fine-grained and coarse-grained droplets are similar. Hence, in order to explain the higher rate of crystal growth, the degree of undercooling must have been lower.

Zoned droplets contain massive MSS and ISS. This texture must have required a lower rate of nucleation and higher rate of diffusion than in the fine-grained and coarse-grained droplets. The presence of segregated MSS and ISS in zoned droplets suggests that sufficient time elapsed between the appearance of MSS and that of the complete solidification of the droplet for the fractionated Cu-Fe-rich liquid to migrate away from the MSS. Moreover, as described above, the ISS in the zoned droplets exist either as fishbone textured grains, representing quenched residual Cu-Fe-rich sulfide liquid and implying a relatively high degree of undercooling, and equant, massive grains representing the crystallization of ISS and implying a relatively low degree of undercooling.

The nucleation process of the zoned sulfide droplets is not clearly defined. In the sulfide droplet of Figure 4c, the M_{ss} is concentrated on the outer part of the droplet and the massive I_{ss} is concentrated in the center. Such texture may have developed by heterogeneous nucleation of M_{ss} crystals on the sulfide droplet wall. Other zoned sulfide droplets do not show this arrangement, suggesting that heterogeneous nucleation from the droplet wall is not the dominant crystallization mechanism.

One could argue that fine-grained and coarse-grained sulfide droplets formed by homogeneous nucleation and that zoned sulfide droplets are formed by heterogeneous nucleation. If heterogeneous nucleation on the droplet wall is a major process, small droplets should be more likely to show zoned textures than larger droplets because they have a higher surface to volume ratio, but this is not observed. Moreover, such interpretation does not take in account the continuum of textural differences from fine-grained to zoned with massive I_{ss} owing to different rates of crystallization. Therefore, we believe that both homogeneous and heterogeneous nucleation can occur but that they are not the main parameters controlling the textures.

Why are the small droplets more undercooled?

The texture of the small fine-grained sulfide droplets implies higher degree of undercooling than large zoned droplets. Observations on droplet sphericity tend to confirm this inference. As pointed out by Czamanske & Moore (1977), the perfect sphericity of fine-grained sulfide droplets implies that they were still liquid when the silicate liquid reached the glass transition, whereas zoned droplets, with crenulated margins, had already started to crystallize at that point.

Emmanuel *et al.* (2010) argued that during nucleation and crystal growth, the solubility of a phase is related to the change of the interfacial energy of the phase. Because small crystals have high surface to volume ratios, high interfacial diffusivity is required to maintain chemical equilibrium, which in turn require more concentrated solution before nucleation and growth can occur (Holness & Sawyer, 2008). This concentration is referred to the effective solubility, S_e . When a crystal forms in a confined volume, the effective solubility becomes a function of the radius of that volume (Emmanuel *et al.*, 2010):

$$S_e = S_0 \exp\left(\frac{2V_m\gamma}{RT r_s}\right) \quad [3]$$

where S_0 is the bulk solubility, R the gas constant, T the temperature and r_s the radius of the confined volume, *i.e.* the sulfide droplet.

The volume influence on the effective solubility leads to supersaturation of the phase components in the solution; such effect have been observed in porous sedimentary rocks (Emmanuel *et al.*, 2010; Putnis & Mauthe, 2001) and in small pores in migmatites (Holness & Sawyer, 2008). Because the solution is supersaturated, high undercooling is needed for crystallization to occur (Bigg, 1953; Putnis & Mauthe, 2001; Holness & Sawyer, 2008).

The sulfide droplet can be considered as a confined volume because the interfacial tension between sulfide melt and silicate melt is larger than those between silicate or oxide minerals and silicate melt (Mungall & Su, 2005). Therefore, the size of the sulfide droplet has an influence on the Ms solubility: small sulfide droplets require a higher

concentration of *Mss* liquid components before *Mss* can crystallize than larger sulfide droplets.

It would be interesting to investigate on the critical size of the volume at which the effective solubility of *Mss* in the sulfide liquid is affected. Quartz crystallization in sandstone does not occur in pore smaller than 10 μm (Emmanuel *et al.*, 2010). Putnis & Mauthe (2001) argued that supersaturation occurs if pore size is around 1 μm and does not occur for pores larger than 100 μm . Bigg (1953) observed that a water droplet of 10 μm could crystallize at -31°C, sustaining high undercooling. Although these systems are different from those dealt with in this paper, the size relation remains relevant. More than 90% of fine-grained sulfide droplets have a diameter lower than 30 μm , whereas droplets with a diameter greater than 50 μm are zoned.

Implication of the undercooling of sulfide droplets on solidification history

The different solidification histories experienced by the different droplets are summarized in Figure 7. As stated above, the crystallization of *Mss* in fine-grained and coarse-grained droplets is delayed (Fig. 7, 3rd and 4th columns). Once the *Mss* starts to crystallize, it is quickly followed by the crystallization of *Iss*. The residual Cu-Fe-rich liquid did have not time to migrate away from the *Mss*, leading to the characteristic intergrowth of *Mss* and *Iss* observed in these droplets (Fig. 2 and 3).

Zoned sulfide droplets (Fig. 7, 1st and 2nd column) experience less undercooling, allowing more time for diffusion and thus enabling formation of equant *Mss* grains. Those of zoned droplets which experience, somewhat, greater degrees of undercooling crystallize *Iss* with oxide in a fishbone texture (Fig. 4a and b). Those that experience

slightly lower degrees of undercooling form massive Iss crystals containing equant oxide crystals (Fig. 4c).

Pentlandite content of sulfide droplets

The pentlandite content of sulfide droplets is variable (Fig. 8). Where whole-rock concentrations of Ni are low (less than 50 ppm), pentlandite does not form and the Ni concentration in the MSS is less than 10%. In samples with higher whole-rock concentrations of Ni, the pentlandite can constitute up to 27% of the droplets, and concentrations of Ni in the MSS are also higher but never exceed 15%. These observations imply even in rapidly quenched system MSS can absorb no more than 15 wt% Ni before pentlandite exsolves.

In fine-grained sulfide droplets, pentlandite occurs as blebs or rims at the MSS-Iss interface (Fig. 2), suggesting formation by heterogeneous nucleation at the interface. In coarse-grained droplets, pentlandite also occurs at MSS-Iss interfaces but is more lozenge-flame-shape. According to Kelly & Vaughan (1983), this characteristic shape is formed by heterogeneous nucleation, but apparently under lower undercooling. Czamanske & Moore (1977) considered such coarse pentlandite to have exsolved at close to its maximum temperature of stability (610°C). Alternatively, the Ni-rich phase could be horomanite, a Ni-Fe sulfide stable to 760°C (Kithakaze *et al.*, 2011). Pentlandite also occurs as oriented, flame-shaped grains in MSS in coarse-grained and zoned droplets (Figs. 3, 4). Kelly & Vaughan (1983) interpreted these to have exsolved by homogeneous nucleation during MSS annealing from 600°C to 300°C.

CONCLUSIONS:

The textural study of quenched sulfide droplets from fresh MORB glass leads to the following conclusions: 1) Textural differences observed in droplets that experienced identical cooling rates are due to differences in the degree of undercooling of the droplets. 2) The differences are mainly controlled by the size of the droplets. In the smaller droplets the effective solubility of M_{ss} is higher, and higher degrees of undercooling are required for crystallization to occur. The effective solubility decreases as droplet size increases. 3) Bulk Fe, Ni and Cu contents of the sulfide droplets do not seem to influence their texture. 4) The amount of pentlandite in sulfide droplets is controlled by the Ni concentration of the magma.

Sulfide droplets in MORB are unique records of near-liquidus phase relations in basaltic systems and provide unique insight into how sulfide-oxide liquids solidify under conditions of rapid cooling. Such insight may be useful in understanding how siderophile and chalcophile elements behave during sulfide crystallization in ore deposits.

ACKNOWLEDGMENTS:

We are grateful to Jim Mungall (University of Toronto) and Bob Martin (McGill University) for the helpful comments during the reviewing process. Sarah Dare (UQAC) and Philippe Pagé (UQAC) are thanked for helpful discussions, George Lozefski of Lamont Doherty Earth Observatory of Columbia University for his assistance in sampling, Dany Savard (UQAC) for his assistance in whole rock analysis and Marc Choquette (Laval University) for his assistance in microprobe analysis. This work was funded by the Canadian Research Chair in Magmatic Metallogeny.

REFERENCES

- BARNES, S.-J., COX, R.A. & ZIENTEK, M.L. (2006): Platinum-group element, gold, silver and base metal distribution in compositionally zoned sulfide droplets from the Medvezky Creek Mine, Noril'sk, Russia. *Contributions to Mineralogy and Petrology* **152**, 187-200.
- BIGG, E.K. (1953): The supercooling of water. *Proceedings of the Physical Society* **66b**, 688-694.
- BOUDREAU, A.E. (1999): PELE — a version of the MELTS software program for the PC platform. *Computers & Geosciences* **25**, 201–203.
- BOCKRATH, C., BALLHAUS, C. & HOLZHEID, A. (2004): Fractionation of the Platinum-Group Elements During Mantle Melting. *Science* **305**, 1951-1953.
- CASHMAN, K.V. & MARSH, B.D. (1988): Crystal size distribution (CSD) in rocks and the kinetics and dynamics of crystallization II: Makaopuhi lava lake. *Contributions to Mineralogy and Petrology* **99**, 292-305.
- CRAIG, J. R. & KULLERUD, G. (1969): Phase relations in the Cu-Fe-Ni-S system and their application to magmatic ore deposits. *Economic Geology Monograph* **4**, 344-358.
- CZAMANSKE, G.K. & MOORE, J.G. (1977): Composition and phase chemistry of sulfide globules in basalt in the Mid-Atlantic Ridge rift valley near 37°N lat. *Geological Society of America Bulletin* **88**, 587-599.
- DALTON, J.A. & LANE, S.J. (1996): Electron microprobe analysis of Ca in olivine close to grain boundaries: the problem of secondary X-ray fluorescence. *American Mineralogist* **81**, 194–201.
- DOWTY, E. (1980): Crystal growth and nucleation theory and the numerical simulation of igneous crystallization. In *Physics of magmatic processes*, ed. R. B. Hargraves, 419-485.
- EBEL, D.S. & NALDRETT, A.J. (1997): Crystallization of sulfide liquids and the interpretation of ore composition. *Canadian Journal of Earth Sciences* **34**, 352-365.
- EMMANUEL, S., AGUE, J. J. & WALDERHAUG, O. (2010): Interfacial energy effects and the evolution of pore size distributions during quartz precipitation in sandstone. *Geochimica et Cosmochimica Acta*, **74**, 3539-3552.
- ETSCHMANN, B., PRING, A., PUTNIS, A., GRGURIC, B.A. & A. STUDER. (2004): A kinetic study of the exsolution of pentlandite (Ni, Fe)₉S₈ from the monosulfide solid solution (Fe, Ni) S. *American Mineralogist* **89**, 39-50.

- FLEET, M.E. & PAN, Y. (1994): Fractional crystallization of anhydrous sulfide liquid in the system Fe-Ni-Cu-S, with application to magmatic sulfide deposits. *Geochimica et Cosmochimica Acta* **58**, 3369-3377.
- GIBB, F.G.F. (1974): Supercooling and the crystallization of plagioclase from a basaltic magma. *Mineralogical Magazine* **39**, 641-653.
- HIGGINS, M.D. (2006): Verification of ideal semi-logarithmic, lognormal or fractal crystal size distributions from 2D datasets. *Journal of Volcanology and Geothermal Research* **154**, 8-16.
- HOLNESS, M. B., & SAWYER, E. W. (2008): On the pseudomorphing of melt-filled pores during the crystallization of migmatites. *Journal of Petrology* **49**, 1343-1363.
- HOLZHEID, A. (2010): Separation of sulfide melt droplets in sulfur saturated silicate liquids. *Chemical Geology* **274**, 127-135
- KELLY, D.P. & VAUGHAN, D.J. (1983): Pyrrhotine-pentlandite ore textures: a mechanistic approach. *Mineralogical Magazine* **47**, 453-463.
- KITAKAZE, A., ITOH, H. & KOMATSU, R. (2011): Horomanite, $(\text{Fe},\text{Ni},\text{Co},\text{Cu})_9\text{S}_8$, and samaniite, $\text{Cu}_2(\text{Fe},\text{Ni})_7\text{S}_8$, new mineral species from the Horoman peridotite massif, Hokkaido, Japan. *Journal of Mineralogical and Petrological Sciences* **106**, 204-210.
- LIU, Y., SAMAHA, N. & BAKER, D. (2007): Sulfur concentration at sulfide saturation (SCSS) in magmatic silicate melts. *Geochimica et Cosmochimica Acta* **71**, 1783-1799.
- MATHEZ, E.A. (1976): Sulfur solubility and magmatic sulfides in submarine basalt glass. *Journal of Geophysical Research* **81**, 4269-4276.
- MATHEZ, EA. (1979): Sulfide relations in hole 418A flows and sulfur contents of glasses. *Initial reports of the Deep Sea Drilling Project* **51**, 1069-1085.
- MATHEZ, E.A. & YEATS, R.S. (1976): Magmatic sulfides in basalt glass from dsdp hole 319a and site 320, Nazca plate. *Initial Reports of the Deep-Sea Drilling Project* **34**, 363-373.
- MOORE, J.G. (1975): Mechanism of formation of pillow lava. *American Scientist* **63**, 269-277.
- MOORE, J.G. & CALK, L.C. (1971): Sulfide spherules in vesicles of dredge pillow basalt. *American Mineralogist* **56**, 476-488.

- MOORE, J.G. & SCHILLING, J.G. (1973): Vesicles, water, and sulfur in Reykjanes Ridge basalt. *Contribution to Mineralogy and Petrology* **41**, 105-118.
- MUNGALL, J.E. (2002): Kinetic Controls on the Partitioning of Trace Elements Between Silicate and Sulfide Liquids. *Journal of Petrology* **43**, 749-768.
- MUNGALL, J.E. (2007): Crystallization of magmatic sulfides: An empirical model and application to Sudbury ores. *Geochimica et Cosmochimica Acta* **71**, 2809-2819.
- MUNGALL, J.E., ANDREWS, D.R.A., CABRI, L.J., SYLVESTER, P.J. & TUBRETT, M. (2005): Partitioning of Cu, Ni, Au, and platinum-group elements between monosulfide solid solution and sulfide melt under controlled oxygen and sulfur fugacities. *Geochimica et Cosmochimica Acta* **69**, 4349-4360.
- MUNGALL, J.E. & SU, S. (2005): Interfacial tension between magmatic sulfide and silicate liquids: Constraints on kinetics of sulfide liquation and sulfide migration through silicate rocks. *Earth and Planetary Science Letters* **234**, 135-149.
- NALDRETT, A.J. (1969): A Portion of the System Fe-S-O between 900 and 1080°C and its Application to Sulfide Ore Magmas. *Journal of Petrology* **10**, 171-201.
- PEACH, C.L., MATHEZ, E.A. & KEAYS, R.R. (1990): Sulfide melt-silicate melt distribution coefficients for noble metals and other chalcophile elements as deduced from MORB: Implications for partial melting. *Geochimica et Cosmochimica Acta* **54**, 3379-3389.
- PRICHARD, H.M., HUTCHINSON, D. & FISHER, P.C. (2004): Petrology and crystallization history of multiphase sulfide droplets in a mafic dike from Uruguay: implications for the origin of Cu-Ni-PGE sulfide deposits. *Economic Geology* **99**, 365-376.
- PUTNIS, A. & MAUTHE, G. (2001): The effect of pore size on cementation in porous rocks. *Geofluids* **1**, 37-41.
- SHELLEY, D. (1993): Igneous and metamorphic rocks under the microscope, Chapman.
- SKINNER, B.J. & PECK, D.L. (1969): An immiscible sulfide melt from Hawai'i. *Economic Geology Monograph* **4**, 310-320.
- WALLACE, P. & CARMICHAEL, I. (1992): Sulfur in basaltic magmas. *Geochimica et Cosmochimica Acta* **56**, 1863-1874.
- YEATS, R.S. & MATHEZ, E.A. (1976): Decorated vesicles in deep-sea basalt glass, eastern pacific. *Journal of Geophysical Research* **81**, 4277-4284.

APPENDIX:

Appendix 1: Sulfide droplets bulk composition calculations

Sulfide droplet bulk compositions were calculated to 100% sulfide with the Image Pro Plus Analysis 6.2 software and the microprobe analysis data using for each element:

$$C_s = \left(\frac{\sum^{n1} c_{Fe\ phase}}{n1} \right) * \%Fe\ phase + \left(\frac{\sum^{n2} c_{Cu\ phase}}{n2} \right) * \%Cu\ phase + \left(\frac{\sum^{n3} c_{Ni\ phase}}{n3} \right) * \%Ni\ phase [6]$$

with C_s , $c_{Fe\ phase}$, $c_{Cu\ phase}$ and $c_{Ni\ phase}$ are respectively the concentration of the element in the sulfide droplet, the Fe-rich phase, the Cu-rich phase and the Ni-rich phase. n1, n2 and n3 are the number of electron microprobe analyses made in each phase. The $\%Fe\ phase$, $\%Cu\ phase$, $\%Ni\ phase$ are the percentage of each phase determined by Image Pro Plus Analysis 6.2. Bulk compositions are calculated to 100% sulfide to be in agreement with experiments values of Ebel & Naldrett (1997) which are oxide free; S and Fe concentrations are slightly overestimated, as the proportion of oxide occurrences varies from nil to 7% in sulfide droplets. Detailed calculations of the Table 2 values are given in Table 3. As Ni-rich phases are present in sulfide droplets either as micrometric flame-shaped exsolution domains or as micrometric grains at the Fe-rich and Cu-rich boundaries their analysis by microprobe was not possible in all droplets. Where a direct analysis of the Ni-rich phase was impossible, the average composition of Ni-rich phase (n=5) was used for the calculation of the bulk composition determined at 33,4% S ($\pm 1,32$), 38,64% Fe ($\pm 4,72$), 24% Ni ($\pm 4,87$) and 2,6% Cu ($\pm 1,47$). For fine-grained sulfide droplets, the phases are too small to be analyzed independently, and the average composition of the whole droplet is used for calculation.

Appendix 2: Whole-rock Ni values

Fresh glass rims of pillow samples were crushed in Al-ceramic mill at the UQAC for whole-rock Ni analysis. The Ni content was determined by atomic absorption spectrometry (AAS) at the LabMaTer, UQAC using a Thermo Atomic Spectrometer (Table 5). KPT reference material was used as monitor.

Appendix 3: Composition of oxide inclusions in sulfide droplets

Euhedral magnetites in sulfide droplets with a size large enough for an electron-microprobe analysis are rare; their compositions are given in Table 4. Three of them were analyzed and gave poor values. Moreover there is a high contamination by the surrounding sulfide owing to secondary fluorescence traduced by high concentration in Ni. However, the results allow a qualitative interpretation as they leave no doubt that the grains are Ti-free magnetite.

FIGURE CAPTIONS

Figure 1

Positive correlation of sulfur content and FeO* concentration in the glass. The values lie between the trend reported by Mathez (1979) and Czamanske & Moore (1977).

Figure 2

Photomicrograph illustrating the textural character of a fine-grained sulfide droplet (sample RC 28 02 24rd). Note the perfect spherical shape of the droplet. MSS and ISS are finely intergrown and contain grains of a Ni-rich phase at their interface.

Figure 3

Photomicrograph illustrating the textural character of a coarse-grained sulfide droplet (sample Cook D37 t.IV). Note the quasi-perfect spherical shape. MSS and ISS are intergrown as in fine-grained droplets (Fig.2), but there are fewer grains and they are larger. The Ni-rich phase is present both at the MSS-ISS interface and as flame-shaped grains inside MSS.

Figure 4

Photomicrographs illustrating the textural character of zoned sulfide droplets. Droplet A is from sample RC 28 02 18rd, droplet B is from sample RC 28 02 13rd and droplet C is from sample Cook D19 tI. Note their crenulated contacts with surrounding glass.

Droplets A and B have quenched ISS with fishbone texture and droplet C has massive ISS and euhedral oxide. Pentlandite (Pn) is present as lozenge-flame-shaped grains within MSS and as grains at the MSS-ISS interface.

Figure 5

Frequencies of apparent sulphide droplet diameters and textural types. Note that sulfide droplets with diameters larger than 50 µm have a zoned texture.

Figure 6

Bulk composition of sulfide droplets in the system Fe-Ni-Cu in weight fraction. The grey zone corresponds to the bulk composition of sulfide droplets from Czamanske & Moore (1977). Dashed line represents the composition of sulfide liquid composition at MSS crystallization at 1100°C, 1050°C and 1000°C from Ebel & Naldrett (1997). Note that texture of sulfide droplets is not dependent on their composition. Droplet liquidii

temperature range between $>1100^{\circ}\text{C}$ to 1050°C . Modified from Czamanske and Moore (1977).

Figure 7

Illustration of the dependency of sulfide droplet cooling history on droplet size. MSS effective solubility increases in droplets as the size decreases leading to a delay in sulfide crystallization during cooling.

Figure 8

Ni content of MSS (symbols) and pentlandite content (bars) of corresponding sulfide droplet versus Ni whole rock content. Overlapping bars refer to droplets from the same sample. Note that Ni concentration in MSS reaches a limit at 12-15% and that pentlandite concentration increases when this limit is reached.

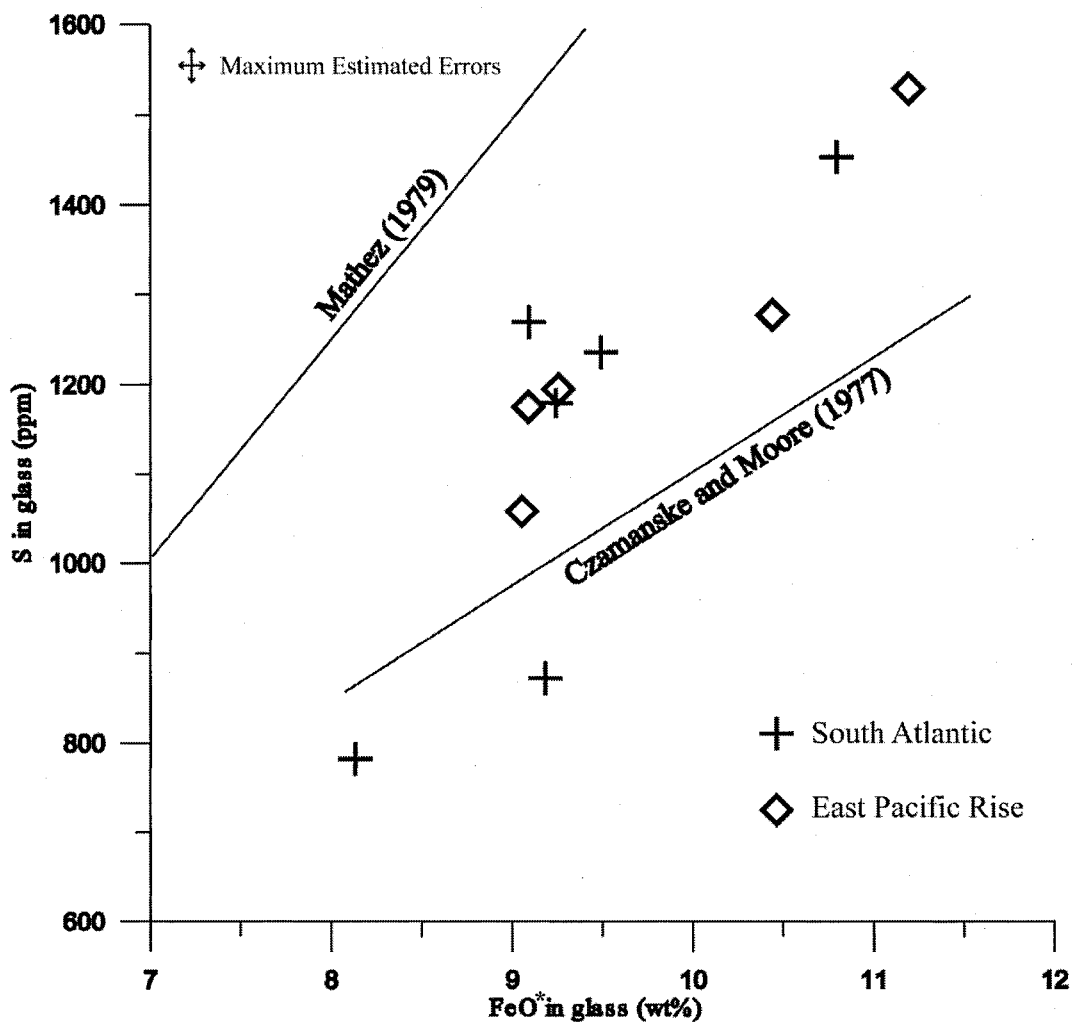


Fig. 1

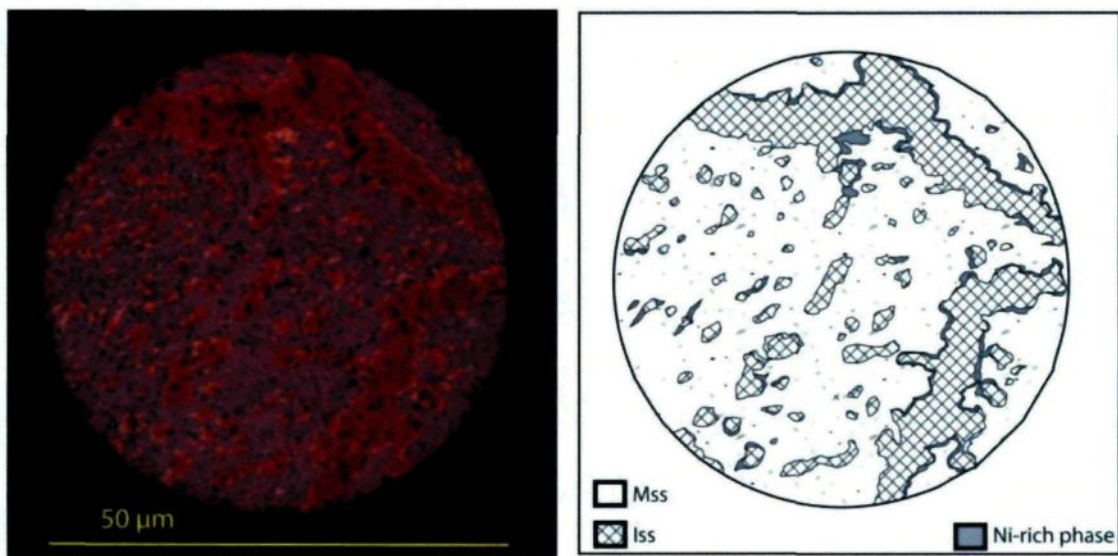


Fig. 2

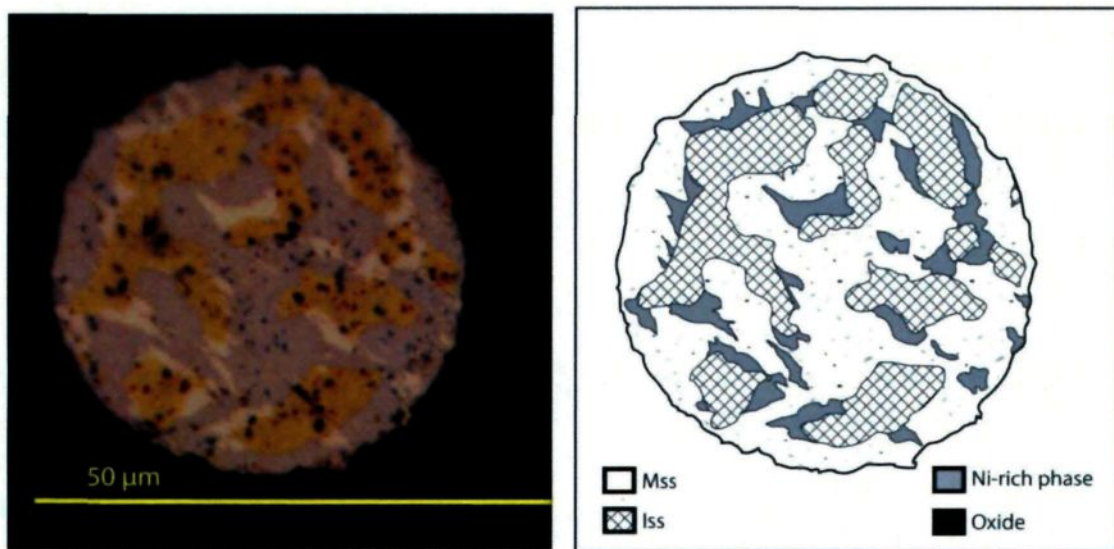


Fig. 3

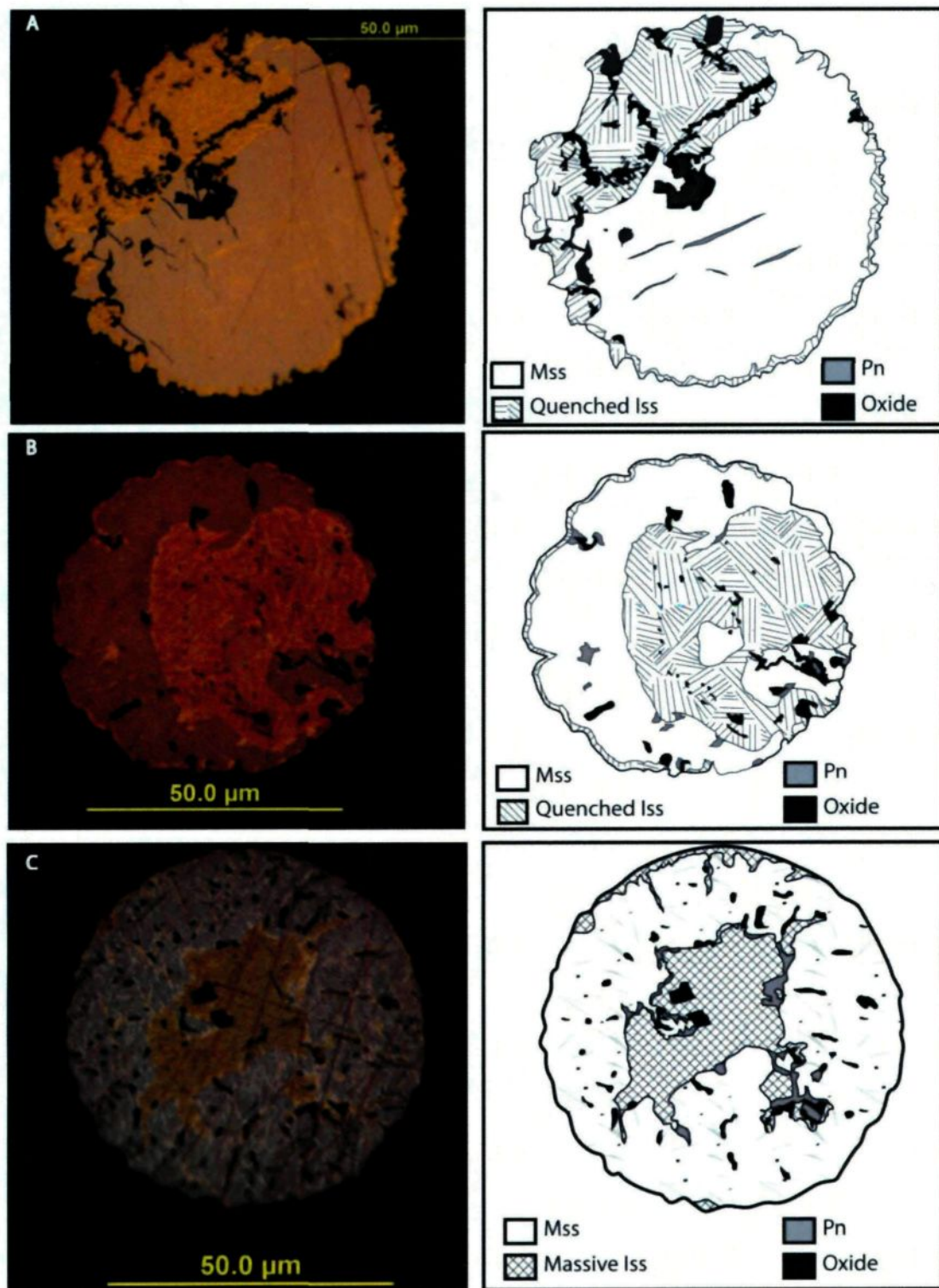


Fig. 4

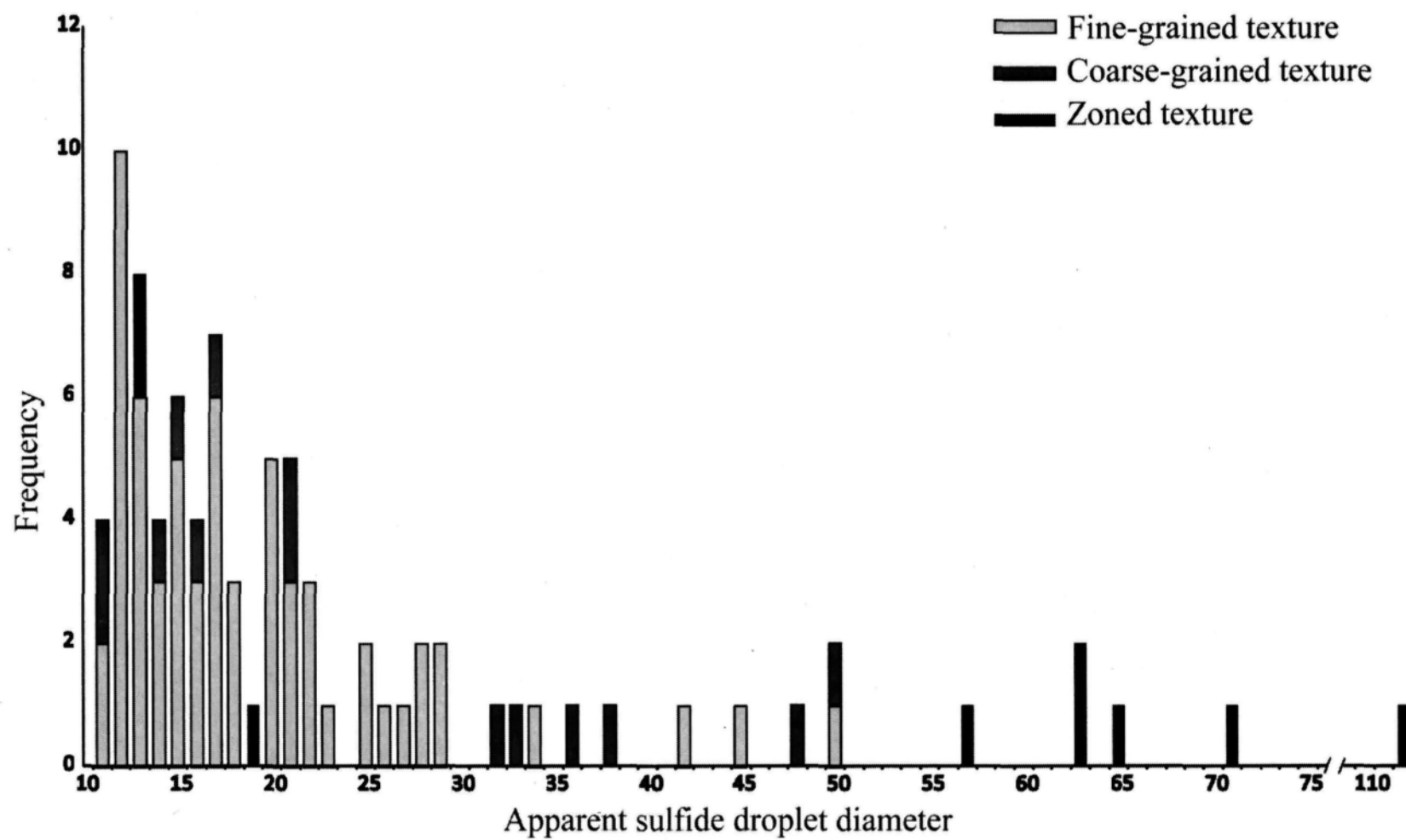


Fig. 5

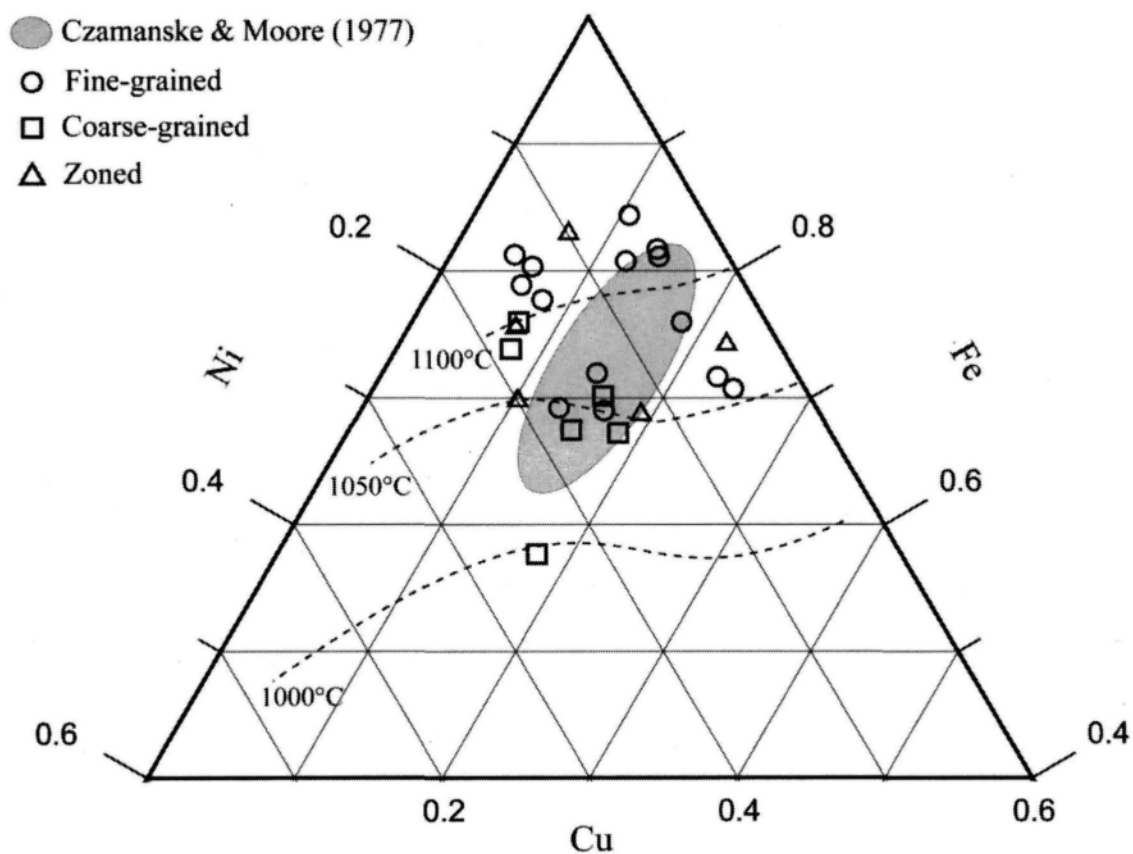


Fig. 6

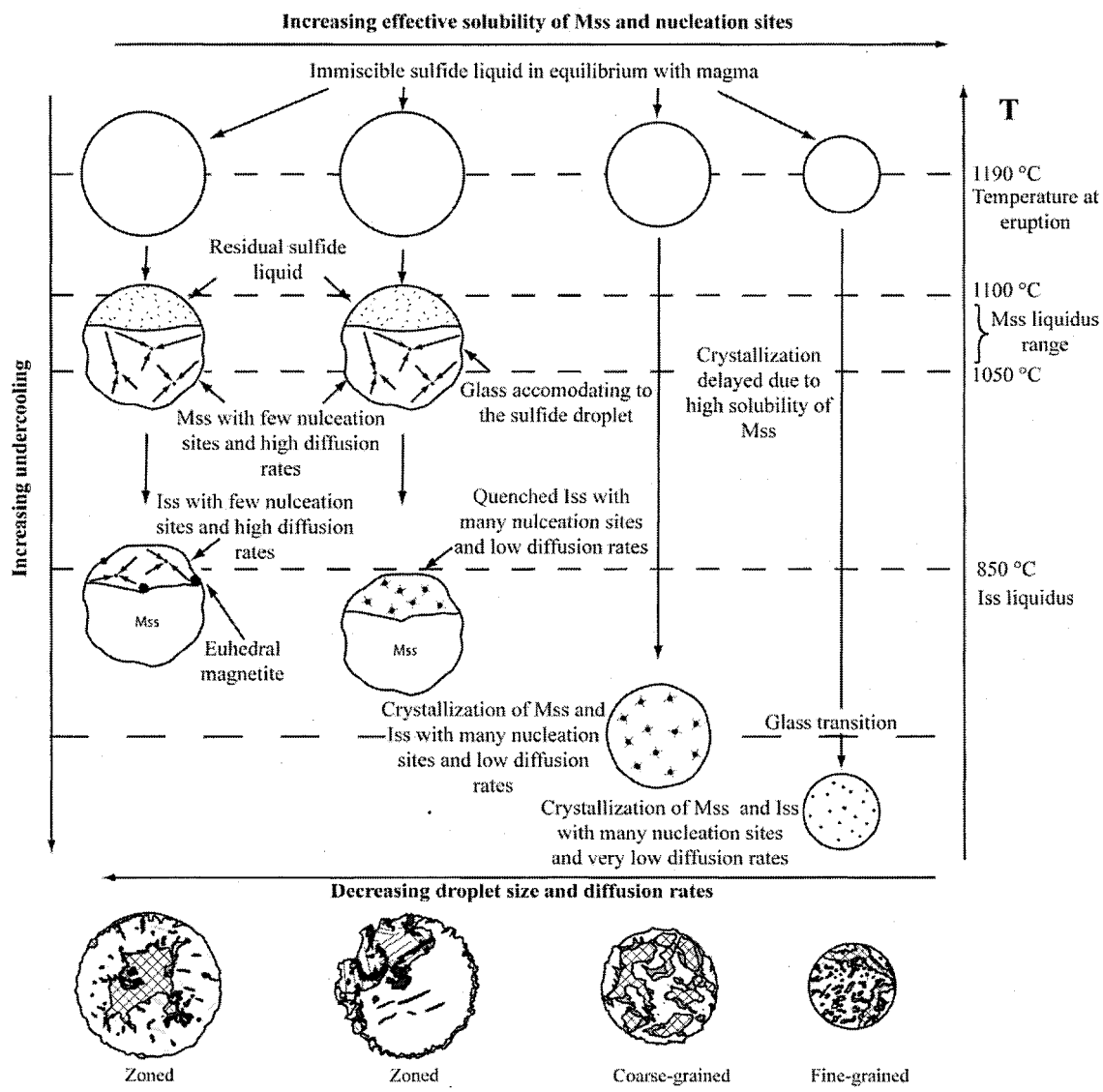


Fig. 7

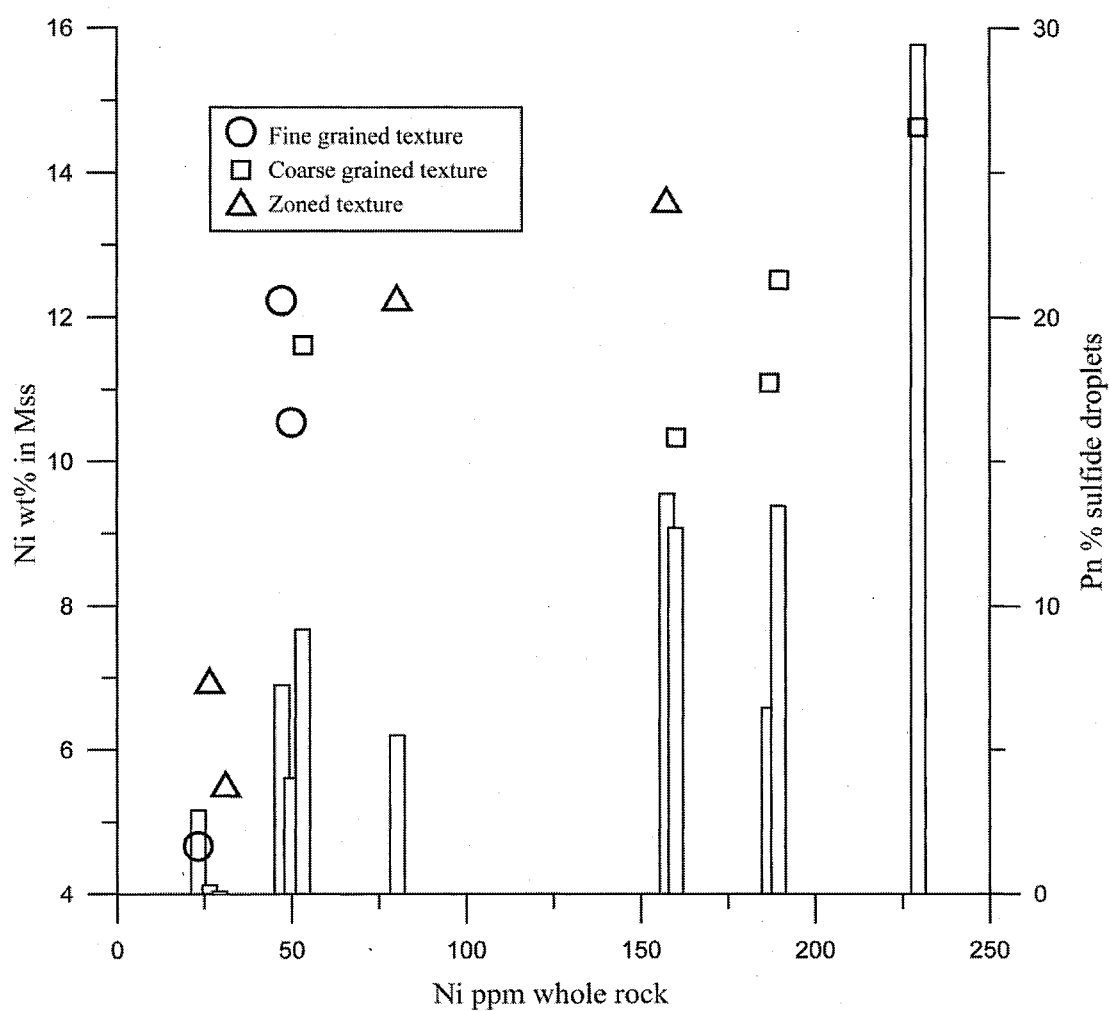


Fig. 8

TABLE 1. BULK COMPOSITION OF THE GLASS

Sample List		SiO ₂	TiO ₂	Al ₂ O ₃	FeO	Cr ₂ O ₃	MgO	CaO	MnO	Na ₂ O	K ₂ O	S (ppm)	Total wt%
		wt%	wt%	wt%	wt%	wt%	wt%	wt%	wt%	wt%	wt%		
South Atlantic Ridge													
RC 28 02 07rd	n=3	49.6	1.2	17.0	9.2	0.04	8.9	11.2	0.2	2.9	0.05	873	100.5
	σ	0.12	0.01	0.05	0.11	0.04	0.09	0.04	0.04	0.03	0.01	88	0.26
RC 28 02 13rd	n=12	50.3	1.6	15.1	9.5	0.07	8.0	11.4	0.2	2.7	0.09	1253	99.3
	σ	0.20	0.04	0.06	0.17	0.04	0.06	0.04	0.03	0.03	0.01	81	0.31
RC 28 02 16rd	n=15	50.4	1.4	14.7	9.1	0.05	7.7	12.2	0.2	2.8	0.05	1275	98.7
	σ	0.31	0.04	0.10	0.23	0.08	0.09	0.10	0.03	0.06	0.01	86	0.57
RC 28 02 18rd	n=3	51.6	1.1	15.3	8.1	0.08	8.4	12.8	0.1	2.7	0.05	782	100.4
	σ	0.26	0.07	0.07	0.13	0.02	0.44	0.36	0.01	0.80	0.01	272	0.43
RC 28 02 22rd	n=9	51.4	1.8	14.0	10.8	0.01	7.0	11.3	0.2	3.0	0.07	1454	99.9
	σ	0.13	0.04	0.04	0.19	0.02	0.06	0.05	0.03	0.03	0.01	88	0.23
RC 28 02 24rd	n=8	50.5	1.6	15.6	9.2	0.06	8.2	11.5	0.2	2.8	0.07	1180	99.8
	σ	0.19	0.05	0.06	0.15	0.04	0.05	0.05	0.02	0.06	0.01	100	0.43
Hotu Sea Mount													
Cook D3 tIII	n=3	47.9	2.9	15.4	11.2	0.0	6.2	9.7	0.2	3.3	0.72	1530	97.9
	σ	0.27	0.08	0.19	0.09	0.02	0.10	0.02	0.02	0.05	0.01	47	0.39
Cook D19 tI n1	n=3	47.6	2.2	16.9	10.4	0.07	7.5	10.1	0.2	3.3	0.58	1278	99.0
	σ	0.18	0.04	0.06	0.12	0.05	0.02	0.04	0.02	0.06	0.01	25	0.36
East Pacific Rise													
Cook D28 tI	n=9	48.8	1.4	16.0	9.0	0.07	8.5	11.9	0.2	3.1	0.12	1054	99.3
	σ	0.10	0.05	0.43	0.31	0.05	0.27	0.03	0.03	0.10	0.01	94	0.27
Cook D37 tIV	n=6	48.7	1.3	16.6	9.3	0.02	8.3	11.7	0.2	2.9	0.12	1195	99.4
	σ	0.25	0.05	0.07	0.13	0.02	0.03	0.09	0.02	0.02	0.01	58	0.36
Cook D37 tVI	n=18	48.6	1.2	16.7	9.1	0.05	8.5	11.7	0.2	2.8	0.11	1167	99.2
	σ	0.29	0.06	0.10	0.13	0.03	0.08	0.03	0.02	0.04	0.01	86	0.45

n= number of analysis; σ= sample standard deviation

Note that samples from the South Atlantic Ridge are slightly richer in SiO₂ and samples from the Hotu Sea Mounts are slightly richer in TiO₂ and K₂O.

Data acquired by electron-microprobe

TABLE 2. BULK COMPOSITION OF THE SULFIDE DROPLETS

Droplet	Texture	Size μm	n (phase)*	Bulk composition (wt%)				
				S	Ni	Cu	Fe	Total
RC 28 02 07rd G1 α	Coarse-grained	48	9 (1,2,3)	34.46 0.74	15.93 3.19	11.36 1.52	37.21 1.58	98.95
RC 28 02 13rd n1 G6 α	Zoned	63	4 (1,2)	35.81 0.70	7.70 0.50	12.17 1.07	44.07 0.62	99.76
RC 28 02 13rd n1 G10 α	Fine-grained	29	2 (4)	35.61 0.63	8.93 0.09	2.68 1.26	50.39 0.88	97.61
RC 28 02 13rd n2 G1 α	Fine-grained	28	3 (4)	34.97 0.44	8.30 0.53	3.64 0.68	48.87 1.01	95.78
RC 28 02 13rd n2 G2 α	Fine-grained	13	3 (4)	35.58 0.43	8.94 0.70	4.98 1.10	48.60 1.63	98.11
RC 28 02 13rd n2 G3 α	Fine-grained	12	3 (4)	35.66 0.41	9.37 0.45	3.70 0.62	48.88 0.56	97.62
RC 28 02 16d n1 G10 α	Fine-grained	45	3 (1,2)	33.69 0.31	3.49 0.02	14.52 0.78	45.53 0.20	97.22
RC 28 02 16rd n1 G3 α	Fine-grained	21	3 (4)	34.51 0.21	3.56 0.54	11.31 2.34	47.06 1.51	96.44
RC 28 02 16rd n1 G4 α	Fine-grained	25	3 (4)	34.78 0.28	4.42 0.23	7.52 0.14	50.14 0.49	96.95
RC 28 02 16rd n2 G2 α	Zoned	18	2 (1,2) a=0	32.43	2.19	13.92	46.98	95.53
RC 28 02 16rd n2 G6 α	Fine-grained	20	3 (4)	33.67 0.16	3.11 1.02	15.52 3.84	44.99 2.75	97.30
RC 28 02 18rd G5 α	Fractionnated	70	4 (1,2)	37.81 0.11	6.10 0.39	4.38 0.63	51.75 0.52	100.03
RC 28 02 22rd G25 α	Fine-grained	29	3 (4)	34.32 0.26	3.16 0.19	6.59 0.24	52.73 0.84	96.81
RC 28 02 22rd G26 α	Fine-grained	26	3 (4)	34.62 0.10	2.95 0.14	8.88 1.18	50.85 0.74	97.29
RC 28 02 22rd G29 α	Fine-grained	41	3 (4)	34.72 0.13	2.84 0.46	8.67 3.03	51.44 2.09	97.67
RC 28 02 24rd G2 α	Fine-grained	33	3 (1,2)	34.49 0.63	9.23 0.26	10.48 2.43	43.88 1.75	98.09
RC 28 02 24rd G3 β	Fine-grained	50	3 (1,2)	34.73 0.20	8.42 0.44	9.06 2.18	44.85 1.49	97.06
RC 28 02 24rd G6 α	Coarse-grained	38	4 (1,2,3)	35.49 0.82	10.53 0.76	4.54 0.08	47.71 1.02	98.27
Cook D19 tI n1 G2 α	Zoned	62	5 (1,2)	33.94 1.70	12.71 0.35	6.48 1.15	44.83 1.09	97.96
Cook D28 tI n1 G1 α	Coarse-grained	32	4 (1,2)	35.54 1.18	10.76 0.89	4.50 1.33	47.74 1.12	98.54
Cook D28 tI n2 G1 α	Coarse-grained	42	4 (1,2)	34.50 0.73	11.26 1.36	9.72 0.84	43.53 0.13	99.01
Cook D37 tIV G2 α	Coarse-grained	32	5 (1,2,3)	35.16 1.08	8.87 0.58	10.05 0.69	44.47 0.47	98.55
Cook D37 tVI n2 G1 α	Coarse-grained	20	3 (4)	35.05 0.46	11.35 0.75	4.78 1.16	45.60 0.93	96.78
Cook D37 tVI n2 G3 α	Fine-grained	13	3 (4)	35.12 0.08	9.26 1.71	11.80 3.06	43.26 1.18	99.44
Cook D37 tVI n3 G8 α	Zoned	15	3 (4)	35.10 0.32	10.99 0.91	8.38 0.61	43.58 0.35	98.05

* Phases analysed: 1) Fe-rich 2) Cu-rich 3) Ni-rich and 4) whole droplet. α= sample

For fine-grained droplets bulk compositions were calculated with whole droplet microprobe analysis. For coarse-grained and zoned sulfide droplets, bulk compositions are calculated by combining microprobe data on the different sulfide phases and Image Pro Plus 6.1 data using equation [6]. Details in Appendix 1 and Table 3.

TABLE 3A. SULPHIDE DROPLET BULK COMPOSITIONS CALCULATED WITH MICROPROBE AND IMAGE PRO PLUS ANALYSIS DATA. BULK COMPOSITIONS IS EITHER CALCULATED WITH 1)WHOLE DROPLET MICROPROBE ANALYSIS AVERAGE OR 2) EQUATION [6].

Droplet	Texture	Size (μm)	Phase	Microprobe analysis					Image pro 100% sulf			Bulk composition				
				S	Ni	Cu	Fe	Total	Fe rich	Cu rich	Ni rich	S	Ni	Cu	Fe	Total
				wt %	wt %	wt %	wt %	wt %				wt %	wt %	wt %	wt %	wt %
South Atlantic Ridge																
RC 28 02 07rd G1	Coarse quenched	48,00	Ni rich	31,29	27,42	5,00	33,97	98,04	31,04	39,52	29,44	34,46	15,93	11,36	37,21	98,95
			Fe rich	35,98	14,51	2,62	46,39	99,71				0,74	3,19	1,52	1,58	
			Cu rich	33,99	1,22	28,40	31,01	94,69								
			Cu rich	34,45	12,17	23,69	30,33	100,82								
			Ni rich	32,70	31,71	3,47	32,05	100,25								
			Cu rich	34,44	12,21	21,39	31,39	99,61								
			Fe rich	36,50	15,52	1,71	46,33	100,38								
			Fe rich	35,51	13,86	2,07	47,45	99,09								
			Ni rich	35,16	22,59	1,88	40,87	100,68								
RC 28 02 13rd n1 G6	Fractionated	63,00	Cu rich	35,46	0,31	26,19	38,52	100,69	47,10	47,39	5,50	33,98	6,37	12,03	41,94	94,32
			Cu rich	33,00	2,20	22,51	40,78	98,64				0,70	0,50	1,07	0,62	
			Fe rich	37,87	12,33	0,74	49,26	100,42								
			Fe rich	37,52	12,21	1,35	49,05	100,44								
RC 28 02 13rd n1 G10	Fine quenched	29,00	whole droplet	36,24	9,02	1,43	51,27	98,14				35,61	8,93	2,68	50,39	97,61
			whole droplet	34,98	8,83	3,94	49,51	97,71				0,63	0,09	1,26	0,88	
RC 28 02 13rd n2 G1	Fine quenched	28,00	whole droplet	34,37	8,84	3,34	48,70	95,50				34,97	8,30	3,64	48,87	95,78
			whole droplet	35,10	8,49	4,58	47,72	96,08				0,44	0,53	0,68	1,01	
			whole droplet	35,44	7,59	3,01	50,18	96,47								
RC 28 02 13rd n2 G2	Fine quenched	13,00	whole droplet	36,00	8,81	5,13	48,27	98,52				35,58	8,94	4,98	48,60	98,11
			whole droplet	35,00	9,85	6,24	46,80	98,06				0,43	0,70	1,10	1,63	
			whole droplet	35,75	8,16	3,57	50,75	98,43								
RC 28 02 13rd n2 G3	Fine quenched	12,00	whole droplet	35,25	9,98	4,56	48,11	98,13				35,66	9,37	3,70	48,88	97,62
			whole droplet	35,50	8,89	3,43	49,39	97,45				0,41	0,45	0,62	0,56	
			whole droplet	36,23	9,25	3,12	49,15	97,97								
RC 28 02 16d n1 G10	Fine quenched	45,00	Fe rich	34,85	4,65	6,18	51,03	97,10	49,31	47,78	2,90	32,72	2,79	14,44	44,40	94,36
			Cu rich	32,83	1,02	23,04	40,47	97,65				0,31	0,02	0,78	0,20	
			Fe rich	34,23	4,69	7,74	50,63	97,61								
RC 28 02 16rd n1 G3	Fine quenched	21,00	whole droplet	34,46	3,23	11,94	46,63	96,54				34,51	3,56	11,31	47,06	96,44
			whole droplet	34,27	3,13	13,82	45,45	96,98				0,21	0,54	2,34	1,51	
			whole droplet	34,79	4,32	8,19	49,09	96,75								

TABLE 3B. SULPHIDE DROPLET BULK COMPOSITIONS CALCULATED WITH MICROPROBE AND IMAGE PRO PLUS ANALYSIS DATA. BULK COMPOSITIONS IS EITHER CALCULATED WITH
1)WHOLE DROPLET MICROPROBE ANALYSIS AVERAGE OR 2) EQUATION [6].

Droplet	Texture	Size (μm)	Phase	Microprobe analysis					Image pro 100% sulf			Bulk composition					
				S	Ni	Cu	Fe	Total	wt %	wt %	wt %	wt %	wt %	wt %	wt %		
				wt %	wt %	wt %	wt %	wt %									
RC 28 02 16rd n1 G4	Fine quenched	25,00	whole droplet	34,60	4,74	7,65	49,46	96,81					34,78	4,42	7,52	50,14	96,86
			whole droplet	34,58	4,25	7,33	50,53	96,92									
			whole droplet	35,18	4,26	7,58	50,43	97,70									
RC 28 02 16rd n2 G2	Fractionated	18,00	Cu rich	31,31	0,83	18,06	44,77	95,12	70,99	29,01	0,00		32,43	2,19	13,92	46,98	95,53
				35,15	5,53	3,80	52,41	97,16									
RC 28 02 16rd n2 G6	Fine quenched	20,00	whole droplet	33,71	4,16	10,84	48,50	97,41					33,67	3,11	15,52	44,99	97,30
			whole droplet	33,85	3,43	15,50	44,69	97,70									
			whole droplet	33,45	1,73	20,24	41,78	97,41									
RC 28 02 18rd G5	Fractionnated	70,00	Cu rich	35,84	1,37	21,70	40,69	99,84		80,59	19,09	0,32	37,70	6,02	4,37	51,63	99,72
				35,58	2,88	19,47	41,79	99,89									
			Fe rich	38,23	6,94	0,70	54,78	100,97									
				38,42	6,99	0,40	53,80	99,85									
RC 28 02 22rd G25	Fine quenched	29,00	whole droplet	33,98	3,43	6,64	51,55	95,80					34,32	3,16	6,59	52,73	96,81
			whole droplet	34,39	2,99	6,85	53,45	98,02									
			whole droplet	34,60	3,07	6,28	53,18	97,38									
RC 28 02 22rd G26	Fine quenched	26,00	whole droplet	34,58	2,77	10,41	49,85	97,79					34,62	2,95	8,88	50,85	97,29
			whole droplet	34,75	2,96	7,54	51,61	97,26									
			whole droplet	34,53	3,10	8,68	51,10	97,60									
RC 28 02 22rd G29	Fine quenched	41,00	whole droplet	34,88	2,94	7,53	52,03	97,68					34,72	2,84	8,67	51,44	97,67
			whole droplet	34,72	3,35	5,66	53,65	97,62									
			whole droplet	34,55	2,24	12,82	48,64	98,62									
RC 28 02 24rd G2	Fine quenched	33,00	Cu rich	33,50	3,40	20,17	40,64	97,95		49,09	43,65	7,25	32,07	7,49	10,29	41,08	90,93
				34,91	12,49	5,45	45,79	98,84									
				36,17	11,97	0,60	49,28	98,35									
RC 28 02 24rd G3	Fine quenched	50,00	Cu rich	33,68	2,10	21,53	38,70	96,30		64,37	31,61	4,02	33,39	7,45	8,96	43,30	93,09
				35,13	10,11	5,53	46,78	97,84									
				35,53	10,98	1,16	49,75	97,66									

TABLE 3C. SULPHIDE DROPLET BULK COMPOSITIONS CALCULATED WITH MICROPROBE AND IMAGE PRO PLUS ANALYSIS DATA. BULK COMPOSITIONS IS EITHER CALCULATED WITH
1)WHOLE DROPLET MICROPROBE ANALYSIS AVERAGE OR 2) EQUATION [6].

Droplet	Texture	Size (μm)	Phase	Microprobe analysis					Image pro 100% sulf			Bulk composition				
				S	Ni	Cu	Fe	Total				wt %	wt %	wt %	wt %	wt %
									Fe rich	Cu rich	Ni rich					
RC 28 02 24rd G6	Coarse quenched	38,00	Cu rich	30,94	1,42	21,67	42,02	96,33	72,91	17,92	9,17	35,49	10,53	4,54	47,71	98,27
			Fe rich	35,95	10,86	0,59	50,75	98,35				0,82	0,76	0,08	1,02	
			Fe rich	37,58	12,38	0,75	48,71	99,69								
			Ni rich	34,22	19,68	1,85	42,78	98,85								
Hotu Seamount																
Cook D19 tl n1 G2	Fractionated	62,00	Cu rich	34,61	1,21	24,41	38,95	99,35	65,99	20,12	13,89	29,30	9,38	6,12	39,47	84,26
			Cu rich	31,52	1,82	21,44	41,13	96,20				1,70	0,35	1,15	1,09	
			Fe rich	36,33	13,53	3,39	46,61	100,06								
			Cu rich	33,77	2,68	22,10	38,80	97,52								
			Fe rich	32,16	13,73	1,35	48,84	96,33								
East Pacific Rise																
Cook D28 tl n1 G1	Coarse quenched	32,00	Fe rich	36,28	11,54	4,03	47,74	99,82	44,54	49,01	6,45	33,39	9,20	4,33	45,25	92,17
			Fe rich	34,05	9,88	1,87	50,48	96,57				1,18	0,89	1,33	1,12	
			Cu rich	33,17	1,17	20,57	44,58	99,56								
			Fe rich	36,77	11,94	0,82	49,07	98,83								
Cook D28 tl n2 G1	Coarse quenched	42,00	Cu rich	34,59	7,62	19,38	39,30	101,36	43,58	42,96	13,46	30,01	8,02	9,37	38,33	85,73
			Fe rich	36,01	11,98	1,17	48,98	98,36				0,73	1,36	0,84	0,13	
			Fe rich	35,62	13,06	0,87	49,04	99,08								
			Cu rich	32,44	4,34	22,16	39,71	98,79								
Cook D37 tIV G2	Coarse quenched	32,00	Cu rich	35,01	2,85	26,50	36,51	101,11	53,10	34,20	12,70	35,16	8,87	10,05	44,47	98,55
			Fe rich	36,98	10,99	1,09	49,28	98,67				1,08	0,58	0,69	0,47	
			Fe rich	34,35	9,59	2,65	50,42	97,21								
			Fe rich	35,52	10,52	1,30	49,76	97,36								
			Ni rich	33,65	18,81	0,81	43,55	97,29								
Cook D37 tVI n2 G1	Coarse quenched	20,00	whole droplet	34,48	12,39	4,70	44,32	96,13				35,05	11,35	4,78	45,60	96,78
			whole droplet	35,07	11,01	3,41	46,48	96,21				0,46	0,75	1,16	0,93	
			whole droplet	35,60	10,65	6,24	46,01	98,77								
Cook D37 tVI n2 G3	Fine quenched	13,00	whole droplet	35,12	7,81	13,60	42,65	99,43				35,12	9,26	11,80	43,26	99,44
			whole droplet	35,02	11,66	7,49	44,91	99,33				0,08	1,71	3,06	1,18	
			whole droplet	35,22	8,31	14,32	42,21	100,22								
Cook D37 tVI n3 G8	Fractionated	15,00	whole droplet	34,68	11,90	7,81	43,48	98,08				35,10	10,99	8,38	43,58	98,05
			whole droplet	35,45	11,33	8,11	43,21	98,32				0,32	0,91	0,61	0,35	
			whole droplet	35,16	9,75	9,23	44,06	98,39								

TABLE 4. WHOLE-ROCK VALUES OF NI DONE BY AAS.

Sample	Ni ppm		Sample	Ni ppm
RC 28 02 07rd	229		Cook D3 tIII	101
RC 28 02 13rd	80		Cook D19 tl n1	157
RC 28 02 16rd	23		Cook D28 tl	187
RC 28 02 18rd	26		Cook D37 tIV	165
RC 28 02 22rd	30		Cook D37 tVI	195
RC 28 02 24rd	47		KPT (n=3) KPT working values	1006 +/- 11 1090 +/- 149

TABLE 5. EUHEDRAL OXIDE MICROPROBE ANALYSIS FROM SULPHIDE DROPLETS.

Droplet	SiO ₂	TiO ₂	Al ₂ O ₃	Fe ₂ O ₃	FeO	MnO	Mgo	CaO	NiO	ZnO	Total
	wt%	wt%	wt%	wt%	wt%	wt%	wt%	wt%	wt%	wt%	wt%
RC 28 02 13rd n1 G6	0.20	0.02	0.01	63.25	23.63	0.24	0.00	0.05	4.65	0.12	92.25
Cook D19 tl n1 G2	0.05	0.00	0.01	56.40	10.09	0.07	0.00	0.30	15.48	0.01	82.45
RC 28 02 18rd G5	0.47	0.05	0.06	57.89	17.50	0.02	0.00	0.28	8.72	0.02	85.32
σ (n=2)	0.05	0.05	0.03	1.40	1.82	0.01	0.00	0.01	2.80	0.02	2.58

Note the high NiO values due to sulphide contamination. oxide are ti free magnetite.

CHAPITRE II

COEFFICIENTS DE PARTAGE LIQUIDE SILICATÉ-LIQUIDE SULFURÉ POUR DES ÉLÉMENTS CHALCOPHILES ET CRISTALLISATION DE GOUTTELETTES SULFUREÉS DE MORB.

Titre du Manuscrit:

Sulphide melt-silicate melt partition coefficients for chalcophile elements and crystallization of sulphide droplets in MORB.

Auteurs:

Clifford Patten, Sarah-Jane Barnes, Edmond A. Mathez, Frances Jenner.

Journal :

Journal of Petrology.

Résumé:

La répartition des Éléments Hautement Sidérophiles (EHS: Ru, Rh, Pd, Re, Os, Ir, Pt et Au) parmi les sulfures de métaux de base, les silicates et les oxydes a reçu un grand intérêt à cause de leur importance pour comprendre des processus pétrogénétiques et pour leur grande valeur économique. A l'opposé, le comportement de nombreux éléments chalcophiles traces ont reçu moins d'attention. L'analyse de gouttelettes sulfurées de verre frais de MORB (Mid-Ocean-Ridge Basalts) par Laser Ablation-Induced Coupled Plasma-Mass Spectrometer (LA-ICP-MS) nous a permis de calculer de nouveaux coefficients de partage entre un liquide silicaté et un liquide sulfuré pour ces éléments

chalcophiles. Ceux-ci sont le Co (45 ± 4.1), Ni (776 ± 91), Cu (1334 ± 194), Zn (3.5 ± 0.79), Se (323 ± 41.7), Ag (1138 ± 219), Cd (107 ± 43), Sn (10.8 ± 1.45), Te (4791 ± 1195), Pb (57 ± 9) et le Bi (487 ± 84). Avec ces valeurs, il est possible de déterminer la contribution des sulfures au coefficient de partage global lors de la fusion partielle du manteau. Excepté pour le Cu et le Te, les éléments chalcophiles se comportent comme des éléments incompatibles pendant la fusion du manteau. Des coefficients de partage minimum pour les Éléments du Groupe du Platine (EGP) et le Re ont également été calculés. Le ratio Cu/Pd des gouttelettes sulfurées suggère qu'elles se sont formées dans la chambre magmatique à l'aplomb de la dorsale et qu'elles ont eu le temps de s'équilibrer avec le liquide silicaté. Les gouttelettes sulfurées de MORB ont des textures variant de grains fins de Solution Solide Monosulfurée (SSM) et de Solution Solide Intermédiaire (SSI) à de la SSM et de la SSI zonées. Les textures à grains fins sont caractéristiques d'un liquide sulfuré trempé tandis que les textures zonées sont caractéristiques d'une étape dans la cristallisation des sulfures après la cristallisation de la SSM et avant la cristallisation de la SSI. La distribution des éléments hautement sidérophiles et des éléments chalcophiles dans les gouttelettes sulfurées indique que le Ni, Co, Re et une partie du Pt et Pd partitionnent dans la SSM; tandis que le Cu, Zn, Ag, Cd, Sn, Te, Bi, Pb et le reste de Pt et Pd sont concentrés dans la SSI. Le Se est présent approximativement en quantité égale dans les deux phases sulfurées. Les gouttelettes sulfurées n'ont pas de Minéraux du Groupe du Platine (MGP) suggérant que l'exsolution est un processus majeur dans la formation de MGP observés dans des sulfures refroidis plus lentement.

Contributions des auteurs :

1^{er} auteur : Clifford Patten:

- Échantillonnage.
- Analyses pétrographiques, LA-ICP-MS, EOMA, MEB et traitement des données.
- Rédaction du manuscrit.

2^{ième} auteur : Sarah-Jane Barnes :

- Planification et direction du projet.
- Aide à la rédaction du manuscrit.
- Correction du manuscrit.

3^{ième} auteur : Edmond A. Mathez :

- Mise à disposition des échantillons.
- Correction du manuscrit.

4^{ième} auteur : Frances Jenner :

- Mise à disposition de données supplémentaires.
- Correction du manuscrit.

SIDEROPHILE AND CHALCOPHILE ELEMENTS DISTRIBUTION IN
 MORB SULPHIDE DROPLETS: DETERMINATION OF NEW
 SULPHIDE MELT-SILICATE MELT PARTITION COEFFICIENTS AND
 EARLY SULPHIDE CRYSTALLISATION HISTORY.

**CLIFFORD PATTEN¹, SARAH-JANE BARNES¹, EDMOND A. MATHEZ² AND
 FRANCES E. JENNER³.**

¹SCIENCES DE LA TERRE, UNIVERSITÉ DU QUÉBEC À CHICOUIMI, CHICOUTIMI, QC., G7H 2B1, CANADA

²DEPARTMENT OF EARTH & PLANETARY SCIENCES, AMERICAN MUSEUM OF NATURAL HISTORY, NEW YORK, NY 10024, UNITED STATES OF AMERICA

³CARNEGIE INSTITUTION OF WASHINGTON, WASHINGTON, DC 20015-1305, UNITED STATES OF AMERICA

ABSTRACT:

The distribution of the Highly Siderophile Elements (HSE: Ru, Rh, Pd, Re, Os, Ir, Pt and Au) among base-metal sulphides, oxides and silicate minerals has received a great deal of attention due to both their importance in understanding petrogenetic processes and their economic value. In contrast the behaviour of many minor and trace chalcophile elements has received less attention. Using Laser Ablation-Induced Coupled Plasma-Mass Spectrometer (LA-ICP-MS) on sulphide droplets in fresh Mid-Ocean-Ridge Basalts (MORB) glass has allowed us to calculate new partition coefficients for chalcophile elements. These are Co (45±4.1), Ni (776±91), Cu (1334±194), Zn (3.5±0.79), Se (323±41.7), Ag (1138±219), Cd (107±43), Sn (10.8±1.45), Te (4791±1195), Pb (57±9) and Bi (487±84). With these values it is possible to estimate the contribution of sulphide minerals to the bulk partition coefficient during mantle melting.

Except for Cu and Te, the chalcophile elements behave as moderately to strongly incompatible during mantle melting. Minimum partition coefficient for Platinum-Group Elements (PGE) and Re are also calculated. The Cu/Pd ratio of the sulphide droplets suggests that they form in the magma chamber beneath the mid-ocean ridge and have time to equilibrate with the silicate liquid. MORB sulphide droplets have texture ranging from fine-grained Monosulphide Solid Solution (Mss) and Intermediate Solid Solution (Iss) to zoned Mss and Iss. Fine-grained textures are characteristic of a quenched sulphide liquid whereas zoned textures are characteristic of a stage in sulphide crystallisation after Mss crystallisation and before Iss crystallisation. The distribution of the HSE and the chalcophile elements in the sulphide droplets show that the Ni, Co, Re and some of the Pt and Pd partition into Mss whereas the Cu, Zn, Ag, Cd, Sn, Te, Bi, Pb and the remaining of Pt and Pd are concentrated in the Iss. Selenium is present in approximately equal amounts in both. The sulphide droplets appear to be PGM free suggesting that exsolution is a major process in the formation of PGM observed in more slowly cooled sulphides.

KEY WORDS: highly siderophile elements, chalcophile elements, sulphide liquid, partition coefficient, sulphide crystallisation

INTRODUCTION:

It is commonly accepted that sulphide liquid and minerals play an important role in the chalcophile and siderophile elements behaviour during Ni-Cu-Platinum-Group Elements (PGE) ore deposit formations and in how the chalcophile and siderophile elements behave during mantle melting (*e.g.* Barnes & Lightfoot, 2005; Peach *et al.*, 1990; Rehkamper *et al.*, 1999; Bézos *et al.*, 2005).

The behaviour of chalcophile elements in the mantle is less well understood because their sulphide melt-silicate melt partition coefficients are poorly known. The partition coefficient, or Nerst partition coefficient, predicts the affinity of an element between two phases. Nickel and Co are controlled by the olivine in the mantle ($D^{\text{ol/melt}} \sim 10$ and $D^{\text{ol/melt}} \sim 2$, *e.g.* Irving, 1978); Sn, Zn, Cd, Ag and Bi behave as lithophile elements (*e.g.* Hertogen *et al.*, 1980; Yi *et al.*, 2000; Kamenetsky, *in press*); Cu and Te are controlled by the sulphides (*e.g.* Yi *et al.* 2000). The complimentary behaviour of Se, Cu and Ag in a range of MORB glasses (Jenner *et al.*, 2010), suggests that the partitioning behaviour of Ag and Se is controlled by mantle sulphides. Hart & Gaetani (2006) propose that the Pb is control by sulphides in the mantle. New sulphide melt-silicate melt partition coefficient values for these elements would allow a better understanding of the role of sulphides the in mantle.

Most models for of the formation of Ni-Cu-PGE ore deposit suggest that a sulphide liquid, segregated from a S-saturated silicate liquid, collect all the chalcophile and siderophile elements from the silicate liquid before accumulating and crystallizing (*e.g.* Naldrett & Duke, 1980). Depending on their ability to substitute for Fe, Ni or Cu the PGE

could be present in the form of solid solution in the sulphide minerals or they could be present as Platinum-Group Minerals (PGM). If PGM are formed they may represent exsolutions from the sulphide minerals (e.g. Barnes et al., 2008) or they may have crystallized from the sulphide liquid (Howell and McDonald, 2010; Dare et al., 2010).

Fresh Mid-Ocean-Ridge Basalt (MORB) glasses contain sulphides that have been quenched from ~1200°C to deep ocean temperature in few minutes (Moore, 1975). Thus, MORB glasses and their sulphide droplets provide a unique opportunity to investigate sulphide melt-silicate melt equilibrium and the possibility of PGM formation in quickly cooled sulphides. Sulphides occurrences in MORB are variable (Moore & Calk, 1971; Moore & Schilling, 1973; Yeats & Mathez 1976; Czamanske & Moore, 1977; Patten *et al.*, accepted). The most common sulphide occurrences are spherical sulphide droplets that formed before eruption and which are likely to have equilibrated with the silicate liquid (Mathez, 1976). They have textures varying from uniform fine-grained intergrowth of monosulphide solid solution (Mss) and intermediate solid solution (ISS) to zoned with one part containing subhedral massive Mss and the other quenched Iss (e.g. Mathez, 1976; Czamanske & Moore, 1977; Patten *et al.*, accepted). These textural differences are controlled by the undercooling of the sulphide droplets (Patten *et al.*, accepted).

Sulphide droplets have already been used to calculate some partition coefficients using Instrumental Neutron Activation Analysis (INAA) and Radiochemical Neutron Activation Analysis (RNAA) (Peach *et al.*, 1990). The Advent of Laser Ablation-Inductively Coupled Plasma-Mass Spectrometry (LA-ICP-MS) allows for the determination of a much larger group of elements at much better spatial resolutions than were available to previous workers.

In this study we have carried out LA-ICP-MS analyses, Electron-Probe-Micro Analyses (EPMA) and Scanning-Electron Microscope (SEM) analyses on sulphide droplets and on the fresh MORB glass surrounding them. The study has 3 objectives: 1) to determine the origin of sulphide droplets and their degree of equilibrium with their host glass, 2) to calculate the sulphide melt-silicate melt partition coefficients for the chalcophile elements Co, Ni, Cu, Zn, Se, Ag, Cd, Sn, Te, Pb and Bi (HSE partition coefficient are also estimated); and 3) to study the chalcophile and siderophile elements distribution among the sulphide phases of the sulphide.

SAMPLING AND ANALYTICAL METHOD:

The fresh MORB glasses are from dredges obtained by the Lamont Doherty Earth Observatory, Columbia University, New York. Of the twenty four samples selected for this study, eleven have sulphide droplets large enough for analyses. All samples came from glassy pillow rims erupted at depths greater than 1000m, which inhibited S outgassing (Mathez, 1976).

Bulk composition of the sulphide droplets were calculated using EPMA data coupled with Image Pro Plus Analysis 6.2 software (see Patten *et al.* (accepted) for details). The EPMA were carried out at Laval University, Quebec, using CAMECA SX-100. Glasses and sulphide droplets were analyzed with an accelerating voltage of 15kV, a beam of 5 μm and wave length dispersive current of 20 nA and a counting time of 20 sec. Astimex standards were used (see Patten *et al.* (accepted) for details). These settings are similar to those of Czamanske & Moore (1977), Wallace & Carmichael (1992) and Liu *et al.* (2007).

Analyses by LA-ICP-MS were carried out at the LabMaTer, Université du Québec à Chicoutimi (UQAC) using a New Wave Research 213-nm YAG UV laser coupled to a Thermo X7 ICP-MS. Data reduction was undertaken using the Plasma Lab software (Thermo Elemental). Analyses were carried out at 20 Hz, with a dwell time of 10ms/peak and a power of 0.3mJ/pulse. The beam diameters range from 50 to 110 μm depending on the sulphide droplet size; the beam was always larger than the analyzed sulphide droplet. Only sulphide droplets with diameter larger or close to 30 μm gave count rates sufficiently above the limit of detection.

Seven fine-grained and coarse-grained sulphide droplets and three zoned sulphide droplets, analysed by LA-ICP-MS, were used for the calculation. Sixty seconds of gas blank signal was collected before ablation. Laser ablation started in the glass at 100 μm from the sulphide droplet and the stage moved at 3 $\mu\text{m.s}^{-1}$ following a line crossing the sulphide droplet and stopping in the glass 100 μm on the other side of the droplet. Raster signal was used rather than local dot ablation for two reasons: 1) it gives results for the sulphide droplet and the surrounding glass in the same run and 2) it gives a stabilized signal of the sulphide droplet. The sulphide droplet signal contains a some glass signal. The real content of analysed elements in the sulphide droplet signal can be determined by:

$$E_{sulf} = E_{ICP\ sulf} - (E_{ICP\ glass} * \left(\frac{Cps\ Si\ sulf}{Cps\ Si\ glass} \right)) \quad [1]$$

with E_{sulf} the concentration of the element in the sulphide droplet, $E_{ICP\ sulf}$ the concentration of the element in the sulphide droplet signal, $E_{ICP\ glass}$ the concentration of the element in the glass signal, $Cps\ Si\ sulf$ the counts per second of silica in the sulphide

signal and *Cps Si glass* the counts per second of silica in the glass. After interference corrections, data were recalculated to 100% sulphide.

The ^{57}Fe was used as the internal standard; Fe concentration in the sulphide was estimated by the combining image analysis and microprobe data. However a similar correction to [1] is needed to calculate the real ^{57}Fe concentration in the sulphide droplet signal:

$$\%^{57}Fe \text{ int std} = \%^{57}Fe_{glass} * \left(\frac{Cps \text{ Si sulf}}{Cps \text{ Si glass}} \right) + \%^{57}Fe_{sulf} * \left(1 - \frac{Cps \text{ Si sulf}}{Cps \text{ Si glass}} \right) \quad [2]$$

with $^{57}Fe \text{ int std}$ the real ^{57}Fe percentage of the internal standard in the signal, $\%^{57}Fe_{glass}$ the percentage of ^{57}Fe in the glass and $\%^{57}Fe_{sulf}$ the percentage of ^{57}Fe in the sulphide.

The following isotopes were monitored ^{24}Mg , ^{29}Si , ^{33}S , ^{34}S , ^{44}Ca , ^{47}Ti , ^{53}Cr , ^{57}Fe , ^{59}Co , ^{60}Ni , ^{61}Ni , ^{63}Cu , ^{65}Cu , ^{66}Zn , ^{68}Zn , ^{75}As , ^{77}Se , ^{82}Se , ^{95}Mo , ^{99}Ru , ^{100}Ru , ^{101}Ru , ^{102}Ru , ^{103}Rh , ^{105}Pd , ^{106}Pd , ^{107}Ag , ^{108}Pd , ^{109}Ag , ^{111}Cd , ^{118}Sn , ^{121}Sb , ^{125}Te , ^{126}Te , ^{128}Te , ^{185}Re , ^{187}Re , ^{189}Os , ^{190}Os , ^{193}Ir , ^{194}Pt , ^{195}Pt , ^{197}Au , ^{208}Pb , ^{209}Bi .

Two reference materials were used to calibrate the laser data: Po727 T1 SRM, a synthetic pyrrhotite doped with 40ppm PGE and Au, supplied by the Memorial University of Newfoundland and MASS-1, a pressed pellet (Fe-Zn-Cu-S) doped with 50-70ppm As, Ag, Bi, Pb, Re, Sb, Se, Sn and Te supplied by the United States Geological Survey. Neither of these reference materials contain Ni or Re thus for these two elements an in-house reference material JB-MSS5, a synthetic FeS sulphide, was used. The values and reference material used to calibrate each elements are listed in Table 1. The accuracy of

the calibration was checked using JB-MSS5 for most elements (Table 2). NIST SRM-610 was used to check Co, Zn, Mo, Cd and Sn and for calibration of the silicate glass analyses (Table 2).

A PGE free Cu-wire was analyzed in order to determine the $^{65}Cu^{40}Ar$ interference for ^{105}Pd and the $^{63}Cu^{40}Ar$ interference for ^{103}Rh . The $^{60}Ni^{40}Ar$ interference for ^{100}Ru and the $^{61}Ni^{40}Ar$ interference for ^{101}Ru and ^{102}Ru were corrected with a PGE free NiS sulphide. The ^{106}Cd interferences for ^{106}Pd and the ^{108}Cd interferences for ^{108}Pd were determined with the Plasma Lab software.

Fresh glass rims of samples were crushed in an Al-ceramic mill at the UQAC for PGE whole rock analysis. They were determined by High Pressure Asher digestion-Isotope Dilution (HPA-ID) at the LabMaTer, UQAC using the techniques described in Savard *et al.* (2010). Results for the OKUM reference material agree with the certificate values.

RESULTS:

Sulphide droplets population:

Of the eleven samples that contain sulphide droplets five are from the East Pacific Rise and six are from the South Atlantic Ridge (sample locations are listed in Table 3). The MORB glasses have low-K tholeiite compositions (Table 3). Two samples are from seamounts and are slightly richer in TiO₂ and K₂O. Sulphur concentrations in the glass vary from 782 to 1530 ppm and show positive correlation with FeO* contents (Figure 1, Patten *et al.*, accepted). These sulphur concentrations are within the same range as those

reported in previous studies (*e.g.* Czamanske & Moore, 1977; Mathez, 1979; Jenner *et al.*, 2010). In the eleven samples of this study, over one hundred sulphide droplets ranging from few micrometers up to 110 μm were observed. Except for a few elliptical ones, all droplets are spherical. Only those with diameters larger than 10 μm were used in this study. The mean diameter of the sulphide droplets is 27 μm for the 85 droplets chosen.

Fresh MORB glass sulphide droplets exhibit a variety of textures which have been already described in other studies (*i.e.* Mathez, 1976; Czamanske & Moore, 1977; Patten *et al.*, accepted). For this study the droplets have been divided into three different groups (Patten *et al.*, accepted). 1) Fine-grained, perfectly spherical, sulphide droplets are composed of fine intergrowths of micrometric MSS and ISS. Pentlandite is present as narrow rims at the MSS-ISS interface. Iron-oxides are present as sub-micron grains randomly disseminated throughout the sulphide droplets (Fig. 1a). These droplets are interpreted to have undergone extreme undercooling before crystallisation (Patten *et al.*, accepted). 2) Coarse-grained sulphide droplets are also composed of MSS and ISS intergrowths similar to group 1 but with fewer and larger grains. They are almost perfectly spherical. The pentlandite forms thicker rims at the MSS-ISS interface and may occur as flame exsolutions in MSS. Oxide phases are present as micron-size grains (Fig. 1b). These textural features imply a lower degree of undercooling before crystallisation than experienced by the group 1 droplets (Patten *et al.*, accepted). 3) Zoned sulphide droplets have separate zone of spheroidal MSS and ISS. Two different textures of ISS are present. The most common is a fishbone texture with disseminated oxides (Fig. 1c). This texture can be interpreted as the quenched residual Cu-Fe rich sulphide liquid that

remained after the M_{ss} crystallisation. The other texture is subhedral I_{ss} containing euhedral oxide (Fig. 1d). Zoned droplets have spherical shapes but with a crenulated margins. The texture of pentlandite is similar to that of pentlandite in coarse-grained sulphide droplets but flame exsolutions in M_{ss} are more abundant. These textural differences can be account by the differences in undercooling before crystallization of the droplets Patten *et al.* (accepted).

The texture of the sulphide droplets is important when interpreting the LA-ICP-MS analyses. In fine-grained and coarse-grained sulphide droplets the HSE and chalcophile element distribution should be homogeneous at the scale of the droplet size. If this is the case, any section of one of these sulphide droplets is representative of the whole droplet and can be used to measure the chalcophile and siderophile elements concentrations. On the other hand, a particular section of a zoned sulphide droplet cannot be considered as representative of the whole droplet and should not be used to estimate the composition of the sulphide droplet. However, such droplets can be used to determine the distribution of the chalcophile and siderophile elements among the sulphide phases composing the droplets.

Table 4 lists the S-Fe-Ni-Cu bulk composition of the fine-grained and the coarse grained sulphide droplets. Details regarding these bulk compositions, which have been determined by EMPA, are given in Patten *et al.* (accepted). Sulphide droplets have low variability in S content 34.71% (standard deviation of the bulks S calculated ± 0.54). Fe, Ni and Cu content are more heterogeneous and have higher variability with respectively 44.59% (± 3.48), 9.54% (± 3.48) and 8.98% (± 3.51). Nickel and Cu concentrations in

droplets are controlled by the degree of fractionation of the melt; in fractionated basalts sulphide droplets are depleted in Ni and Cu (Czamanske & Moore; 1977).

LA-ICP-MS results for fine-grained and coarse-grained sulphide droplets:

Figure 2 shows the LA-ICP-MS traverses for chalcophile elements across the quenched sulphide droplets and the surrounding glass. The first 60s represent the gas blank. Glass signals are characterized by high Si and low S count rates and sulphide by low Si and high S count rates. The sulphide droplet signals have bell shapes because near the margins of the droplets the signal originates from both silicate and sulphide. The chalcophile elements present in the sulphide droplet also have a bell shape signal (Fig. 2) but with no peak characteristic of inclusions implying that these elements are in solid solution in the sulphide droplets.

Concentrations of chalcophile elements in the glasses and the sulphides determined by LA-ICP-MS are listed in Table 5. In sulphide droplets Ni and Cu concentrations are respectively $10.3 \pm 3.5\%$ and $8.7 \pm 2\%$, respectively similar to the range determined by EPMA. Cobalt concentrations are in the thousands of ppm range; Zn and Se are in the hundreds of ppm range; Ag, Cd, Te and Pb are in the tens of ppm range and Sn and Bi are in the ppm range. The Mo content of sulphide droplets is too close to detection limit to give reliable values, while As concentrations are variable, from ppm levels to below the detection limit. The variability in As value could be due to an O-Co interference that has not been corrected.

Highly siderophile elements concentrations are also given in Table 5. Palladium, Pt and Au are in the ppm range. Iridium, Os, Ru and Re concentrations are an order of

magnitude lower. Rhodium concentrations are usually below detection limit. All the HSE all have a bell shape signals similar to the S signal (Figure 3) and do not have peaks characteristics of inclusions. Prior to the laser study the droplets were inspected for PGM using a SEM and none were observed. Hence, it appears that, as for the chalcophile elements, the HSE exist in solid solution in the sulphide phases.

LA-ICP-MS results for the host glass:

The concentrations of the chalcophile and siderophile elements in the glass are much lower than in the sulphides droplets (Table 5). Nickel is in the hundreds of ppm range; Co, Cu and Zn are in the tens of ppm range; Ag, Cd, Sn, Sb and Pb are in the tens of ppb range and Se, Te and Bi could not be detected in all of the glasses. For comparison concentrations of these elements determined in other studies of MORB glasses (Yi *et al.*, 2000; Jenner *et al.*, 2012) are shown Appendix 1. The concentrations of the HSE are less than or too close to the detection levels in our glasses.

Partition coefficients:

For Co, Ni, Cu, Zn, Ag, Cd, Sn and Pb concentrations from both the glass and sulphide droplets are available (Table 5) and partition coefficients can be directly calculated from our data (Table 6). None of the elements show a correlation between the partition coefficient and the Mg# of the glass (Table 6). Thus, there does not appear to be a correlation between partition coefficients and degree of fractionation.

The Se, Te and Bi the concentrations in the glass were too low to be determined by our analytical methods. However, Yi *et al.* (2000) and Jenner *et al.* (2012) reports values for many of the chalcophile elements from MORB glasses with similar

compositions to our glasses. We have used the concentrations in their MORB glasses and our sulphide droplets to calculate partition coefficients (Table 7). There is good agreement between the partition coefficients we determined for Co, Ni, Cu, Zn, Ag, Sn, Cd and Pb and those we calculate using the glasses of Yi *et al.* (2000) or Jenner *et al.* (2012) and our sulphide droplets (Table 7) suggesting that using their glasses to estimate the Se, Te and Bi concentrations of our glasses is reasonable.

The Co, Ni and Cu partition coefficients are similar to previously published values (Table 7). Our Pb partition coefficient is somewhat higher ($D=57$) to a previously published value (Hart & Gaetani, 2006). Based on Ag/Cu ratios in MORB, Jenner *et al.* (2010) estimated that the partition coefficients for Ag should be similar to Cu. Indeed, the value we have determined for Ag (1138) is similar to the partition coefficient calculated for Cu (1334).

The Se partition coefficient values are in the range of 295-394 which are lower than those reported by Peach *et al.* (1990) of 1770, but overlap with the lower range recently determined by Brenan (personal communication as quote in Barnes *et al.*, 2008). The Te partition coefficient values are in the range of 4442-5107 and are similar to those of Brenan (personal communication as quote in Barnes *et al.*, 2008) but it is one order of magnitude lower than the estimate of Yi *et al.* (2000) based on the correlation between Cu and Te in MORB.

For Zn, Cd and Sn we are not aware of published values for these elements however the similarity of the Co, Ni and Cu partition coefficients to published values suggests to us that our method is valid and thus these values are reasonable.

For the PGE and Re minimum partition coefficients values can also be estimated using the whole rock values for each sample (Table 8). Table 9 shows that the PGE partition coefficients are in the range 5000 to 40000 and are similar to previously published values (e.g. Peach *et al.*, 1990; Fleet *et al.*, 1999). The Re partition coefficient is similar to that estimated for MORB by Brenan (2008) at \approx 400-800. However, these values have extremely high standard deviation and it must still be pointed out that the values are still minimum estimates because the whole rock values include the sulphide droplets.

LA-ICP-MS analyses of zoned sulphide droplets:

Four zoned sulphide droplets have been analyzed by LA-ICP-MS. Three of them have good zonation between the MSS and the ISS (Fig. 1c) and it was possible to reduce the data for both the sulphide phases separately. It was not possible to reduce separately the signals of the MSS and the ISS in the fourth zoned sulphide droplet (Cook D19 G1, Fig. 1d). Figure 4 shows time-resolved analytical profiles for two of the zoned sulphide droplets. The chalcophile have a smooth bell shape similar to S implying that they exist in solid solution in the sulphide phases. In the profiles, the MSS is characterized by the Ni-rich portion and the ISS by the Cu-rich portion (Figure 4). The Co signal mirrors that of the Ni and thus must be concentrated in the MSS, while signals of Zn, Ag, Sn, Cd, Te, Pb and Bi correlate with that of Cu, indicating that these elements are concentrated in the ISS. The Se does not show preference between the MSS and the ISS. These sulphide droplets were As and Mo free.

Figure 5 shows the profile of the same two sulphide droplets for the HSE. The HSE signals follow S and do not form peaks which would indicate the presence of PGM. Only the profiles for Pt, Pd, Au and Re are sufficiently robust for interpretation. Gold follows Cu and therefore must be concentrated in the Iss. Rhenium correlates with Ni and must be concentrated in the MSS, consistent with the data of Brenan (2002). Platinum and Pd do not show a particular preference for either MSS or Iss.

DISCUSSION:

The time required for a sulphide droplet to equilibrate with surrounding silicate liquid depends on the size of the droplet, the diffusivity of the elements in the silicate liquid and the partition coefficient (Mungall, 2005). During MORB genesis it is not clear when and where the sulphide droplets are formed. Mid-Ocean-Ridge Basalt magma forms by 10-20% mantle melting (Langmuir *et al.*, 1992) and is thought to be S-saturated at its source (Mavrogenes & O'Neill, 1999). However the decrease of pressure during the magma rising from the mantle source to the surface increases the Sulphur Content at Sulphide Saturation (SCSS) which would lead the magma to be sulphur under-saturated when it reaches the surface (Mavrogenes & O'Neill, 1999) and yet most MORB appears to be sulphur saturated. Thus some processes during MORB genesis must bring the magma to sulphide saturation.

MORB differentiation:

The sulphide droplets found in fresh MORB glass could form in the ridge magmatic chamber and transport to the ocean floor during eruption. Li and Ripley (2005) have calculated that only 10% of fractional crystallisation is needed to attain SCSS in

MORB magma chamber. Some sulphide droplets in fresh MORB glass are included inside plagioclase and olivine phenocrysts (Yeats & Mathez, 1976; Mathez, 1976; Danyushevsky *et al.*, 2002) implying that sulphur saturation occurred at the same time than those crystals formed.

Figure 6 shows the simulation of MORB fractional crystallisation and sulphide saturation. The degree of fractional crystallisation was determined using PELE v.7 (Boudreau, 1999) and the composition of the least fractionated glass sample (RC 28 02 7RD) as the initial composition. Simulation was made at 1.46×10^8 Pa for a magma chamber at 4km depth, at $fO_2 = QFM$ and with 0.2% H₂O. Based on their Mg# content, the samples experienced, at least, 15% to 35% fractional crystallisation. This simulation does not take in account the refilling of the magma chamber. Using the equation given by Li and Ripley (2005) to calculate the SCSS; up to 696 ppm sulphide can segregate from the magma after 33% fractional crystallisation (Fig. 6). Barnes and Lightfoot (2005) have demonstrated the utility of Cu/Pd to determine the sulphide segregation in magma. From the equation for Rayleigh fractionation equation:

$$Cf = Ci * F^{(\overline{D}_s - 1)} \quad [3]$$

where Cf is the concentration in the residual magma, Ci the initial concentration in the magma, F the weight fraction liquid remaining and \overline{D}_s the partition coefficient of the element into sulphide multiplied by the weight fraction sulphide in the cumulate. The Cu/Pd estimated in sulphides segregating during fractional segregation versus the Mg# content of the magma is shown in Fig. 7. The Cu/Pd is calculated for $D_{Pd} = 23000$ (Peach *et al.*, 1990) and for $D_{Pd} = 10000$ (this study). Actual Cu/Pd from LA-ICP-MS

analyses on sulphide droplets from the South Atlantic Ridge samples are also plotted. In the three sets of data, Cu/Pd increases in sulphides as fractional segregation occurs because $D_{Pd} \gg D_{Cu}$ ($D_{Cu} = 1334$, Table 7). The simulation shows the correlation with the values from the real sulphide droplets especially the one with the D_{Pd} of 10000. This correlation indicates that MORB sulphide droplets of this study have formed in the magma chamber before eruption and evolved by fractional segregation.

Sulphide droplets transport to the surface:

Using Stoke's law, the estimated settling speed of a sulphide droplets of 10 to 100 μm in a basaltic MORB is 6.46 to 646 cm.year^{-1} with the viscosity of the basalt at 117 Pa.s (Sato, 2005) and the density of the sulphide liquid of 4000Kg.m^{-3} (Ballhaus *et al.*, 2006). This speed is negligible compare to speed of magma rising at eruption which is in the order of meters per seconds (Schubert *et al.*, 2001). Considering the magmatic chamber at 1-4 km depth (Sinton *et al.* 1992) the pressure drop will be 0.29kb to 1.16kb during eruption which will have negligible effect on the SCSS allowing the melt to remain sulphide saturated (Mavrogenes & O'Neill, 1999). Sulphide droplets observed in this study are then likely to be a part of the sulphide liquid segregating in the magmatic chamber. In this case the mass transfer from the silicate liquid to the sulphide liquid would be high as it is more efficient in dynamic system such as magma rising (Mungall, 2005) leading faster to equilibrium state.

Quenching of sulphide droplets:

As described above, sulphide droplets in fresh MORB glass have different textures varying from fine-grained to zoned. One might expect that such textural

differences could arise from different times of formation of the sulphide droplets, with the droplets displaying zoned textures forming before eruption and those with fine-grained and coarse-grained textures during eruption. In this case quenched sulphide droplets may not have attained equilibrium with the surrounding silicate melt. We do not believe that sulphide droplets textural differences are related to the time of formation the sulphide droplets. Using PELE 7.3, the liquidus temperatures of the MORB glasses are in the 1250-1170°C range and M_{ss} liquidus in MORB sulphide droplet is estimated to be at 1100°C (Patten *et al.*, accepted) preventing the crystallisation of sulphide before eruption.

If fine and coarse-grained sulphide droplets had formed during or just before eruption one might expect that the sulphide droplet would absorb the chalcophile and siderophile elements in the vicinity and that the glass would therefore be depleted in these elements. Considering a sulphide droplet of 30 μm in diameter containing 0.21ppm Pd (RC 28 02 24rd gte1) forming from MORB magma with 2.1ppb Pd (Barnes & Lightfoot, 2005) the radius of the silicate volume from which the sulphide extracted the Pd to attain this concentration would be 1.5mm. For a similar size droplet containing 45.4 ppm Pd (RC 28 02 7rd gte1) the radius would be 32.4cm. Pd diffusivity in the magma is $\approx 9.5 \cdot 10^{-7} \text{ cm}^2 \cdot \text{s}^{-1}$ (Mungall, 2005) and quenching event is only few minutes long ($\approx 3\text{min}$, Moore, 1975) implying that Pd only had time to diffuse $\approx 1.7\mu\text{m}$ in the silicate liquid. Considering the same sulphide droplet with 10.25% Ni forming from MORB magma with 150ppm Ni the radius of the silicate volume needed to attain such concentration would be 9.8mm. Ni diffusivity is similar to Pd ($\approx 8.5 \cdot 10^{-7} \text{ cm}^2 \cdot \text{s}^{-1}$, Mungall, 2005) and would have time to diffuse only on $\approx 1.5\mu\text{m}$ during eruption. It appears that if the fine-grained and coarse-grained sulphide droplets were formed during

the quenching event they could never acquire the high concentrations in chalcophile and siderophile elements observed in this study. Therefore, the sulphide droplets analyzed in this study essentially equilibrated with the host magma.

Sulphide importance in the mantle:

The behaviour of an element during partial melting depends on the bulk partition coefficient between the silicate melt and the residuum. The bulk partition coefficient (\bar{D}) is defined by:

$$\bar{D} = \sum D_i X_i + D_j X_j + \dots$$

with \bar{D} the bulk partition coefficient, D_i the partition coefficient of the element in the mineral i , and X_i the weight fraction of the mineral i in the residuum. The quantity of sulphide minerals present in the mantle is very low: the S concentration of the mantle is ≈ 200 ppm (Palm & O'Neill, 2003) and is considered to be controlled by sulphides with $\approx 38\text{--}40\%$ S (Alard *et al.*, 2000) which in turn is $5.10^{-4} - 5.26.10^{-4}$ weight fraction sulphides. Thus in order for the sulphides to contribute significantly to the bulk partition coefficient the partition coefficient between sulphide melt and silicate melt has to be very high. The sulphide contributions to \bar{D} are summarized in Table 7. We consider that the conditions of pressure, temperature and oxygen fugacity at the eruption and during upper mantle melting are sufficiently close for the sulphide melt-silicate melt partition coefficients to be similar. The overall bulk partition coefficient also have a contribution from the residual mantle silicate phases (olivine and orthopyroxene) and spinels.

Cobalt, Ni and Zn are moderately to strongly compatible with most of the silicates and oxides present in the mantle (e.g Bedard, 2005; Bedard, 2007; Page *et al.*, 2009). Hence, as the silicates represent the largest fraction of minerals in the mantle, the Co, Ni and Zn are controlled by the silicates phases even though their concentrations in the sulphides are high.

For Ag, Sn, Pb and Bi the partition coefficient data base for the silicates is much more limited, but recent experimental work (Adams & Green, 2006) indicates that these elements are incompatible in silicate phases. Hart and Gaetani (2006) are in agreement with this conclusion stating that Pb is largely contained in sulphides in the mantle. The sulphide contribution to the bulk D for Pb and Sn is very low (0.03 and 0.01, Table 7) and thus they should behave as essentially incompatible elements. In contrast the high partition coefficients for Bi and Ag into sulphide liquid results in these elements being only moderately incompatible with a sulphide contribution to the bulk D of 0.26 and 0.60 respectively (Table 7).

There is a limited data base suggesting that Cu and Cd partition slightly into some silicate phases (Adam & Green, 2006). The high partition coefficient of Cu into sulphide liquid results in a contribution of 0.7 to the bulk D from the sulphides (Table 7) suggesting that, in addition to the contribution of silicates partition coefficient to the bulk D, the Cu behaves as a compatible element during melting. In contrast the contribution of sulphides to the bulk D of Cd is very low (0.06) and hence it might be expected to behave as an incompatible element.

There is no data on partitioning of Se and Te into mantle silicates known to the authors. The contribution of sulphides to the bulk D for both elements, and in particular for Te, is substantial (0.17 and 2.52). Tellurium might therefore be expected to behave as compatible element and Se as moderately incompatible.

Fractionation of the different chalcophile elements by retention of a sulphide phase during melting of the mantle is summarized in Figure 8. It shows the concentration factor of each chalcophile elements in the melt after 10% batch melting of the mantle using the sulphide contributions to the bulk D partition coefficient. Ce, which is an incompatible element in sulphide and which has a very low D for the other phases, is used to illustrate the behaviour of incompatible elements and has an enrichment factor of 10. Zn and Sn have enrichment factors of 9.8 and 9.5 respectively indicating incompatible behaviour. The concentration factors decrease from Co to Te down by a factor 0.4 relative to Ce indicating an increasing compatible behaviour. In the mantle, sulphides poorly control the chalcophile elements (except those with high partition coefficient), but they have a great impact on the variation of the ratios of these elements during mantle melting.

The fractionation between these different elements might be slightly different than that expected from Figure 8 during actual mantle melting. The partition coefficients used for this pattern are the ones calculated from a sulphide melt and a silicate but during mantle melting sulphides are not homogenous phases. Alard *et al.* (2000) showed that mantle derived rock contain different type of sulphides classified in two groups which could behave differently during mantle melting.

Crystallisation of a sulphide liquid:

Figure 9 summarizes the behaviour of the chalcophile and the highly siderophile elements in the first stages of sulphide differentiation. Before the crystallization of the MSS, as represented by the fine- and coarse-grained droplets, all of the elements are homogeneously distributed in the sulphide liquid and there is no evidence of PGM by neither LA-ICP-MS nor SEM analyses. Thus no crystallization or exsolution of PGM is expected to occur at this stage.

The analyzed zoned sulphide droplets are composed of massive MSS and quenched ISS with fishbone texture. Such texture is representative of the stage after MSS crystallisation and before ISS crystallisation. The data clearly show that Ni, Co and Re partition into MSS and Cu, Zn, Cd, Sn, Ag, Te, Au, Pb and Bi partition into the quenched ISS (Fig. 9). The signals for Ir, Os, Ru and Rh are too poor to determine their distribution within the differentiated sulphide droplets but they are likely to be present in solid solution in the MSS as they have $D_{\text{MSS}}^{\text{sulfide liquid}} \geq 1$ (Fleet *et al.*, 1993). Given that the partition coefficient for Pt and Pd into MSS are ≈ 0.2 (Fleet *et al.*, 1993) it is surprising that Pt and Pd do not show a preference toward the ISS. However, the profiles for Au, Pt and Pd indicate that $D_{\text{Pd}}^{\text{MSS}} \approx D_{\text{Pt}}^{\text{MSS}} > D_{\text{Au}}^{\text{MSS}}$.

Zoned sulphide droplets are also PGM free, implying that although these sulphide droplets have sustained lower undercooling rates there is little evidence for the formation of PGM by crystallisation from a late residual sulphide liquid or by exsolution from the sulphide phases.

The *in situ* analyses of MORB sulphide droplets confirms the previous patterns about the behaviour of chalcophile and siderophile elements at high temperature during the early stages of sulphide crystallisation ($>850^{\circ}\text{C}$, before the ISS crystallisation), which has not previously been observed *in situ* before. Moreover, the rapidly cooled MORB sulphide droplets appear to be PGM free supporting the idea that many of PGM observed in more slowly cooled sulphides are the product of exsolution (e.g. sulphide blebs in Noril'sk, Russia; Barnes *et al.* 2006).

CONCLUSIONS:

The analyses of MORB sulphide droplets by LA-ICP-MS lead to the following conclusions: 1) MORB sulphide droplets have a chemical composition similar to the sulphides segregating during low-pressure fractional crystallization in a magma chamber prior to eruption. It implies sufficient time for the sulphide droplets to maintain equilibrium with their host magma. 2) As sulphide droplets are close to the equilibrium state, partition coefficients for Co, Ni, Cu, Zn, Se, Ag, Cd, Sn, Te, Pb and Bi have been calculated. Minimum partition coefficients for PGE have also been estimated. 3) Using these values we calculate the contribution of the sulphides to the \bar{D} in the mantle. Sulphides have a great importance on the variation of the fractionation of the elements during melting; *i.e.* the variation of the ratios. 4) Fine-grained and coarse-grained sulphide droplets are representative of the sulphide liquid before the MSS crystallisation. Zoned sulphide droplets are representative of the stage after the MSS crystallisation and before the ISS crystallisation. 5) Distribution of chalcophile and the HSE in MORB sulphide droplets allow us to determine their behaviour in the earliest stages of sulphide differentiation. The MSS integrates Ni, Co, Re and part of the Pt and Pd at high temperature. The quenched ISS is enriched in Cu, Zn, Cd, Ag, Sn, Te, Bi, Au and the rest of the Pt and Pd. Se partitions approximately evenly between the MSS and the quenched ISS. 6) The MORB sulphide droplets appear to be PGM free. The high undercooling rates sustained during the quenching event did not allow the PGM exsolution during sulphide crystallisation.

ACKNOWLEDGMENTS:

The Lamont Doherty Earth observatory of the Columbia University is thanked for allowing sampling fresh glass from dredges collection. Sarah Dare and Philippe Page are thanked for the useful comments. George Lozefski (LDEO) for his assistance in sampling; Dany Savard (UQAC) for assistance in whole rock analysis and in situ LA-ICP-MS analyses; Marc Choquette (Laval University) for assistance in EPAM and SEM analyses. This work was funded by the Canadian Research Chair in Magmatic Ore Deposit.

REFERENCES:

- Adam, J., & Green, T. (2006). Trace element partitioning between mica- and amphibole-bearing garnet lherzolite and hydrous basanitic melt: 1. Experimental results and the investigation of controls on partitioning behaviour. *Contributions to Mineralogy and Petrology* **152**, 1-17.
- Alard, O., Griffin, W. L., Lorand, J. P., Jackson, S. E., & O'Reilly, S. Y. (2000). Non-chondritic distribution of the highly siderophile elements in mantle sulphides. *Nature* **407**, 891-894.
- Ballhaus, C., Bockrath, C., Wohlgemuth-Ueberwasser, C., Laurenz, V., & Berndt, J. (2006). Fractionation of the noble metals by physical processes. *Contributions to Mineralogy and Petrology* **152**, 667-684.
- Barnes, S. J., & Lightfoot, P. C. (2005). Formation of magmatic nickel-sulphide ore deposits and processes affecting their copper and platinum-group element contents. *Economic Geology 100th Anniversary Volume* 179-213.
- Barnes, S. J., Cox, R. A., & Zientek, M. L. (2006). Platinum-group element, gold, silver and base metal distribution in compositionally zoned sulphide droplets from the Medvezky Creek Mine, Noril'sk, Russia. *Contributions to Mineralogy and Petrology* **152**, 187-200.
- Barnes, S.-J., Prichard, H. M., Cox, R. A., Fisher, P. C., & Godel, B. (2008). The location of the chalcophile and siderophile elements in platinum-group element ore deposits (a textural, microbeam and whole rock geochemical study): Implications for the formation of the deposits. *Chemical Geology* **248**, 295-317.
- Bedard, J. H. (2005). Partitioning coefficients between olivine and silicate melts. *Lithos* **83**, 394-419.
- Bedard, J. H. (2007). Trace element partitioning coefficients between silicate melts and orthopyroxene: Parameterizations of D variations. *Chemical Geology* **244**, 263-303.
- Bezos, A., Lorand, J. P., Humler, E., & Gros, M. (2005). Platinum-group element systematics in Mid-Oceanic Ridge basaltic glasses from the Pacific, Atlantic, and Indian Oceans. *Geochimica et Cosmochimica Acta* **69**, 2613-2627.
- Boudreau, A. E. (1999). PELE — a version of the MELTS software program for the PC platform. *Computers & Geosciences* **25**, 201–203.
- Brenan, J. M. (2002). Re-Os fractionation in magmatic sulphide melt by monosulphide solid solution. *Earth and Planetary Science Letters* **199**, 257-268.
- Brenan, J. M. (2008). Re–Os fractionation by sulphide melt–silicate melt partitioning: A new spin. *Chemical Geology* **248**, 140-165.

- Cabri, L.J. (2002). The platinum group minerals. *Canadian Institute of Mining, Metallurgy and Petroleum, Special Volume 54*, 13-129.
- Chou , C.-L. (1978). Fractionation of siderophile elements in the earth's upper mantle. *Proceedings Of The 9th Lunar And Planetary Science Conference 1*, 219-230.
- Czamanske, G. K., & Moore, J. G. (1977). Composition and phase chemistry of sulphide globules in basalt from the Mid-Atlantic Ridge rift valley near 37°N lat. *Geological Society of America Bulletin 88*, 587-599.
- Danyushevsky, L. V., McNeill, A. W., & Sobolev, A. V. (2002). Experimental and petrological studies of melt inclusions in phenocrysts from mantle-derived magmas: an overview of techniques, advantages and complications. *Chemical Geology 183*, 5-24.
- Dare, S., Barnes, S.-J., & Prichard, H. (2010). The distribution of platinum group elements (PGE) and other chalcophile elements among sulphides from the Creighton Ni–Cu–PGE sulphide deposit, Sudbury, Canada, and the origin of palladium in pentlandite. *Mineralium Deposita 45*, 765-793.
- Dare, S., Barnes, S.-J., Prichard, H., & Fisher, P. (2011). Chalcophile and platinum-group element (PGE) concentrations in the sulphide minerals from the McCreedy East deposit, Sudbury, Canada, and the origin of PGE in pyrite. *Mineralium Deposita 46*, 381-407.
- Ebel, D. S., & Naldrett, A. J. (1997). Crystallisation of sulphide liquids and the interpretation of ore composition. *Canadian Journal of Earth Sciences 34*, 352-365.
- Fleet, M. E., Chryssoulis, S. L., Stone, W. E., & Weisener, C. G. (1993). Partitioning of platinum-group elements and au in the Fe-Ni-Cu-S system - experiments on the fractional crystallization of sulfide melt. *Contributions to Mineralogy and Petrology 115*, 36-44.
- Fleet, M. E., Crocket, J. H., Liu, M., & Stone, W. E. (1999). Laboratory partitioning of platinum-group elements (PGE) and gold with application to magmatic sulphide–PGE deposits. *Lithos 47*, 127-142.
- Francis, R. D. (1990). Sulfide globules in mid-ocean ridge basalts (MORB), and the effect of oxygen abundance in Fe-S-O liquids on the ability of those liquids to partition metals from MORB and komatiite magmas. *Chemical Geology 85*, 199-213.
- Gaetani, G. A., & Groves, T. L. (1997). Partitioning of moderately siderophile elements among olivine, silicate melt, and sulfide melt: Constraints on core formation in the Earth and Mars. *Geochimica et Cosmochimica Acta 61*, 1829-1846.

- Godel, B., & Barnes, S.-J. (2008). Platinum-group elements in sulphide minerals and the whole rocks of the J-M Reef (Stillwater Complex): Implication for the formation of the reef. *Chemical Geology* **248**, 272-294.
- Hart, S. R., & Dunn, T. (1993). Experimental cpx/melt partitioning of 24 trace elements. *Contributions to Mineralogy and Petrology* **113**, 1-8.
- Hart, S., & Gaetani, G. (2006). Mantle Pb paradoxes: the sulphide solution. *Contributions to Mineralogy and Petrology* **152**, 295-308.
- Hertogen, J., Janssens, M. J., & Palme, H. (1980). Trace elements in ocean ridge basalt glasses: implications for fractionations during mantle evolution and petrogenesis. *Geochimica et Cosmochimica Acta* **44**, 2125-2143.
- Holwell, D. A., & McDonald, I. (2010). A review of the behaviour of platinum group elements within natural magmatic sulphide ore systems. *Platinum Metals Review* **54**, 26-36.
- Horn, I., Foley, S. F., Jackson, S. E., & Jenner, G. A. (1994). Experimentally determined partitioning of high field strength- and selected transition elements between spinel and basaltic melt. *Chemical Geology* **117**, 193-218.
- Irving, A. J. (1978). A review of experimental studies of crystal/liquid trace element partitioning. *Geochimica et Cosmochimica Acta* **42**, 743-770.
- Jenner, F. E., O'Neill, H. S. C., Arculus, R. J., & Mavrogenes, J. A. (2010). The magnetite crisis in the evolution of arc-related magmas and the initial concentration of Au, Ag and Cu. *Journal of Petrology* **51**, 2445-2464.
- Jenner, F. E., & O'Neill, H. S. (2012). Analysis of 60 elements in 616 ocean floor basaltic glasses. *Geochemistry Geophysics Geosystems* **13**.
- Kamenetsky, V. S., & Eggins, S. M. (in press). Systematics of metals, metalloids, and volatiles in MORB melts: effects of partial melting, crystal fractionation and degassing (a case study of Macquarie Island glasses). *Chemical Geology*.
- Langmuir, C. H., Klein, E. M., & Plank, T. (1992). Petrological systematics of mid ocean ridge basalts - constraints on melt generation beneath ocean ridges. In J. P. Morgan, D. K. Blackman & J. M. Sinton (Eds.), *Mantle Flow and Melt Generation at Mid-Ocean Ridges* **71**, 183-280.
- Li, C., & Ripley, E. (2005). Empirical equations to predict the sulfur content of mafic magmas at sulphide saturation and applications to magmatic sulphide deposits. *Mineralium Deposita* **40**, 218-230.

- Liu, Y., Samaha, N.-T., & Baker, D. R. (2007). Sulfur concentration at sulphide saturation (SCSS) in magmatic silicate melts. *Geochimica et Cosmochimica Acta* **71**, 1783-1799.
- Lorand, J.-P., Luguet, A., Alard, O., Bezios, A., & Meisel, T. (2008). Abundance and distribution of platinum-group elements in orogenic lherzolites; a case study in a Fontete Rouge lherzolite (French Pyrénées). *Chemical Geology* **248**, 174-194.
- Lorand, J.-P., Alard, O., & Luguet, A. (2010). Platinum-group element micronuggets and refertilization process in Lherz orogenic peridotite (northeastern Pyrenees, France). *Earth and Planetary Science Letters* **289**, 298-310.
- Maaløe, S., & Aoki, K.-I. (1977). The major element composition of the upper mantle estimated from the composition of lherzolites. *Contributions to Mineralogy and Petrology*, **63**, 161-173.
- Mathez, E. A. (1976). Sulfur solubility and magmatic sulphides in submarine basalt glass. *Journal of Geophysical Research* **81**, 4269-4276.
- Mathez, E. A. & Yeats, R. S. (1976). Magmatic sulphides in basalt glass from dsdp hole 319a and site 320, Nazca plate. *Initial Reports of the Deep-Sea Drilling Project* **34**, 363-373.
- Mathez, E. A. (1979). Sulphide relations in hole 418a flows and sulfur contents of glasses. *Initial reports of the Deep Sea Drilling Project* **51**, 1069-1085.
- Mavrogenes, J. A., & O'Neill, H. S. C. (1999). The relative effects of pressure, temperature and oxygen fugacity on the solubility of sulphide in mafic magmas. *Geochimica et Cosmochimica Acta*, **63**, 1173-1180.
- Mitchell, R. H., & Keays, R. R. (1981). Abundance and distribution of gold, palladium and iridium in some spinel and garnet lherzolites: implications for the nature and origin of precious metal-rich intergranular components in the upper mantle. *Geochimica et Cosmochimica Acta* **45**, 2425-2442.
- Moore, J. G. (1975). Mechanism of formation of pillow lava: pillow lava, produced as fluid lava cools underwater, is the most abundant volcanic rock on earth, but only recently have divers observed it forming. *American Scientist* **63**, 269-277.
- Moore, J. G., and L. C. Calk. (1971). Sulphide spherules in vesicles of dredge pillow basalt. *American Mineralogist* **56**, 476-488.
- Moore, J. G., & Schilling, J. (1973). Vesicles, water, and sulfur in Reykjanes Ridge basalts. *Contributions to Mineralogy and Petrology* **41**, 105-118.
- Mungall, J. E. (2002). Kinetic controls on the partitioning of trace elements between silicate and sulphide liquids. *Journal of Petrology* **43**, 749-768.

- Naldrett, A. J., & Duke, J. M. (1980). Platinum metals magmatic sulphide ores. *Science* **208**, 1417-1424.
- Palme, H., & O'Neill, H. S. C. (2007). 2.01 - Cosmochemical estimates of mantle composition. In D. H. Editors-in-Chief: Heinrich & K. T. Karl (Eds.), *Treatise on Geochemistry*, 1-38.
- Page, P., & Barnes, S.-J. (2009). Using trace elements in chromites to constrain the origin of podiform chromitites in the Thetford mines ophiolite, Québec, Canada. *Economic Geology* **104**, 997-1018.
- Patten, C., Barnes, S.-J., Mathez, E. A. (accepted). Textural variations in MORB sulfide droplets caused by differences in crystallization history. *The Canadian Mineralogist*.
- Peach, C. L., Mathez, E. A., & Keays, R. R. (1990). Sulphide melt silicate melt distribution coefficients for noble-metals and other chalcophile elements as deduced from MORB - implications for partial melting. *Geochimica et Cosmochimica Acta* **54**, 3379-3389.
- Peregoedova, A., Barnes, S.-J., & Baker, D. R. (2004). The formation of Pt-Ir alloys and Cu-Pd-rich sulphide melts by partial desulfurization of Fe-Ni-Cu sulphides: results of experiments and implications for natural systems. *Chemical Geology* **208**, 247-264.
- Prichard, H. M., Hutchinson, D., & Fisher, P. C. (2004). Petrology and crystallisation history of multiphase sulphide droplets in a Mafic Dike from Uruguay: Implications for the origin of Cu-Ni-PGE sulphide deposits. *Economic Geology and the Bulletin of the Society of Economic Geologists* **99**, 365-376.
- Rajamani, V., & Naldrett, A. J. (1978). Partitioning of Fe, Co, Ni, and Cu between sulfide liquid and basaltic melts and the composition of Ni-Cu sulfide deposits. *Economic Geolog*, **73**, 82-93.
- Rehkämper, M., Halliday, A. N., Fitton, J. G., Lee, D. C., Wieneke, M., & Arndt, N. T. (1999). Ir, Ru, Pt, and Pd in basalts and komatiites: new constraints for the geochemical behaviour of the platinum-group elements in the mantle. *Geochimica et Cosmochimica Acta* **63**, 3915-3934.
- Sato, H. (2005). Viscosity measurement of subliquidus magmas: 1707 basalt of Fuji volcano. *Journal of Mineralogical and Petrological Sciences* **100**, 133-142.
- Savard, D., Barnes, S.-J., & Meisel, T. (2010). Comparison between nickel-sulfur fire assay Te Co-precipitation and isotope dilution with high-pressure ashing acid digestion for the determination of Platinum-Group Elements, Rhenium and Gold. *Geostandards and Geoanalytical Research* **34**, 281-291.

- Schubert, G., Turcotte, D. L., & Olson, P. (2001). Mantle convection in the earth and planets. *Cambridge University Press, Cambridge*, 940p.
- Sinton, J. M., & Detrick, R. S. (1992). Mid ocean ridge magma chambers. *Journal of Geophysical Research-Solid Earth* **97**, 197-216.
- Wallace, P., & Carmichael, I. S. E. (1992). Sulfur in basaltic magmas. *Geochimica et Cosmochimica Acta*, **56**, 1863-1874.
- Wilson, S. A., Ridley, W. I., & Koenig, A. E. (2002). Development of sulphide calibration standards for the laser ablation inductively-coupled plasma mass spectrometry technique. *Journal of Analytical Atomic Spectrometry*, **17**, 406-409.
- Yeats, R. S., & Mathez, E. A. (1976). Decorated vesicles in deep-sea basalt glass, eastern pacific. *Journal Geophysical Research* **81**, 4277-4284.
- Yi, W., Halliday, A. N., Alt, J. C., Lee, D. C., Rehkamper, M., Garcia, M. O., Su, Y. J. (2000). Cadmium, indium, tin, tellurium, and sulfur in oceanic basalts: Implications for chalcophile element fractionation in the Earth. *Journal of Geophysical Research-Solid Earth* **105**, 23761-23761.

FIGURE CAPTIONS:

Figure 1:

Sulphide droplet textures. A) Fine-grained texture composed of a micrometric intergrowth of MSS and ISS; note the perfect spherical shape. Pentlandite is not present in this droplet. B) Coarse-grained texture with coarse MSS-ISS intergrowth. Pentlandite is present at the MSS-ISS interface. C) Zoned texture with massive MSS and quenched ISS with fishbone texture. Pentlandite is present at the MSS-ISS interface and as exsolution in the MSS. D) Zoned texture with massive MSS and ISS. Note the euhedral magnetite grains. Pentlandite is present at the MSS-ISS interface and as exsolution in the MSS.

Figure 2:

LA-ICP-MS signals for chalcophile elements from fine-grained and coarse-grained sulphide droplets. The glass signal is characterized by high Si signal and low S signal. The sulphide droplets signals are characterized by the zones where S signal increases as bell shape.

Figure 3:

LA-ICP-MS signals for highly siderophile elements from fine-grained and coarse-grained sulphide droplets. The sulphide droplets are the same that Fig. 2. Highly siderophile elements signal are above detection limits only in the sulphide droplets signals.

Figure 4:

LA-ICP-MS signals for chalcophile elements from zoned sulphide droplets. The Ni-rich portion corresponds to the MSS and the Cu-rich portion to the ISS. The MSS signal is Ni-rich relatively to Cu. The chalcophile elements have bell shapes similar to the Ni or the Cu.

Figure 5:

LA-ICP-MS signals for HSE elements from zoned sulphide droplets. The sulphide droplets are the same that Fig. 4. The HSE have signals similar to Ni and Cu. The Ni-rich portion corresponds to the MSS and the Cu-rich portion to the ISS. The sulphide droplet RC 02 18rd G1 is Ir, Os, Ru and Rh free and their signals are not shown.

Figure 6:

Simulation of the variation of the degree of the fractional crystallisation, the SCSS and the amount of sulphide segregating in the magma chamber using PELE v.7. The crosses represent the degree of fractional crystallisation in percent. The open circles represent the sulphides segregated in ppm. The open squares represent the SCSS in ppm.

Figure 7:

Variation of the Pd/Cu depending on the Mg#. Open circles with solid line represent the Cu/Pd in sulphide simulated with $D_{Pd}=23000$ (Peach *et al.*). With a lower Pd partition coefficient ($D_{Pd} = 10000$) the simulation (open triangle with dash line) is closer to the real concentrations of sulphide droplets analyzed in this study (filled squares).

Figure 8:

Fractionation of HSE and chalcophile elements during 10% of sulphide mantle melting. Cerium is used as an incompatible and has an enrichment factor of 10. Zn and Sn are poorly retained by sulphides. Co, Pb and Cd are moderately retained in sulphides and Se, Bi, Ni, Ag, Cu and Te are strongly retained in sulphides.

Figure 9:

Early stages of sulphide crystallisation pattern showing the repartition of HSE and chalcophile elements. The parameters that control textural differences of the sulphide are developed in Patten et al., (accepted).

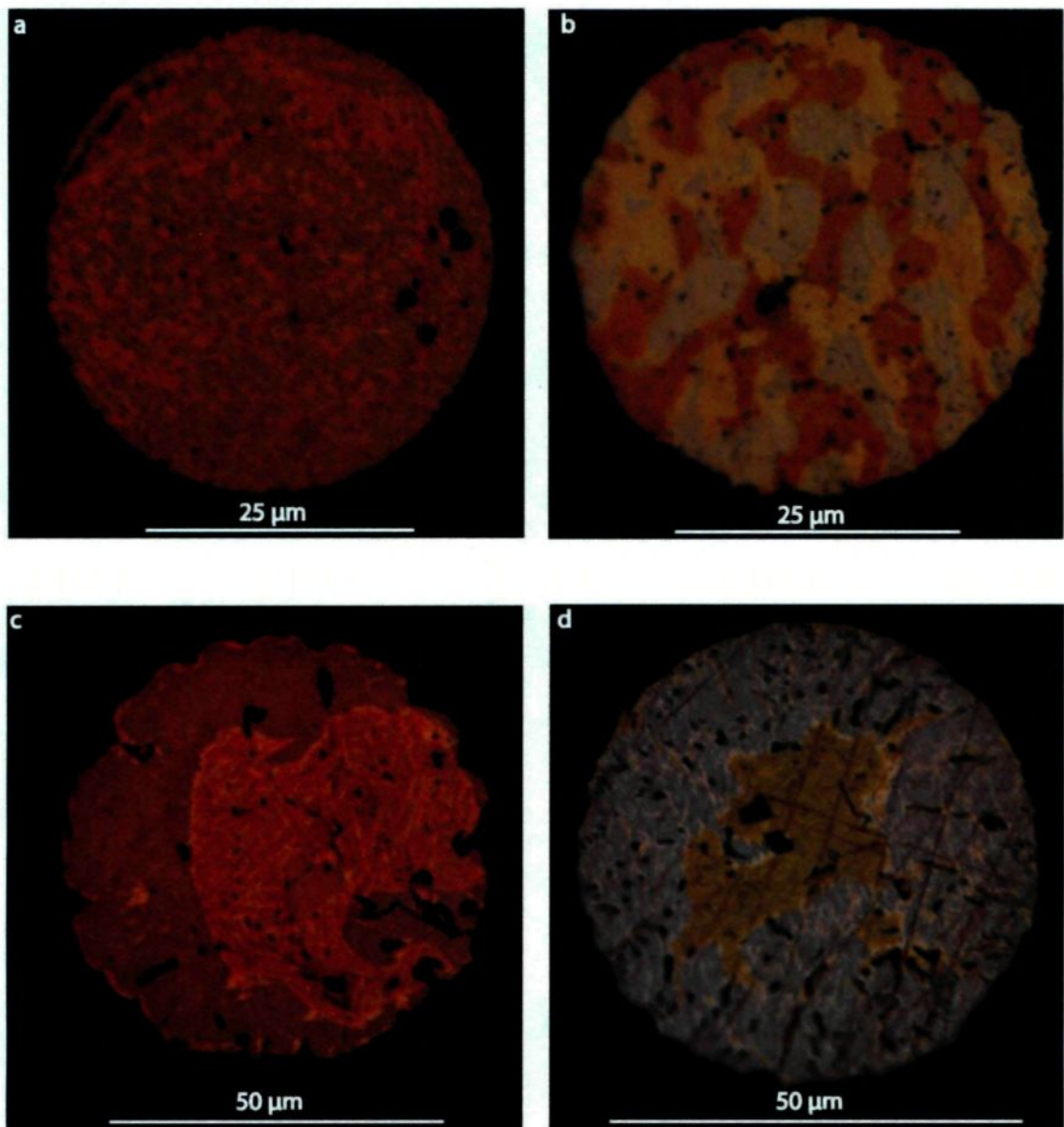


Figure 1.

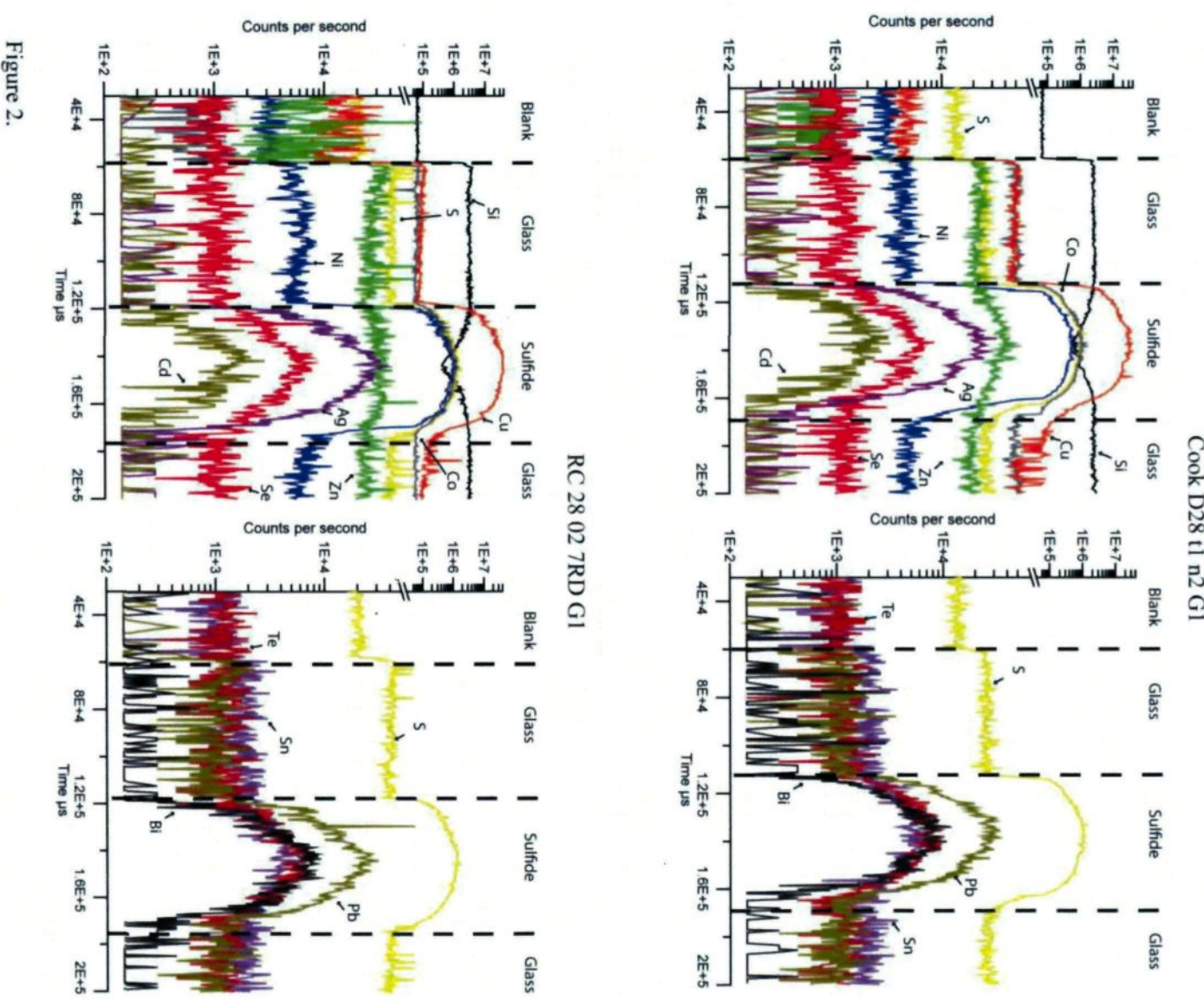


Figure 2.

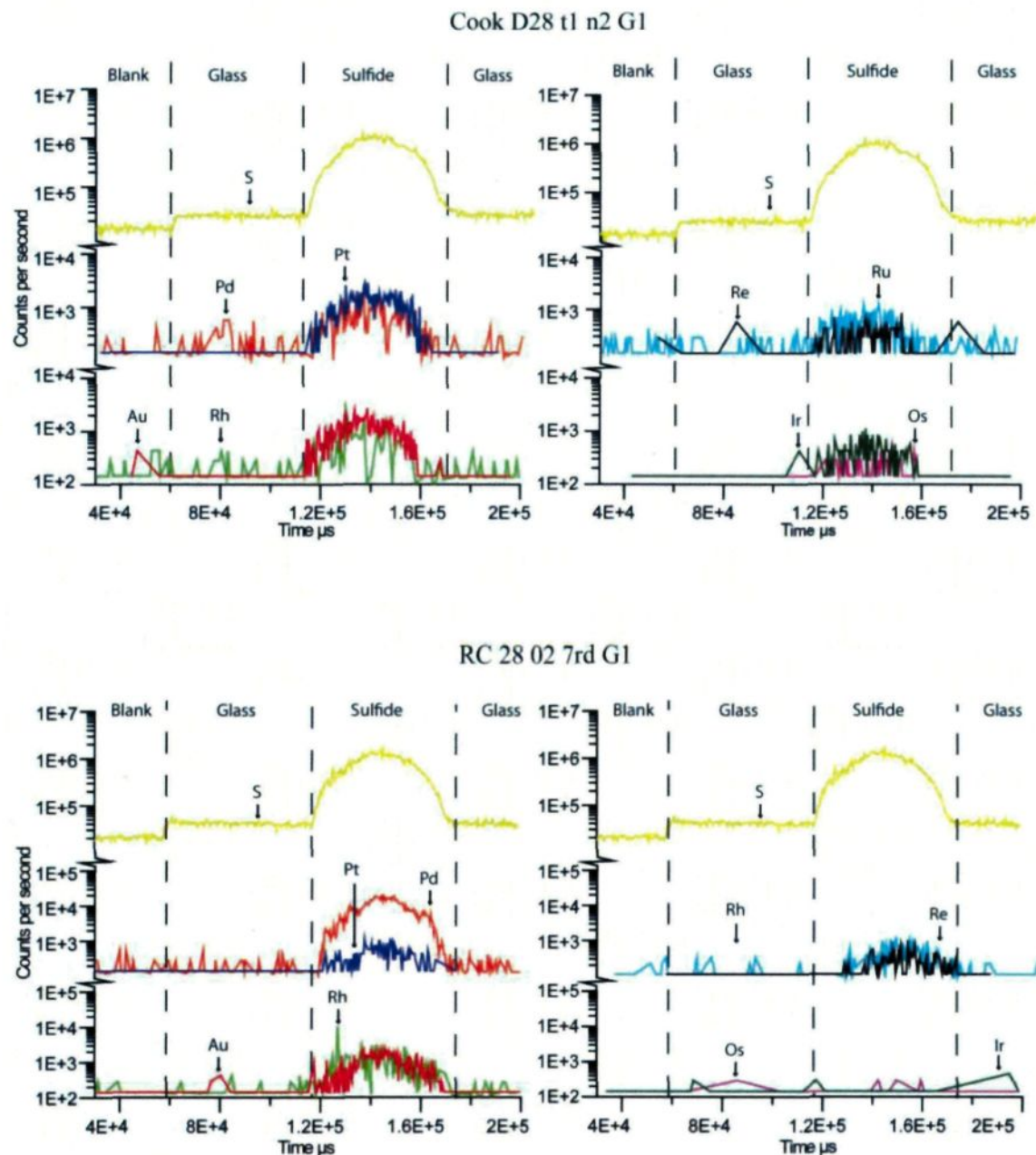


Figure 3.

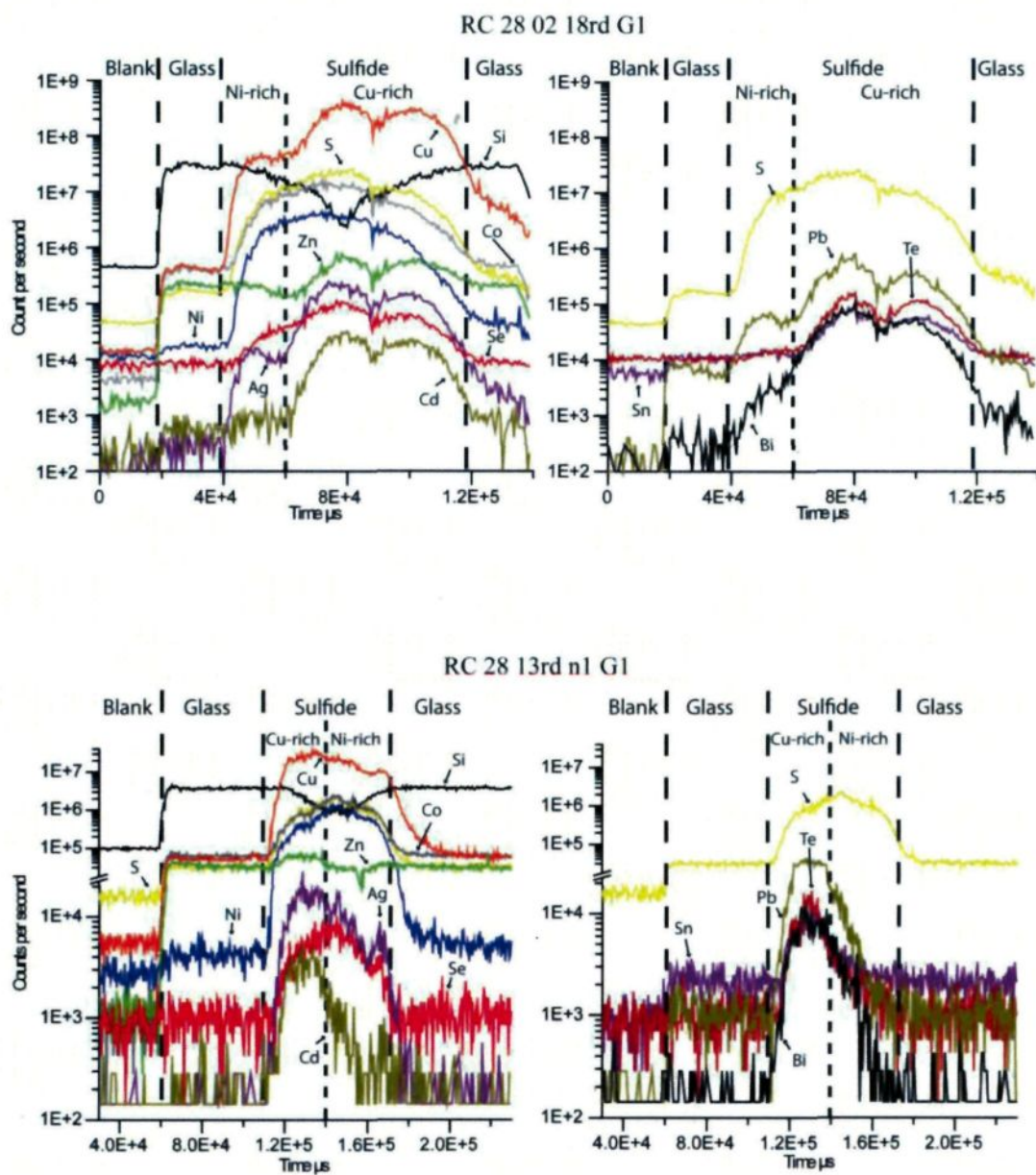


Figure 4.

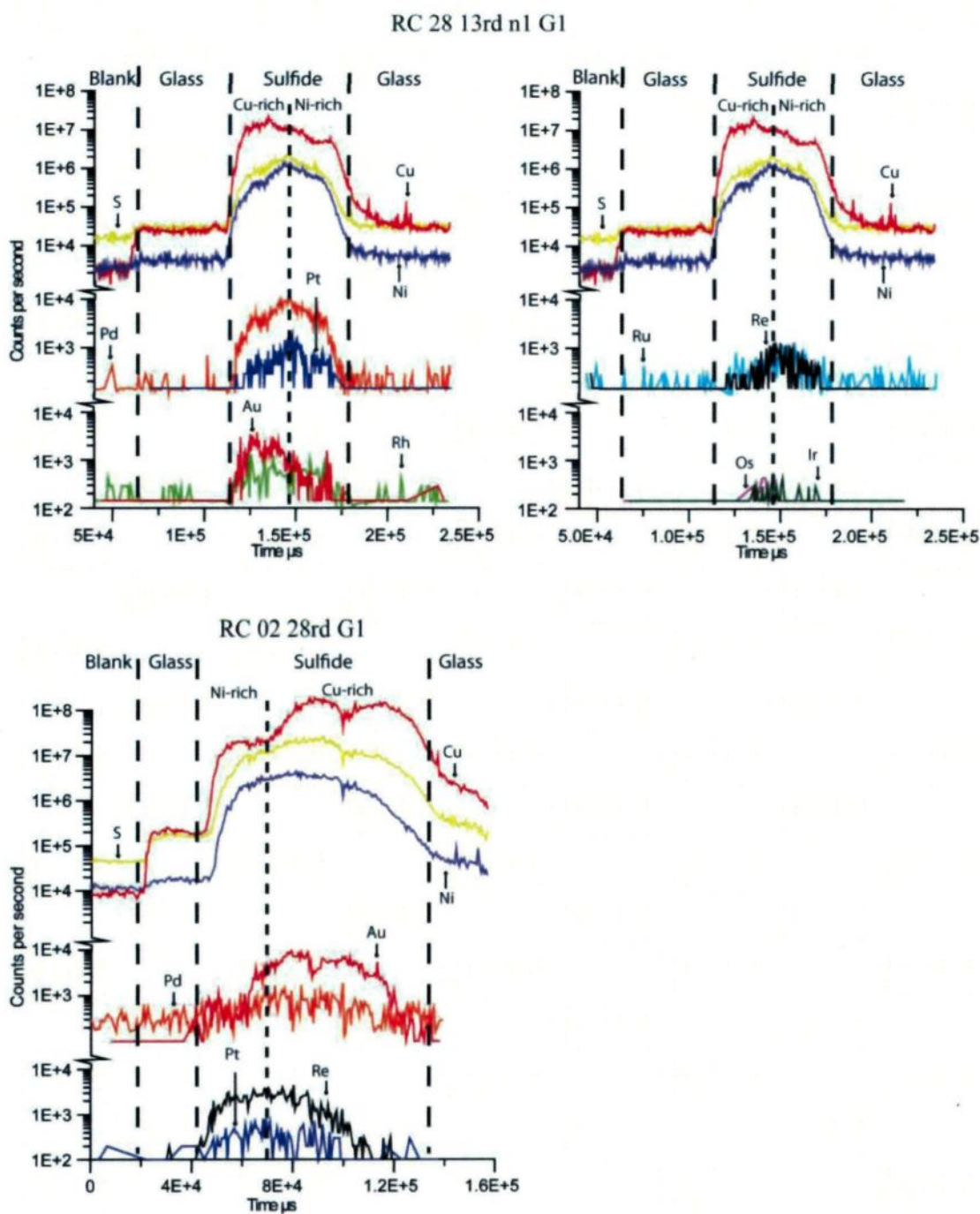


Figure 5.

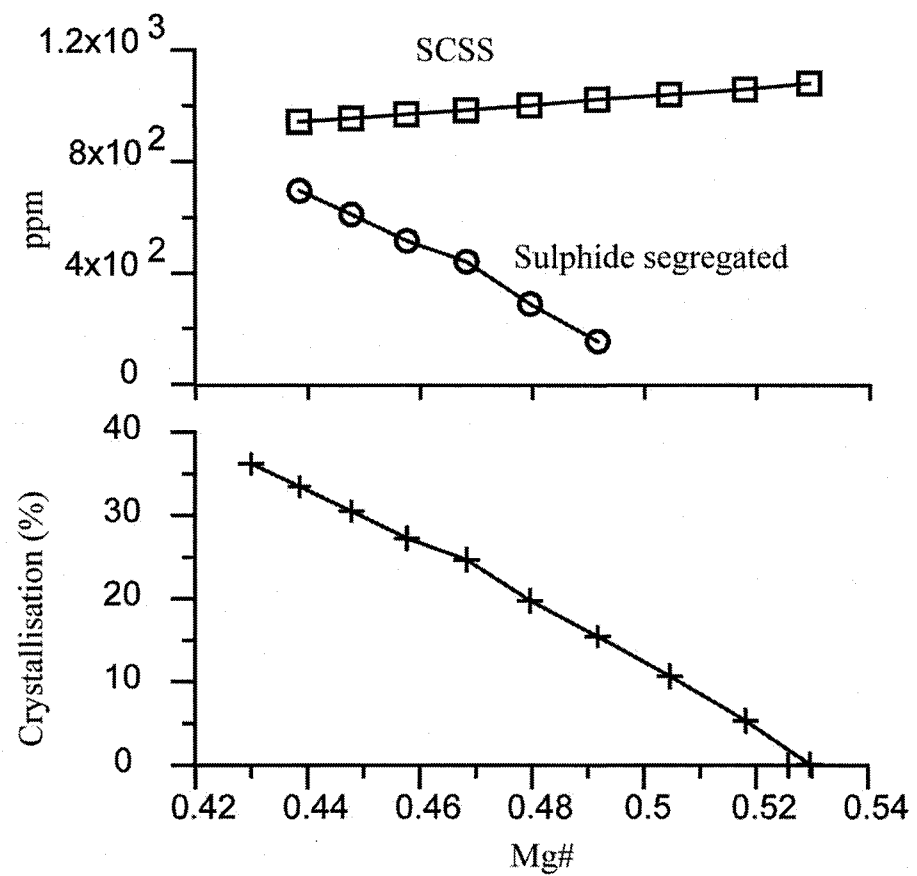


Figure 6.

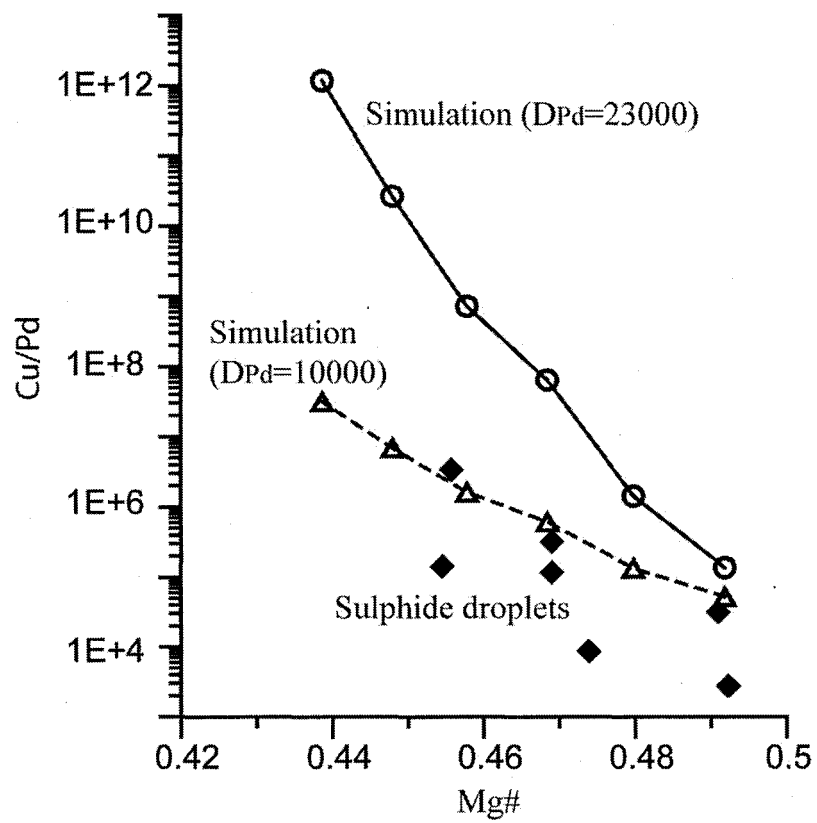


Figure 7.

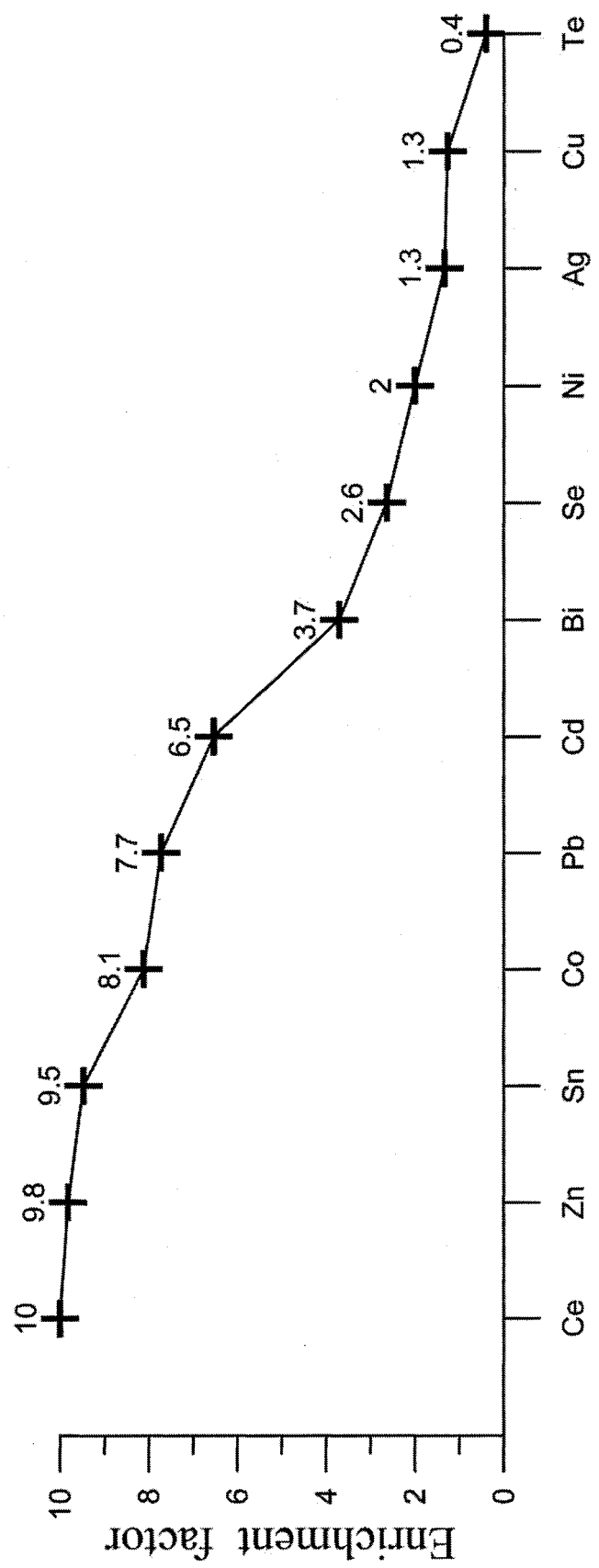


Figure 8.

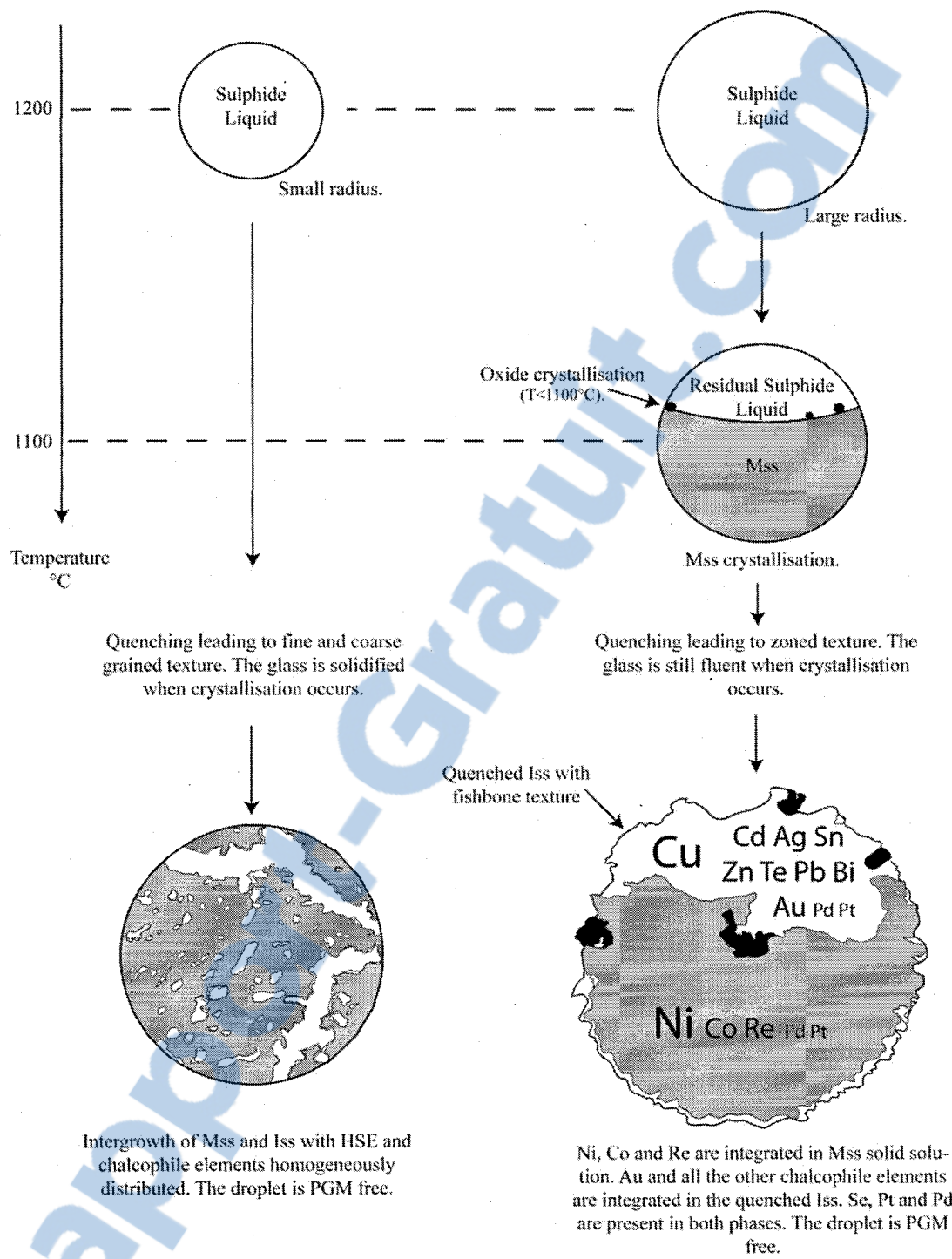


Figure 9.

Table 1: Reference materials and values used to calibrate the laser data

Isotope	34S %	57Fe %	59Co ppm	61Ni ppm	63Cu %	66Zn %	75As ppm	82Se ppm	95Mo ppm	101Ru ppm	103Rh ppm	107Ag ppm
Ref. material	po-727	po-727	Mass-1	JB-mss-5	Mass-1	Mass-1	Mass-1	Mass-1	Mass-1	po-727	po-727	Mass-1
This study	39.2	Int. Std.	67.82	10529	13.4	21.1	64.79	52.87	60.87	35.67	40.92	66.97
σ	2.3		1.68	155.79	0.1	0.3	0.58	0.23	0.25	2.80	3.23	0.19
Working values	39.09	61.07	67	10487	13.4	21	65	53	61	36.26	41.62	67
Based on	certificate	certificate	Wilson (2002)	AA-sol	Wilson (2002)	Wilson (2002)	Wilson (2002)	Wilson (2002)	Wilson (2002)	certificate	certificate	Wilson (2002)
Isotope	108Pd ppm	111Cd ppm	118Sn ppm	121Sb ppm	125Te ppm	185Re ppm	189Os ppm	193Ir ppm	195Pt ppm	197Au ppm	208Pb ppm	209Bi ppm
Ref. material	po-727	Mass-1	Mass-1	Mass-1	Mass-1	JB-mss-5	po-727	po-727	po-727	po-727	Mass-1	Mass-1
This study	42.73	69.12	54.83	54.80	21.03	20.76	46.18	47.22	35.01	45.82	79.59	65.80
σ	2.28	2.16	0.28	0.34	0.14	0.66	3.55	3.59	2.26	1.26	0.65	0.48
Working values	43.82	70	55	55	21	20.7	46.85	47.81	35.37	45.79	80.26	66
Based on	certificate	Wilson (2002)	Wilson (2002)	Wilson (2002)	LA-NIST- 610	ID-ICP-MS	certificate	certificate	certificate	certificate	LA-NIST- 610	LA-NIST- 610

Mass-1 FeCuZnS pressed powder pellet supplied by National Institute for Standards and Technology; JB-mss-5 synthetic FeS in house reference material; po-727 synthetic FeS supplied by Memorial University; po-62 synthetic FeS in house reference material; LA-NIST-610 = LA-ICP-MS on Mass-1 made at the UQAC using NIST-SRM-610 as the reference material; σ = sample standard deviation

Table 2: Reference materials used as monitors

Isotope	34S %	57Fe %	59Co ppm	61Ni %	63Cu ppm	66Zn ppm	75As ppm	82Se ppm	95Mo ppm	101Ru ppm	103Rh ppm	107Ag ppm
JB-mss-5 working values	40	57	0.28	1.05	208	13	63	48	0.23	21.7	61.4	53.0
σ	0.6	0.9	0.02	n.d.	7	9	10	14	0.02	0.4	7.2	4.9
based on this run n=9	po-727	po-727	LA-NIST-610	AA-sol	AA-sol	Mass-1	LA-NIST-610	LA-NIST-610	LA-NIST-610	ID-ICP-MS	sol-ICP-MS	sol-ICP-MS
std dev	41	Int. Std.	0.16	1.05	235	16	61	57	0.41	22.7	65.0	67.0
	1.7		0.07	0.007	12.0	10.2	4.1	4.9	0.08	1.1	3.6	3.0
Isotope	108Pd ppm	111Cd ppm	118Sn ppm	121Sb ppm	125Te ppm	185Re ppm	189Os ppm	193Ir ppm	195Pt ppm	197Au ppm	208Pb ppm	209Bi ppm
JB-mss-5 working values	61.4	0.13	0.34	61.3	66	20.7	42.5	44.0	39.9	35.9	71.5	76.1
σ	1.3	0.04	0.03	7.3	11	0.41	0.28	1.3	1	4.8	4.5	2.9
based on this run n=9	ID-ICP-MS	LA-NIST-610	NIST-610	sol-ICP-MS	LA-semi-q	ID-ICP-MS	sol-ICP-MS	ID-ICP-MS	sol-ICP-MS	sol-ICP-MS	sol-ICP-MS	sol-ICP-MS
std dev	56.8	0.18	0.57	52.8	43.5	20.8	64.7	46.2	41.1	35.9	79.1	84.5
	3.3	0.06	0.21	2.9	4.5	0.66	5.86	3.7	4.4	3.4	4.4	4.5
Isotope	34S %	57Fe %	59Co ppm	61Ni ppm	63Cu %	66Zn %	75As ppm	82Se ppm	95Mo ppm	107Ag ppm	111Cd ppm	118Sn ppm
NIST-610 working values	0.069	0.046	405	458	430	456	317	112	410	239	259	396
σ	0.013	0.000	46	4	48	38	24	4	58	38	10	36
this run n=6	0.054	0.061	457.8	464.3	Int. Std.	443.3	271.4	100.9	413.4	232.7	205.1	352.7
std dev	0.21	0.016	74.64	3.62		59.16	29.18	18.6	28.80	12.83	26.98	20.26
Isotope	121Sb ppm	125Te ppm	185Re ppm	208Pb ppm	209Bi ppm							
NIST-610 working values	368	302	47	426	357							
σ	56	n.d.	14	1	98							
this run n=6	314.5	267	56.2	379.8	338.1							
σ	20.63	55.31	9.96	30.82	25.57							

JB-mss-5 synthetic FeS in house reference material; NIST-610 = glass NIST-SRM-610 standard reference material, values are from GeoReM database; LA-semi-q = laser ablation using the semi-quantitative mode; σ = sample standard deviation

Table 3. Fresh MORB glass composition.

Sample List	SiO ₂ wt%	TiO ₂ wt%	Al ₂ O ₃ wt%	Cr ₂ O ₃ wt%	FeO wt%	MnO wt%	MgO wt%	CaO wt%	Na ₂ O wt%	K ₂ O wt%	S (ppm)	Total wt%
South Atlantic Ridge												
RC 28 02 07rd n=3	49.6	1.2	17.0	0.04	9.2	0.2	8.9	11.2	2.9	0.05	873	100.5
σ	0.10	0.01	0.04	0.03	0.09	0.03	0.07	0.03	0.03	0.01	72	0.22
RC 28 02 13rd n=12	50.3	1.6	15.1	0.07	9.5	0.2	8.0	11.4	2.7	0.09	1253	99.3
σ	0.18	0.04	0.05	0.03	0.16	0.02	0.05	0.03	0.03	0.01	75	0.28
RC 28 02 16rd n=15	50.4	1.4	14.7	0.05	9.1	0.2	7.7	12.2	2.8	0.05	1275	98.7
σ	0.29	0.04	0.09	0.03	0.22	0.02	0.08	0.10	0.05	0.01	80	0.53
RC 28 02 18rd n=3	51.6	1.1	15.3	0.08	8.1	0.1	8.4	12.8	2.7	0.05	782	100.4
σ	0.21	0.06	0.06	0.02	0.11	0.01	0.36	0.30	0.65	0.01	222	0.35
RC 28 02 22rd n=9	51.4	1.8	14.0	0.01	10.8	0.2	7.0	11.3	3.0	0.07	1454	99.9
σ	0.12	0.03	0.04	0.02	0.18	0.02	0.06	0.05	0.03	0.00	83	0.21
RC 28 02 24rd n=8	50.5	1.6	15.6	0.06	9.2	0.2	8.2	11.5	2.8	0.07	1180	99.8
σ	0.18	0.05	0.06	0.04	0.14	0.02	0.05	0.04	0.06	0.00	94	0.41
Hotu Sea Mount												
Cook D3 tIII n=3	47.9	2.9	15.4	0.0	11.2	0.2	6.2	9.7	3.3	0.72	1530	97.9
σ	0.22	0.07	0.15	0.02	0.07	0.02	0.08	0.01	0.04	0.01	38	0.32
Cook D19 tI n=3	47.6	2.2	16.9	0.07	10.4	0.2	7.5	10.1	3.3	0.58	1278	99.0
σ	0.15	0.03	0.05	0.04	0.10	0.01	0.01	0.04	0.05	0.01	21	0.30
East Pacific Rise												
Cook D28 tI n=9	48.8	1.4	16.0	0.07	9.0	0.2	8.5	11.9	3.1	0.12	1054	99.3
σ	0.09	0.04	0.35	0.04	0.26	0.02	0.22	0.02	0.08	0.01	80	0.23
Cook D37 tIV n=6	48.7	1.3	16.6	0.02	9.3	0.2	8.3	11.7	2.9	0.12	1195	99.4
σ	0.23	0.04	0.06	0.02	0.12	0.02	0.03	0.08	0.02	0.01	53	0.33
Cook D37 tVI n=18	48.6	1.2	16.7	0.05	9.1	0.2	8.5	11.7	2.8	0.11	1167	99.2
σ	0.27	0.05	0.10	0.03	0.13	0.02	0.08	0.03	0.04	0.01	81	0.42

n= number of analysis; σ= analysis standard deviation

Note that samples from the South Atlantic Ridge are slightly richer in SiO₂ and samples from the Hotu Sea Mounts are slightly richer in TiO₂ and K₂O.

Table 4. Sulfide droplets bulk composition.

Droplet	Texture	Size μm	n (phase)*	S wt%	Bulk composition				Total wt%
					Ni wt%	Cu wt%	Fe wt%		
RC 28 02 07rd G1	Coarse-grained	48	9	34.46	15.93	11.36	37.21	98.95	
σ			(1.2,3)	0.74	3.19	1.52	1.58		
RC 28 02 13rd n2 G1	Fine-grained	28	3	34.97	8.30	3.64	48.87	95.78	
σ			(4)	0.44	0.53	0.68	1.01		
RC 28 02 16rd n1 G10	Fine-grained	45	3	33.69	3.49	14.52	45.53	97.22	
σ			(1.2)	0.31	0.02	0.78	0.20		
RC 28 02 24rd G3	Fine-grained	50	3	34.73	8.42	9.06	44.85	97.06	
σ			(1.2)	0.20	0.44	2.18	1.49		
RC 28 02 24rd G6	Coarse-grained	38	4	35.49	10.53	4.54	47.71	98.27	
σ			(1.2,3)	0.82	0.76	0.08	1.02		
Cook D28 tI n2 G1	Coarse-grained	42	4	34.50	11.26	9.72	43.53	99.01	
σ			(1.2)	0.73	1.36	0.84	0.13		
Cook D37 tIV G2	Coarse-grained	32	5	35.16	8.87	10.05	44.47	98.55	
σ			(1.2,3)	1.08	0.58	0.69	0.47		

* Phases analysed: 1) Fe-Ni rich (Mss) 2) Cu-Fe rich (Iss) 3) Ni-Fe rich (Pentlandite) and 4) Whole droplet

n= number of microprobe analysis; σ= microprobe analysis standard deviation

Details of bulk composition are given in Patten et al. (sub.).

Table 5a. LA-ICP-MS analyses of the sulphide droplets and the surrounding glasses.

	Sulphide droplet	Droplet Size	S wt.% 34	Fe* wt.% 57	Co ppm 59	Ni ppm 61	Cu ppm 65	Zn ppm 68	As ppm 75	Se ppm 77	Mo ppm 95	Ru ppm 102	Rh ppm 103	Pd ppm 108	Ag ppm 109
Isotope															
RC 28 02 16rd n1 GI	Sulphide	45	33.18	46.68	1.554	48.401	104.717	288	<d.l.	110.51	<d.l.	<d.l.	<d.l.	<d.l.	38.12
	d.l.		6.61E-03		0.06	14.2	0.6	1.19	0.41	1.38	0.16	0.04	0.012	0.032	0.020
	Glass				32.3	74.96	65.97	61	<d.l.	<d.l.	0.16	<d.l.	<d.l.	<d.l.	<d.l.
RC 28 02 7rd GI	Sulphide	48	34.641	37.49	2.371	174.404	125.126	188	0.85	129.05	0.34	2.19	0.841	45.46	42.77
	d.l.		7.61E-03		0.12	22.5	1.1	2.10	0.50	1.63	0.19	0.04	0.017	0.051	0.018
	Glass				57.0	243.1	96.6	78	<d.l.	<d.l.	0.20	<d.l.	<d.l.	<d.l.	0.028
Cook D37 tIV G2	Sulphide	32	37.26	45.10	2.438	105.808	74.395	301	3.30	119.80	<d.l.	2.01	0.613	8.60	22.17
	d.l.		7.97E-03		0.11	19.4	0.5	1.51	0.48	1.64	0.15	0.05	0.015	0.043	0.024
	Glass				49.0	140.9	71.4	83	<d.l.	<d.l.	0.22	<d.l.	<d.l.	<d.l.	0.026
Cook D28 tI n2 GI	Sulphide	42	33.12	46.70	2.192	100.702	86.778	291	3.15	120.40	0.56	1.27	<d.l.	2.75	32.51
	d.l.		8.94E-03		0.12	21.4	0.6	1.63	0.55	1.74	0.18	0.06	0.021	0.042	0.025
	Glass				50.9	131.3	72.5	91	<d.l.	<d.l.	0.33	<d.l.	<d.l.	0.091	0.029
RC 28 02 24rd G6	Sulphide	38	34.87	47.71	1.784	109.279	66.640	324	1.15	114.66	<d.l.	0.26	<d.l.	0.208	21.09
	d.l.		6.83E-03		0.07	14.9	0.5	1.25	0.39	1.25	0.15	0.04	0.014	0.034	0.019
	Glass				35.5	113.3	49.1	72	<d.l.	<d.l.	0.23	<d.l.	<d.l.	<d.l.	0.020
RC 28 02 24rd G3	Sulphide	50	36.10	44.62	1.715	94.589	80.797	259	<d.l.	112.41	<d.l.	<d.l.	<d.l.	0.689	24.94
	d.l.		6.63E-03		0.08	14.6	0.5	1.10	0.37	1.19	0.15	0.04	0.012	0.037	0.016
	Glass				37.6	121.1	49.8	78	<d.l.	<d.l.	0.11	<d.l.	<d.l.	<d.l.	0.022
RC 28 02 13rd n2 GI	Sulphide	28	33.62	51.02	1.901	84.459	67.443	276	5.75	83.67	<d.l.	0.12	<d.l.	0.472	21.55
	d.l.		1.01E-02		0.11	17.7	0.8	1.94	0.52	2.55	0.18	0.04	0.016	0.040	0.022
	Glass				49.7	105.2	54.7	101	<d.l.	<d.l.	0.52	<d.l.	<d.l.	<d.l.	<d.l.
Mean	Sulphide		34.68		1.994	102.520	86.556	275	2.84	113	0.45	1.17	0.73	9.70	29.02
	σ		1.44		317	34.939	19.859	40	1.76	13	0.11	0.86	0.11	16.25	8.16
	Glass				44.2	128.9	64.0	81			0.25			0.025	
	σ				8.1	47.1	15.2	11.4			0.13			0.003	

Sulphide droplets analyzed are fine and coarse grained quenched texture and have a diameter $\geq 30\mu\text{m}$.

*Fe: Iron 57 is the internal standard, values were determined by electronic microprobe.

d.l.= detection limit, the detection limit is three times the square root of the blank

σ= standard deviation

Table 5b. LA-ICP-MS analyses of the sulphide droplets and the surrounding glasses.

	Sulphide droplet Isotope	Droplet Size	Cd ppm 111	Sn ppm 118	Sb ppm 121	Te ppm 128	Re ppm 187	Os ppm 190	Ir ppm 193	Pt ppm 195	Au ppm 197	Pb ppm 208	Bi ppm 209	Total %
RC 28 02 16rd n1 G1	Sulphide	45	19.51	6.95	<d.l.	9.95	0.25	<d.l.	0.01	0.01	0.11	19.56	3.66	95.38
	d.l.		0.11	0.09	0.03	0.27	0.002	0.01	0.004	0.01	0.01	0.01	0.01	
	Glass		0.10	0.58	<d.l.	0.27	0.008							
	d.l.		0.08	0.07	0.02	0.13	0.002	0.01	0.003	0.01	0.005	0.01	0.01	
RC 28 7rd G1	Sulphide	48	10.14	5.73	<d.l.	12.78	0.31	0.08	0.01	1.52	1.70	16.55	3.02	102.37
	d.l.		0.13	0.12	0.03	0.26	0.00	0.01	0.01	0.01	0.01	0.01	0.01	
	Glass		<d.l.	0.62	<d.l.	0.30	<d.l.							
	d.l.		0.08	0.07	0.02	0.13	0.002	0.013	0.010	0.010	0.005	0.01	0.004	
Cook D37 tIV G2	Sulphide	32	8.30	5.39	0.13	18.06	0.30	1.19	0.52	9.35	2.60	11.64	3.02	100.68
	d.l.		0.10	0.10	0.03	0.27	0.00	0.01	0.00	0.01	0.01	0.01	0.01	
	Glass		0.14	0.60	0.03	<d.l.	<d.l.	<d.l.	<d.l.	<d.l.	<d.l.	0.26	0.014	
	d.l.		0.06	0.06	0.02	0.12	0.002	0.007	0.003	0.005	0.005	0.01	0.004	
Cook D28 tI n2 G1	Sulphide	42	12.57	7.75	<d.l.	19.29	0.25	0.86	0.54	4.44	1.81	20.15	3.29	98.83
	d.l.		0.11	0.11	0.03	0.27	0.00	0.03	0.00	0.01	0.01	0.02	0.01	
	Glass		0.12	0.79	<d.l.	0.38	0.028							
	d.l.		0.07	0.07	0.02	0.13	0.002	0.021	0.004	0.009	0.006	0.01	0.005	
RC 28 02 24rd G6	Sulphide	38	13.56	8.22	<d.l.	13.89	0.27	0.04	0.01	0.41	0.56	21.62	2.95	100.41
	d.l.		0.08	0.09	0.03	0.20	0.00	0.01	0.00	0.01	0.00	0.01	0.01	
	Glass		0.19	0.80	0.02	<d.l.	<d.l.	<d.l.	<d.l.	<d.l.	<d.l.	0.36	<d.l.	
	d.l.		0.05	0.05	0.02	0.09	0.002	0.009	0.003	0.005	0.001	0.01	0.005	
RC 28 02 24rd G3	Sulphide	50	13.89	9.09	<d.l.	16.09	0.26	<d.l.	0.01	0.26	0.59	21.81	2.81	98.47
	d.l.		0.08	0.09	0.02	0.18	0.00	0.02	0.00	0.01	0.00	0.01	0.01	
	Glass		0.12	0.71	0.03	<d.l.	<d.l.	<d.l.	<d.l.	<d.l.	<d.l.	0.32	<d.l.	
	d.l.		0.05	0.06	0.02	0.09	0.002	0.016	0.002	0.006	0.002	0.01	0.004	
RC 28 02 13rd n2 G1	Sulphide	28	13.40	8.80	<d.l.	11.96	0.20	0.07	0.01	0.58	0.78	18.61	2.52	100.06
	d.l.		0.11	0.11	0.03	0.29	0.00	0.03	0.00	0.01	0.00	0.01	0.01	
	Glass		0.15	0.72	0.02	<d.l.	<d.l.	<d.l.	<d.l.	<d.l.	<d.l.	0.39	<d.l.	
	d.l.		0.08	0.08	0.02	0.17	0.004	0.024	0.005	0.011	0.005	0.01	0.005	
Mean	Sulphide		13.05	7.42	0.13	14.57	0.26	0.45	0.16	2.37	1.16	18.56	3.04	
	std. dev.		3.25	1.34	0.00	3.13	0.04	0.48	0.23	3.18	0.82	3.28	0.33	
	Glass		0.14	0.70								0.32	0.02	
	std. dev.		0.03	0.08								0.04	0.01	

Sulphide droplets analyzed are fine and coarse grained quenched texture and have a diameter $\geq 30\mu\text{m}$.

*Fe: Iron 57 is the internal standard, values were determined by electronic microprobe.

d.l.= detection limit, the detection limit is three times the square root of the blank

std. dev.= standard deviation

Table 6. Sulfide melt-silicate melt partition coefficient determine from each sulphide droplet

Partition coefficient	Mg#	Co	Ni	Cu	Zn	Ag	Cd	Sn	Pb
RC 28 02 13rd G2	0.42	38	803	1233.0	2.73		89	12.2	48
RC 28 02 16rd n1 G1	0.42	48	646	1587.3	4.69		193	12.1	71
RC 28 02 24rd G6	0.43	50	965	1357.8	4.53	1054	72	10.3	60
RC 28 02 24rd G3	0.43	46	781	1623.7	3.33	1134	120	12.8	68
Cook D37 tIV G2	0.44	50	751	1041.8	3.64	853	61	9.0	45
Cook D28 tI n2 G1	0.45	43	767	1196.4	3.19	1121	107	9.8	54
RC 28 02 7rd G1	0.46	42	717	1294.9	2.42	1528		9.2	54

Table 7. Summarized partition coefficient values and sulphide contribution to the mantle bulk partition coefficient.

Values for the Glass	Method*	Co	Ni	Cu	Zn	Se	Ag	Cd	Sn	Te	Pb	Bi
This study UQAC	LA-ICP-MS	38-50	646-965	1042-1624	2.42-4.69		853-1528	61-193	8.96-12.8		45-71	118-458
Mean		45	776	1334	3.50		1138	107	10.8		57	264
Std dev		4.1	91	194	0.79		219	43	1.45		9.0	143
Jenner et al. (2012) UNA	LA-ICP-MS	36-48	395-1155	748-1398	2.33-3.56	247-375	806-1656	88-138	6.44-10.38		30-96	361-613
Mean		41	756	1013	2.91	323	1143	106	8.87		51	487
Std dev		4.4	245	222	0.39	42	314	18	1.47		24	84
Yi et al. (2000) ID ICP-MS							97-169	8.41-12.11	3506-6380			
Mean							126	10.3	4791			
Std dev							24	1.42	1195			
Preferred Partition Coeffecient Value		45	776	1334	3.5	323	1138	107	10.8	4791	57	487
Std dev		4.1	91	194	0.79	41.7	219	43	1.45	1195	9.0	84
Glass		This study	This study	This study	This study	Jenner et al. (2012)	This study	This study	This study	Yi et al. (2000)	This study	Jenner et al. (2012)
Rajamani and Naldrett (1978)		61-80										
Peach et al. (1990)		36-45	574-836	1383		1770						
Francis (1990)			350-424	913-1006								
Gaetani and Groove (1997)		17-24	410-580	250-313								
Yi et al. (2000)										3.10 ⁴ -6.10 ⁴		
Hart and Gaetani (2006)											14	
Brenan et al., p.c. [†]				620-1513		397-793						
Sulfide Contribution to Bulk D Mantle		0.024	0.41	0.70	0.002	0.17	0.60	0.06	0.01	2.52	0.03	0.26

*Method of analysis of the galss; [†]Personal communication in Barnes et al., 2009.

All the partition coefficient are calculated with the sulphide droplets values from Table 5.

Table 8. Whole rock values for PGE.

Sample	Ru (ppb)	Pd (ppb)	Re (ppb)	Ir (ppb)	Pt (ppb)	Os (ppb)
RC 28 02 16rd n1	0.037	0.50	0.35	<d.l.	<d.l.	0.005
RC 28 7rd	0.176	2.88	0.36	0.041	0.968	0.321
Cook D37 tIV	0.067	0.51	0.42	0.017	0.070	0.205
Cook D28 t1 n2	0.046	0.48	0.39	0.020	0.183	0.024
RC 28 02 24rd	0.062	0.02	0.22	0.002	0.014	0.001
RC 28 02 13rd n2	0.032	0.11	0.34	0.011	0.034	0.008
Okum	r.f.	4.89	12.01	0.61	1.03	11.83
Okum	r.f.	4.67	11.88	0.42	1.03	11.13
Certificate		4.25	11.70	n.d.	0.99	11.00
						n.d.

Whole rock analyses made by High Pressure Asher digestion and Isotope Dilution(HPA-ID) at the LabMaTer, UQAC; Detection limits are at 0.01ppb; r.f.= reference material

Table 9. Minimum partition coefficients for PGE and Re.

	102Ru	108Pd	187Re	190Os	193Ir	195Pt
Range	3 610-30 145	5 700-16 735	597-1 218	252-73 660	261-27 219	1 569-132 704
Mean	15 524	10 666	870	24 771	11 637	37 301
Std dev	11 224	4 670	248	27 366	12 435	43 513

The partition coefficients are estimated with whole rock values instead of glass LA-ICP-MS values.

Annex 1a. Glass composition used from Jenner et al. (2012) for the calculation of partition coefficient.

Sample	Lat.	Long.	Mgr	S (ppm)	Co (ppm)	Ni (ppm)	Cu (ppm)	Zn (ppm)	Se (ppm)	Ag (ppm)	Cd (ppm)	Sn (ppm)	Pb (ppm)	Bi (ppm)
4081	45.51	-29.48	0.417		35.4	90.2	60.3	82.9	0.32	0.02	0.13	1.08	1.37	0.009
4083	45.51	-29.48	0.418		34.9	79.6	62.9	88.2			0.11	1.26	1.48	0.013
193	-21.87	-11.85	0.418	1176.8	43.0	84.1	77.5	94.2	0.36	0.02	0.15	1.12	0.40	0.006
3798	36.45	-33.68	0.419	1008.5	44.3	107.1	80.9	88.6		0.03	0.10	0.69	0.33	bdl
197	-21.87	-11.85	0.419		42.5	84.0	89.3	87.3			0.14	1.14	0.29	0.004
7220	-41.26	-16.6	0.420		44.2	142.1	74.4	103.9			0.15	1.13	0.52	0.006
1695	51.84	-30.07	0.420		43.2	114.9	78.1	98.1			0.12	1.07	0.39	0.007
626	34.9	-61.17	0.420	1049.2	47.6	147.2	110.2	94.5	0.41	0.03	0.12	0.61	0.33	0.007
7234	-40.44	-16.75	0.420	1103.4	45.5	145.6	76.9	98.0		0.02	0.14	0.94	0.45	0.007
3619	11.97	-43.7	0.421		43.1	129.5	76.0	96.8			0.14	1.27	0.45	0.007
760	25.4	-45.3	0.421	1121.8	41.0	128.4	66.9	89.9	0.32	0.02	0.13	1.10	0.47	0.005
3627	-0.56	-16.02	0.421		41.7	122.8	74.4	96.4			0.16	1.28	0.60	0.008
193	-21.87	-11.85	0.422		43.1	134.3	72.8	95.3			0.16	1.29	0.41	0.007
201	42.96	-29.18	0.422		37.0	90.3	76.0	85.0			0.15	1.15	1.08	0.007
990	25.77	-45.16	0.422	1037.0	42.7	132.5	72.0	96.1		0.02	0.15	1.22	0.55	0.005
7226	-40.44	-16.75	0.422		45.6	145.7	80.8	104.1			0.14	1.08	0.47	0.006
7209	-42.92	-16.37	0.422		45.7	137.6	72.3	104.0			0.19	1.17	0.61	0.007
7232	-40.44	-16.75	0.422	1074.4	46.8	152.8	78.2	100.2		0.02	0.15	0.92	0.42	0.005
627	34.9	-61.17	0.423	1066.7	48.2	159.2	117.2	93.0	0.37	0.03	0.12	0.61	0.34	0.007
3965	36.46	-33.62	0.423		46.4	72.5	85.4	95.4			0.13	0.81	0.35	0.006
3618	11.97	-43.7	0.423		43.0	126.6	73.9	97.6			0.14	1.29	0.47	0.008
7233	-40.44	-16.75	0.423	1158.6	45.4	148.3	77.2	98.6		0.02	0.13	0.97	0.43	0.007
7204	-46.22	-14.08	0.423		45.8	149.5	80.7	99.3			0.15	1.16	0.60	0.008
7235	-40.44	-16.75	0.424	1090.2	47.0	150.8	78.6	100.4		0.02	0.13	0.91	0.43	0.007
3625	11.52	-43.6	0.424		43.4	126.5	71.6	99.6			0.18	1.24	0.46	0.010
7266	-37.19	-17.52	0.425		41.7	92.0	86.1	91.5			0.13	1.03	0.82	0.010
4080	45.51	-29.48	0.425		35.5	94.3	38.9	81.9	0.31	0.02	0.12	1.09	1.37	0.010
307	45.33	-28.03	0.425	963.7	40.9	116.4	65.2	87.8	0.33	0.02	0.12	0.81	0.66	0.007
7229	-40.44	-16.75	0.425		45.4	146.4	80.4	102.5			0.16	1.08	0.49	0.007
7207	-42.92	-16.37	0.425		46.0	162.9	71.1	102.6			0.14	1.21	0.61	0.007
3620	11.97	-43.7	0.426	988.3	43.4	132.6	78.9	101.6			0.14	1.28	0.47	0.009
3795			0.426		42.3	102.1	78.3	84.7		0.03	0.11	0.63	0.29	bdl
7200	-46.22	-14.08	0.426		44.5	135.7	72.4	97.7			0.15	1.12	0.62	0.006
7205	-46.22	-14.08	0.426		45.0	136.8	79.8	99.2			0.15	1.15	0.60	0.007
7201	-46.22	-14.08	0.426		45.4	143.1	83.0	99.1			0.13	1.12	0.60	0.007
199	42.96	-29.18	0.427		37.8	96.2	75.9	84.7			0.14	1.15	1.11	0.007
7225	-40.44	-16.75	0.427		46.3	155.5	80.7	104.2			0.14	1.07	0.47	0.007
3617	11.97	-43.7	0.427		40.1	57.2	77.4	91.9			0.14	1.43	0.48	0.007
7265	-37.19	-17.52	0.427		41.3	90.0	84.4	91.2			0.11	1.07	0.79	0.009
7228	-40.44	-16.75	0.428		45.5	153.0	79.3	102.7			0.15	1.05	0.48	0.007
621	34.9	-61.17	0.428	1045.8	48.8	157.5	112.9	92.8		0.03	0.12	0.62	0.38	0.005
314	45.12	-28.33	0.428	1081.0	43.3	126.8	67.8	89.3	0.31	0.02	0.12	0.85	0.58	bdl
3925	36.76	-31.29	0.429	994.6	43.2	111.5	74.5	94.9	0.32	0.02	0.14	0.69	0.32	0.005
3966	36.46	-33.62	0.429		45.2	106.8	82.7	92.9			0.12	0.73	0.33	0.009
7227	-40.44	-16.75	0.429		46.3	157.5	79.1	105.2			0.17	1.09	0.47	0.006
1629	53.19	-35.09	0.429	1111.0	45.2	112.3	94.4	90.8	0.34	0.03	0.13	0.59	0.12	0.006
311			0.430	989.2	43.5	165.3	66.4	89.2	0.31	0.02	0.13	0.72	0.56	bdl
7208	-42.92	-16.37	0.431		46.7	163.6	75.0	103.2			0.14	1.16	0.58	0.008
5387	-5.36	5.26	0.431		50.1	145.9	112.6	79.0			0.15	0.67	0.21	0.005
622	34.9	-61.17	0.432	1047.8	47.8	156.3	116.3	92.3	0.36	0.03	0.12	0.62	0.31	0.007
3331	36.46	-33.58	0.433	935.6	43.4	116.0	80.6	85.0	0.24	0.02	0.11	0.67	0.36	0.005
7202	-46.22	-14.08	0.434		46.5	137.5	85.9	94.2			0.13	1.09	0.64	0.005
309	45.33	-28.03	0.434	933.7	39.2	115.1	64.0	86.5	0.31	0.02	0.12	0.82	0.69	0.008
624	34.9	-61.17	0.434	1056.8	47.5	154.2	117.4	92.9	0.38	0.03	0.12	0.62	0.34	0.006
312	45.22	-28	0.436	961.6	43.8	142.2	69.2	92.1	0.33	0.02	0.13	0.74	0.52	bdl
5388	-34.37	5.26	0.436		50.1	145.2	112.5	78.1			0.13	0.67	0.22	0.008
623	34.9	-61.17	0.436	1069.3	47.4	143.6	67.9	92.9	0.38	0.03	0.12	0.62	0.33	0.007
3458	28.9	-43.32	0.438		49.5	159.4	121.8	82.2	0.34	0.03	0.12	0.62	0.20	0.005
1696	51.84	-30.07	0.438		44.2	109.6	84.8	93.9			0.13	1.07	0.38	0.006
3092	28.9	-43.32	0.438		51.2	175.3	126.7	86.2			0.12	0.82	0.21	0.005
7203	-46.22	-14.08	0.438		34.1	199.1	87.7	84.3			0.15	0.90	0.49	0.005
625	34.9	-61.17	0.439	1046.6	47.8	155.7	115.8	92.5	0.36	0.03	0.12	0.61	0.33	0.007
3456	28.9	-43.32	0.440		49.2	152.3	120.6	81.5	0.37	0.03	0.12	0.62	0.20	0.005
3766	36.78	-33.3	0.441	987.2	46.2	86.2	101.5	84.4	0.32	0.03	0.12	0.63	0.42	0.007
3967	36.46	-33.63	0.441		45.3	108.6	92.4	87.2			0.12	0.68	0.34	0.007
3056	27.2	-43.55	0.441	1112.6	44.7	162.0	87.3	90.2	0.33	0.03	0.13	0.96	0.38	0.005
3090	28.9	-43.32	0.441		50.3	179.3	122.0	85.1			0.12	0.83	0.20	0.008
1698	51.84	-30.07	0.443		45.2	152.5	75.7	100.0			0.13	1.11	0.39	0.005
1693	51.84	-30.07	0.443		43.8	108.8	81.3	93.6			0.14	1.03	0.38	0.007
1676	70.37	-14.69	0.444	1077.8	48.6	93.6	121.9	85.1	0.44	0.03	0.12	0.42	0.16	0.006
3927	36.45	-33.68	0.445		43.8	109.0	89.9	86.9			0.14	0.81	0.38	0.007
3071	28.9	-43.32	0.446	913.8	49.3	163.6	117.6	80.2	0.34	0.03	0.11	0.64	0.23	0.005
204	42.95	-29.23	0.446		43.2	104.0	86.2	82.1			0.14	0.88	0.66	0.007
3330	36.58	-33.52	0.446	998.0	48.8	157.0	101.2	84.8	0.32	0.03	0.12	0.57	0.29	0.005
3073	28.9	-43.32	0.446	905.8	48.6	163.6	116.2	79.2	0.35	0.03	0.11	0.61	0.20	0.005
1678	70.37	-14.69	0.447	1114.6	49.2	70.0	125.7	82.0	0.40	0.03	0.12	0.41	0.13	0.006
3074	28.9	-43.32	0.447	965.0	49.6	162.7	120.0	81.0	0.36	0.03	0.13	0.63	0.22	0.009
3076	28.9	-43.32	0.447	941.6	50.2	178.0	117.4	81.1	0.33	0.03	0.11	0.65	0.21	0.006
3077	28.9	-43.32	0.447	930.5	49.3	163.6	120.0	81.7	0.34	0.03	0.11	0.63	0.19	0.005
3924	36.76	-33.29	0.447		46.0	93.0	93.6	93.5			0.12	0.78	0.38	0.005
3334	36.4													

Annexe 1b. Glass composition used from Yi et al. (2012) for the calculation of partition coefficient.

Sample	Mg#	S (ppm)	Cd (ppm)	Sn (ppm)	Te (ppm)
AII 127 D15-1	0.417	725	0.117	0.62	0.00125
AII 127 D11-1	0.430	1220	0.113	0.71	0.0049
AII 127 D27-S	0.431	800	0.109	0.78	0.00315
AII 127 D5-S	0.488	1050	0.079	0.49	0.00531
AII 127 D8-2	0.489	970	0.1	0.46	0.00492
AII 127 D17-3	0.490	460	0.102	0.83	0.00083

CONCLUSIONS GÉNÉRALES

Ce projet de maîtrise en Sciences de la Terre s'axe sur deux chapitres qui abordent trois problématiques spécifiques au comportement des éléments hautement sidérophiles et des éléments chalcophiles dans des sulfures magmatiques. Chaque chapitre correspond à un manuscrit ayant été ou étant en voie de soumission à une revue scientifique et ayant été corrigé par différents relecteurs.

Ces deux chapitres se basent sur des données acquises par l'analyse de verre frais de MORB. Ces échantillons, provenant de dragages principalement effectués au niveau de la dorsale Sud Atlantique et de la dorsale Est Pacifique, nous ont été mis à disposition par le Lamont Doherty Earth Observatory de New York. Différentes méthodes d'analyses ont été utilisées pour l'acquisition des données: les observations pétrographiques ainsi que les analyses LA-ICP-MS et HPA-ID ont été effectuées à l'UQAC au LabMaTer. Les analyses EPMA et MEB ont quant à elles été effectuées à l'Université Laval de Québec.

Le premier article, accepté par *The Canadian Mineralogist*, propose une approche thermodynamique permettant d'expliquer les différentes textures des gouttelettes sulfurées. En effet, des gouttelettes sulfurées présentes dans les mêmes échantillons de verre frais, et ayant donc subi le même refroidissement, avaient des textures très variables.

Les observations pétrographiques ont permis de mettre en évidence la relation entre la taille des gouttelettes sulfurées et leur texture. Les gouttelettes les plus petites ($\approx 10\text{-}30\mu\text{m}$) ont tendance à présenter des textures trempées et les gouttelettes les plus grosses ($>50\mu\text{m}$) ont tendance à présenter des textures différencierées. Ainsi, la taille des

gouttelettes affecte leur texture. Des analyses par EPMA ont permis de déterminer que la composition des gouttelettes n'affectait pas la température de cristallisation de la SSM et donc les textures.

Durant la nucléation et la croissance d'un cristal, la solubilité d'une phase est dépendante du changement d'énergie d'interface de cette phase. Puisque de petits grains ont un ratio surface sur volume élevé, une diffusion élevée à l'interface est nécessaire afin de maintenir l'équilibre chimique. Cela nécessite donc une solution plus élevée avant que la nucléation et la croissance aient lieu. Cette concentration est appelée solubilité effective et est dépendante du rayon du cristal. Cependant, lorsque la nucléation et la croissance ont lieu dans un volume confiné, tel qu'une gouttelette sulfurée, la solubilité effective n'est plus dépendante du rayon du cristal mais du rayon du volume. Les petites gouttelettes nécessitent donc une saturation plus élevée afin que la nucléation et la croissance aient lieu.

Ce phénomène a pour conséquence de retarder la cristallisation des différentes phases sulfurées des petites gouttelettes sulfurées au moment de l'éruption et du refroidissement par rapport aux gouttelettes plus larges. Ainsi, les petites gouttelettes subissent un refroidissement plus brutal que les grosses gouttelettes provoquant une variation dans les taux de nucléation et de diffusion aboutissant à des textures trempées. Les gouttelettes plus grosses, ayant une solubilité effective moins élevée, n'ont pas leur cristallisation qui est retardée au moment de l'éruption ce qui permet une bonne diffusion et le développement de textures zonées.

La compréhension des processus de cristallisation des gouttelettes sulfurées dans les verres frais de MORB est fondamentale avant de pouvoir aborder le comportement des éléments hautement sidérophiles et chalcophiles lors de l'évolution de systèmes magmatiques. Ainsi, ce premier chapitre permet la compréhension de ces processus de cristallisation et sert d'étude préliminaire au second chapitre.

Le second chapitre, correspondant à un article qui sera soumis au *Journal of Petrology*, s'intéresse au comportement géochimique des EHS et chalcophiles dans les gouttelettes sulfurées de MORB.

En effet, bien que la répartition des EHS parmi les sulfures de métaux de base, les silicates et les oxydes ait reçu un grand intérêt à cause de leur importance scientifiques et économiques, le comportement de nombreux éléments chalcophiles traces a reçu moins d'attention. Les analyses par LA-ICP-MS des gouttelettes sulfurées avec des textures d'intercroissances fines permettent de calculer des nouvelles valeurs de coefficients de partage permettant de mieux comprendre le comportement général des éléments chalcophiles.

De nouveaux coefficients de partage ont été calculés pour le Co, Ni, Cu, Zn, Se, Ag, Cd, Sn, Te, Pb et Bi. De plus, l'analyse des gouttelettes zonées ont pu permettre de déterminer la distribution des éléments chalcophiles et sidérophiles dans les différents minéraux sulfurés; permettant ainsi de comprendre leur comportement durant les premières étapes de la différenciation d'un liquide sulfuré. Ainsi, les conclusions suivantes ont pu être mises en évidence:

1. Les gouttelettes analysées au LA-ICP-MS ont un rapport Cu/Pd similaire aux sulfures ségrégant dans la chambre magmatique à l'aplomb de la dorsale océanique. Ces gouttelettes ont donc probablement été formées dans la chambre magmatique et ont eu le temps de s'équilibrer avec le magma silicaté. Ainsi il est réaliste de pouvoir utiliser ces gouttelettes pour calculer des coefficients de partage.
2. Étant proche de l'état d'équilibre, il a été possible de calculer des coefficients de partage entre le liquide silicaté et le liquide sulfuré pour : Co (45±4.1), Ni (776±91), Cu (1334±194), Zn (3.5±0.79), Se (323±41.7), Ag (1138±219), Cd (107±43), Sn (10.8±1.45), Te (4791±1195), Pb (57±9) et Bi (487±84). Des coefficients de partage minimums ont également été calculés pour les EGP en utilisant les analyses roches totales.
3. En utilisant ces coefficients de partage, il est possible de déterminer la contribution des sulfures pendant la fusion partielle du manteau. Excepté pour le Cu et le Te, les éléments chalcophiles se comportent comme des éléments incompatibles pendant la fusion partielle du manteau. Les sulfures jouent un rôle primordial dans le fractionnement des ces éléments entre eux et avec les éléments lithophiles.
4. Les gouttelettes sulfurées ont des textures représentatives des différentes étapes de cristallisation des sulfures allant du liquide sulfuré jusqu'à la cristallisation de la SSI. Les gouttelettes ayant des textures avec des intercroissances fines et grossières sont représentatives du liquide sulfuré avant la cristallisation de la SSM. Les gouttelettes ayant une texture zonée et une SSI trempée sont

caractéristiques d'une étape après la cristallisation de la SSM et avant la cristallisation de la SSI. Les gouttelettes zonées avec la SSI massive sont caractéristiques d'une étape après la cristallisation de la SSI.

5. La répartition des EHS et des éléments chalcophiles dans les gouttelettes sulfurées confirme les précédents modèles. Le Ni, Co et le Re ainsi qu'une partie du Pt et du Pd sont intégrés en solution solide dans la SSM. Le Zn, Cd, Ag, Sn, Te, Bi, Au et le reste de Pt et Pd sont concentrés dans le liquide résiduel riche en Cu.
6. Les gouttelettes sulfurées étudiées ne contiennent pas de MGP. Puisqu'elles ont subi un refroidissement brutal, l'exsolution de MGP par diffusion n'a pas pu avoir lieu. Cela confirme que le processus d'exsolution est un processus majeur dans la formation de MGP à partir de sulfures qui ont refroidi lentement.

REMERCIEMENTS

Je tiens à remercier tout particulièrement Mme Sarah-Jane Barnes, directrice du projet de recherche, pour l'attention, le soutien et l'accompagnement tout au long de cette maîtrise.

Je tiens également à remercier Mr Edmond Mathez qui a permis l'accès aux échantillons du Lamont Doherty Earth Observatory (LDEO) ainsi que sa contribution intellectuelle au projet. Sont également remerciés les membres du comité interne qui ont participé à l'évaluation de ce mémoire, ainsi que Philippe Pagé et Sarah Dare pour leurs corrections et leurs précieux conseils, Dany Savard pour les analyses au LA-ICP-MS ainsi que les analyses roches totales au LabMaTer à l'UQAC, Marc Choquette pour les analyses microsondes à l'Université de Laval, Georges Lozefski pour l'échantillonnage (LDEO).

Je voudrais également remercier tous les membres de la Chaire de Recherche du Canada en Métallogénie Magmatique qui ont permis de créer une dynamique de travail propice à l'épanouissement intellectuel.

RÉFÉRENCES

- Alard, O., Griffin, W. L., Lorand, J. P., Jackson, S. E., & O'Reilly, S. Y. (2000). Non-chondritic distribution of the highly siderophile elements in mantle sulphides. *Nature* 407, 891-894.
- Ballhaus, C., & Sylvester, P. (2000). Noble metal enrichment processes in the Merensky Reef, Bushveld Complex. *Journal of Petrology* 41, 545-561.
- Barnes, S. J., & Lightfoot, P. C. (2005). Formation of magmatic nickel-sulphide ore deposits and processes affecting their copper and platinum-group element contents. *Economic Geology 100th Anniversary Volume* 179-213.
- Barnes, S. J., Cox, R. A., & Zientek, M. L. (2006). Platinum-group element, gold, silver and base metal distribution in compositionally zoned sulphide droplets from the Medvezky Creek Mine, Noril'sk, Russia. *Contributions to Mineralogy and Petrology* 152, 187-200.
- Barnes, S.-J., Prichard, H. M., Cox, R. A., Fisher, P. C., & Godel, B. (2008). The location of the chalcophile and siderophile elements in platinum-group element ore deposits (a textural, microbeam and whole rock geochemical study): Implications for the formation of the deposits. *Chemical Geology* 248, 295-317.
- Cabri, L.J. (2002). The platinum group minerals. *Canadian Institute of Mining, Metallurgy and Petroleum, Special Volume* 54, 13-129.
- Chou , C.-L. (1978). Fractionation of siderophile elements in the earth's upper mantle. *Proceedings Of The 9th Lunar And Planetary Science Conference* 1, 219-230.
- Czamanske, G. K., & Moore, J. G. (1977). Composition and phase chemistry of sulphide globules in basalt from the Mid-Atlantic Ridge rift valley near 37°N lat. *Geological Society of America Bulletin* 88, 587-599.
- Dare, S., Barnes, S.-J., & Prichard, H. (2010). The distribution of platinum group elements (PGE) and other chalcophile elements among sulphides from the Creighton Ni-Cu-PGE sulphide deposit, Sudbury, Canada, and the origin of palladium in pentlandite. *Mineralium Deposita* 45, 765-793.
- Fleet, M. E., Crocket, J. H., Liu, M., & Stone, W. E. (1999). Laboratory partitioning of platinum-group elements (PGE) and gold with application to magmatic sulphide-PGE deposits. *Lithos* 47, 127-142.
- Godel, B., & Barnes, S.-J. (2008). Platinum-group elements in sulphide minerals and the whole rocks of the J-M Reef (Stillwater Complex): Implication for the formation of the reef. *Chemical Geology* 248, 272-294.

- Hart, S., & Gaetani, G. (2006). Mantle Pb paradoxes: the sulphide solution. *Contributions to Mineralogy and Petrology* 152, 295-308.
- Hertogen, J., Janssens, M. J., & Palme, H. (1980). Trace elements in ocean ridge basalt glasses: implications for fractionations during mantle evolution and petrogenesis. *Geochimica et Cosmochimica Acta* 44, 2125-2143.
- Holwell, D. A., & McDonald, I. (2010). A review of the behaviour of platinum group elements within natural magmatic sulphide ore systems. *Platinum Metals Review* 54, 26-36.
- Irving, A. J. (1978). A review of experimental studies of crystal/liquid trace element partitioning. *Geochimica et Cosmochimica Acta* 42, 743-770.
- Lorand, J.-P., Luguet, A., Alard, O., Bezos, A., & Meisel, T. (2008). Abundance and distribution of platinum-group elements in orogenic lherzolites; a case study in a Fontete Rouge lherzolite (French Pyrénées). *Chemical Geology* 248, 174-194.
- Mathez, E. A. (1976). Sulfur solubility and magmatic sulphides in submarine basalt glass. *Journal of Geophysical Research* 81, 4269-4276.
- Mathez, E. A. & Yeats, R. S. (1976). Magmatic sulphides in basalt glass from dsdp hole 319a and site 320, Nazca plate. *Initial Reports of the Deep-Sea Drilling Project* 34, 363-373.
- Mitchell, R. H., & Keays, R. R. (1981). Abundance and distribution of gold, palladium and iridium in some spinel and garnet lherzolites: implications for the nature and origin of precious metal-rich intergranular components in the upper mantle. *Geochimica et Cosmochimica Acta* 45, 2425-2442.
- Moore, J. G., and L. C. Calk. (1971). Sulphide spherules in vesicles of dredge pillow basalt. *American Mineralogist* 56, 476-488.
- Moore, J. G., & Schilling, J. (1973). Vesicles, water, and sulfur in Reykjanes Ridge basalts. *Contributions to Mineralogy and Petrology* 41, 105-118.
- Moore, J. G. (1975). Mechanism of formation of pillow lava: pillow lava, produced as fluid lava cools underwater, is the most abundant volcanic rock on earth, but only recently have divers observed it forming. *American Scientist* 63, 269-277.
- Naldrett, A. J., & Duke, J. M. (1980). Platinum metals magmatic sulphide ores. *Science* 208, 1417-1424.
- Peach, C. L., Mathez, E. A., & Keays, R. R. (1990). Sulphide melt silicate melt distribution coefficients for noble-metals and other chalcophile elements as deduced from MORB - implications for partial melting. *Geochimica et Cosmochimica Acta* 54, 3379-3389.

- Peregoedova, A., Barnes, S.-J., & Baker, D. R. (2004). The formation of Pt-Ir alloys and Cu-Pd-rich sulphide melts by partial desulfurization of Fe-Ni-Cu sulphides: results of experiments and implications for natural systems. *Chemical Geology* 208, 247-264.
- Prichard, H. M., Hutchinson, D., & Fisher, P. C. (2004). Petrology and crystallisation history of multiphase sulphide droplets in a Mafic Dike from Uruguay: implications for the origin of Cu-Ni-PGE sulphide deposits. *Economic Geology and the Bulletin of the Society of Economic Geologists* 99, 365-376.
- Tredoux, M., Lindsay, N. M., Davies, G., & McDonald, I. (1995). The fractionation of platinum-group elements in magmatic systems, with the suggestion of a novel causal mechanism. *South African Journal of Geology* 98, 157-167.
- Yeats, R. S., & Mathez, E. A. (1976). Decorated vesicles in deep-sea basalt glass, Eastern Pacific. *Journal Geophysical Research* 81, 4277-4284.
- Yi, W., Halliday, A. N., Alt, J. C., Lee, D. C., Rehkamper, M., Garcia, M. O., Su, Y. J. (2000). Cadmium, indium, tin, tellurium, and sulfur in oceanic basalts: Implications for chalcophile element fractionation in the Earth. *Journal of Geophysical Research-Solid Earth* 105, 23761-23761

ANNEXES

Annexe A: Localisation des échantillons

Les 24 échantillons de ce projet, mis à disposition par le Lamont Doherty Earth Observatory, Columbia University, New York, proviennent de dragages principalement le long de la dorsale océanique de l'Atlantique Sud et de la dorsale Est Pacifique (Tableau 1). Parmi ces 24 échantillons, seuls 11 contiennent des gouttelettes sulfurées pouvant être analysées (Figure 1).

Tableau 1. Coordonnées des échantillons

Dragage	RC13-5RD	RC21-2RD	RC28-12RD	RC28-13RD	RC28-16RD	RC28-18RD	RC28-21RD	RC28-22RD	RC28-24RD
Latitude	9.96	10.65	-25.70	-25.72	-25.93	-26.01	-26.12	-26.24	-26.44
Longitude	-5.39	-44.42	-13.92	-13.92	-13.88	-13.86	-13.86	-13.81	-13.76
<hr/>									
Dragage	RC28-6RD	RC28-7RD	VM25-1RD	VM33-24RD	VM33-4RD	COOK 16MV D37	COOK 16MV D3	COOK 16MV D3	
Latitude	-26.57	-26.54	25.40	14.75	-50.22	-13.08	-14.13	-14.13	
Longitude	-13.92	-13.93	-45.30	54.80	137.56	-112.05	-116.13	-116.13	
<hr/>									
Dragage	COOK 16MV D3	COOK 16MV D28	COOK 16MV D28	COOK 16MV D37	COOK 16MV D37	COOK 16MV D19	COOK 16MV D38	COOK 16MV D38	
Latitude	-14.13	-13.07	-13.07	-13.08	-13.08	-15.03	-13.02	-13.02	
Longitude	-116.13	-113.02	-113.02	-112.05	-112.05	-117.00	-113.04	-113.04	

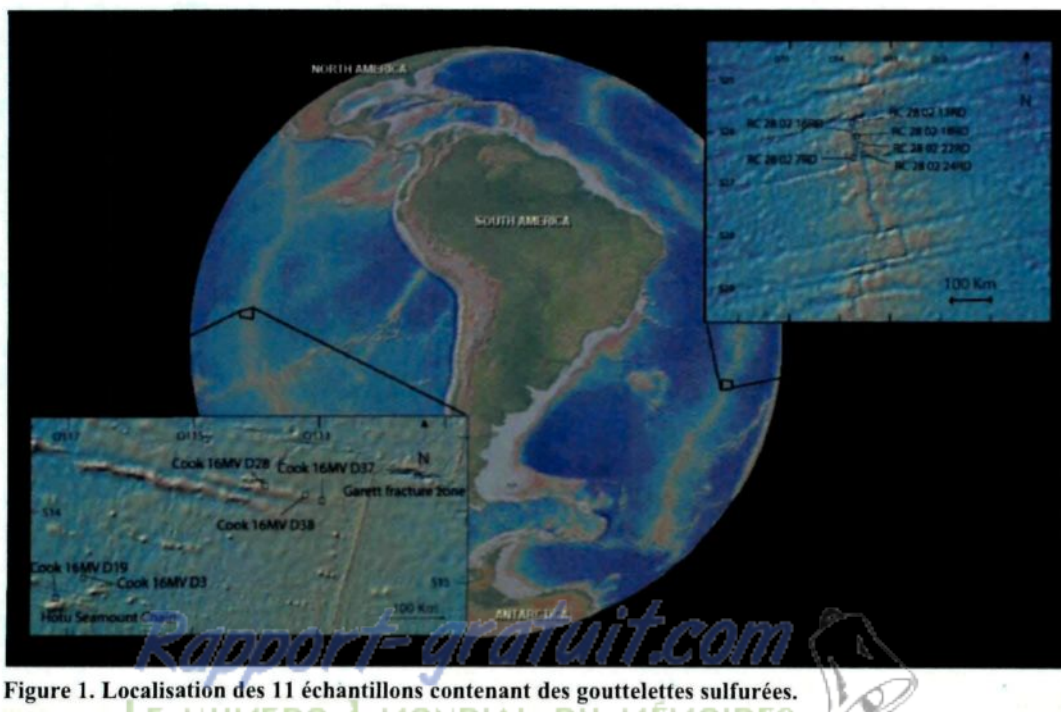


Figure 1. Localisation des 11 échantillons contenant des gouttelettes sulfurées.



Annexe B: Cartographie d'une gouttelette sulfurée au LA-ICP-MS

Une gouttelette zonée de l'échantillon RC-28-02-18RD a été cartographiée au LA-ICP-MS au LabMaTer à l'UQAC avec un laser ArF-193nm M-50 de Resonetics et un ICP-MS Agilent 7700X. Ce LA-ICP-MS est différent de celui utilisé dans les chapitres précédents et c'est pourquoi ces résultats sont mis en annexe. L'ablation a été effectuée avec un faisceau de $5\mu\text{m}$, une fréquence de 20Hz et une vitesse de $3\mu\text{m}/\text{s}$. Il est possible de voir la distribution des éléments chalcophiles au sein de la gouttelette (Figure 2). Cette technique d'analyse mériterait d'être développée afin d'acquérir de meilleures données sur la distribution spatiale des EHS et des éléments chalcophiles au sein des gouttelettes sulfurées.

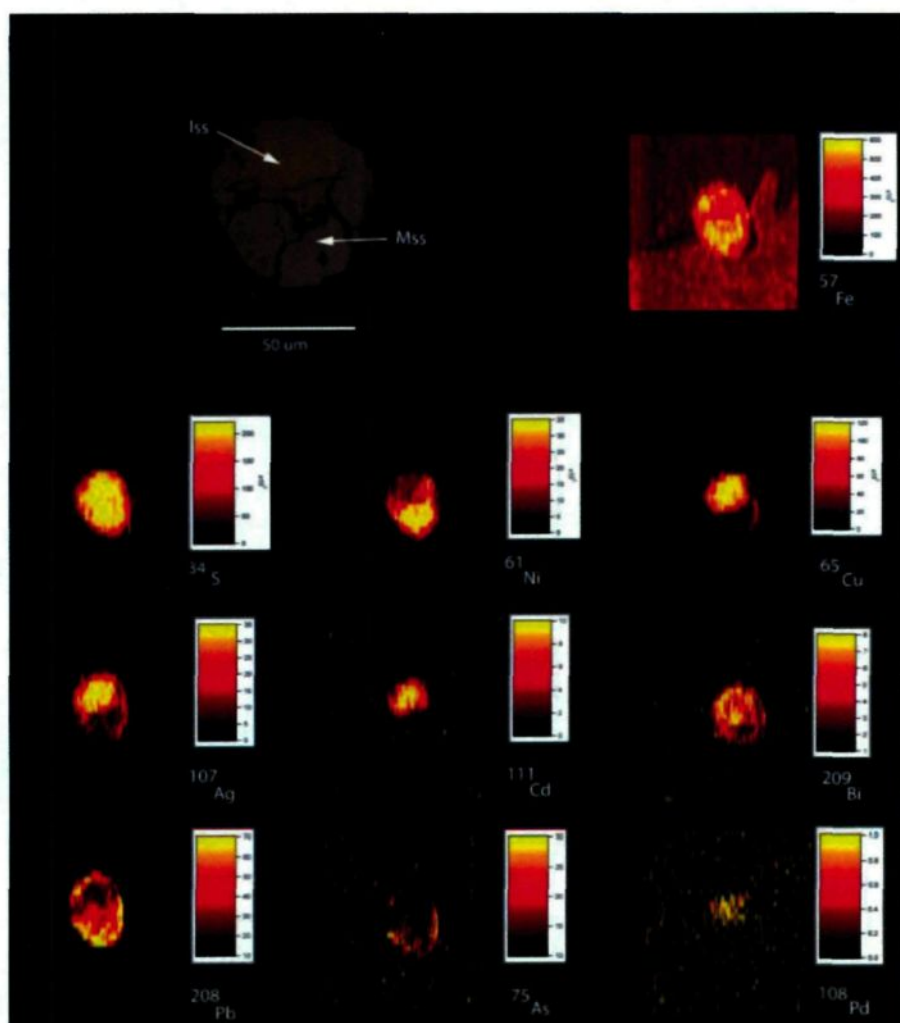


Figure 2. Cartographie au LA-ICP-MS d'une gouttelette zonée. Les échelles sont en compte par seconde excepté pour le S, Fe et Pd qui sont en ppm.

Annexe C: Conférence au 11th Platinum Symposium, Sudbury

Présentation orale en Juin 2010 au 11th Platinum Symposium à Sudbury, Ontario, Canada.

Résumé étendu soumis:**PLATINUM-GROUP ELEMENT AND CHALCOPHILE ELEMENTS
CONTENT IN SULPHIDE DROPLETS FROM MORB GLASS.****C. Patten, S.-J. Barnes.**

Sciences de la Terre, Université du Québec à Chicoutimi
clifford.patten@uqac.ca
Sarah-Jane_Barnes@uqac.ca

E. A. Mathez.

Department of Earth and Planetary Sciences, American Museum of Natural History, New York
mathez@amnh.org

ABSTRACT. Most models of how PGE deposits form suggest that a sulphide liquid collects the PGE and concentrates them in a zone sufficiently rich in PGE to be exploited. If this were the case then one might expect the PGE to be present in the ores in solid solution in magmatic sulphides such as pyrrhotite (Py), pentlandite (Pn) and chalcopyrite (Ccp). However in most ores studied to date PGM account for a large part of the PGE budget. The origin of these PGM could be: exsolution from the BMS, crystallization from the sulphide liquid, precipitation from a deuterian fluid. Sulphide droplets from MORB represent natural examples of rapidly quenched sulphide liquid. Thus it is possible that exsolution has not occurred and deuterian processes were not important. Furthermore the sulphide liquid would not have fractionated sufficiently to crystallize PGM. To test these ideas we are determining PGE and chalcophile elements content of sulphide droplets in MORB glasses.

1 INTRODUCTION

Barnes et al. (2008) found that platinum-group elements are largely found in solid solution in pyrrhotite and pentlandite in Noril'sk's sulphide droplets. Platinum is an exception to this and is found as platinum-group minerals (PGM) within the sulphide minerals. In contrast to the Noril'sk droplets PGE in the Merensky, Main Sulphide, JM, PV and AP reefs are found both in sulphides (Py and Pn) and in PGM associated with the sulphides. Barnes et al. (2008) suggest that as is the case at Noril'sk originally all the PGE were in the reef sulphides, but because the sulphides occur in large layered intrusions the sulphides cooled very slowly and that during cooling the PGM exsolved from the sulphides (Makovicky et al. 2002). There are other possible means of forming PGM. The first phase to crystallize from a sulphide liquid is monosulphide solid solution (mss) and Pt, Pd and most semi-metals do not partition into mss. Thus these elements concentrate into the fractionated liquid and could eventually crystallize from the sulphide liquid as PGM. Alternatively late deuteritic fluids could dissolve some S and reduced the solubility of PGE in the sulphides (Peregoedova et al. 2004). Finally some of the deposits have been deformed and metamorphosed and PGM could have exsolved during metamorphism. Sulphide droplets in MORB glasses have been quenched from liquidus temperature at water depths of greater than 2000 m (Mathez, 1976). The rapid quenching and lack of metamorphism eliminates many of the processes outlined above and suggests that all of the PGE should be present in the sulphides. This study intends to investigate the distribution of chalcophile elements and PGE among sulphide droplets, PGM and silicate glass.

2. METHODOLOGY

Fifty dredge samples were selected of MORB glass from the Lamont Doherty Earth Observatory

of Columbia University collection based on their fresh glass content. The glasses were impregnated with epoxy and then made into polished sections. These were then inspected for sulphide droplets. Twelve contain droplets and are the subject of our study. The samples are being investigated with a scanning electron microscope for PGM. The major element composition of the glass and the S content of the glass are being determined by microprobe, the whole rock major elements, trace elements, S and PGE contents by all rock analyses and the composition of the droplets by laser ablation. Then a mass balance will be carried out.

3 PRELIMINARY RESULTS - PETROGRAPHIC OBSERVATIONS

The sulphide content of 12 sulphur saturated glass MORB samples from the South Atlantic Ridge and the East Pacific Ridge has been observed. These MORBs contain sulfide droplets ranging from a few micrometres up to 150 micrometres, with a mean of 40 micrometres. They present variable textures ranging from intergrowth of pn, py, and ccp to a well-differentiated texture with classic base metal sulphides (figure 1). In those presenting intergrowth textures the droplet was quenched very quickly and at a temperature superior to 1200°C (figure 1.1). Other droplets with more differentiated textures show some oxide, chalcopyrite, pyrrhotite and pentlandite (figures 1. 2-3-4). The pentlandite is either at the edge of the pyrrhotite or in the form of flame inside the latter. These droplets have undergone a less intense cooling rate than those with eutectic textures.

Five samples, with different textures, have been examined with the scanning electron microscope and no PGM were observed.

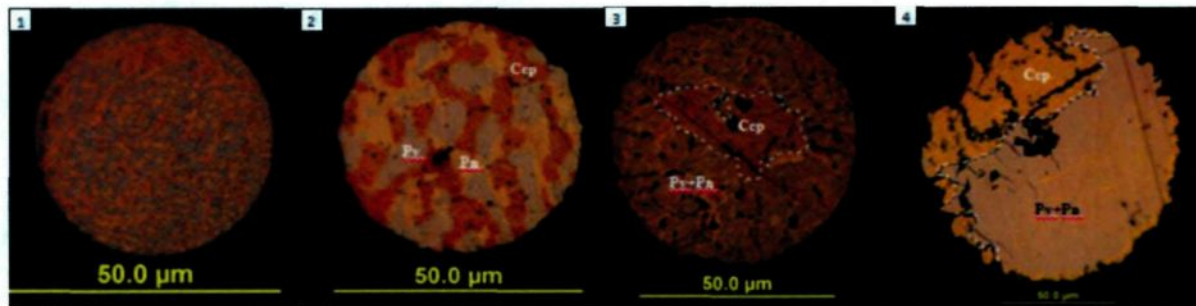


Figure 1. Sulphide droplets: ccp= chalcopyrite, py = pyrrhotite, pn = pentlandite.

- 1- Droplet with eutectic texture from the South Atlantic Ridge.
- 2- Droplet in intermediate state between eutectic and well-differentiated texture from the South Atlantic Ridge. Note the relatively large amount of pentlandite at pyrrhotite edge.
- 3- Droplet with well differentiated chalcopyrite phase in the heart, exsolution of pentlandite inside the pyrrhotite. Sample from the East Pacific Ridge.
- 4- Well-differentiated droplet poor in pentlandite; note the much bigger size than the others. Sample from the South Atlantic Ridge.

4. PRELIMINARY RESULTS - PGE AND CHALCOPHILE ELEMENT CONTENT IN SULPHIDE DROPLETS

The analysis at the LA-ICP-MS of droplets from four samples revealed the presence of several chalcophile elements and also noble metals. For Ni and Cu their concentrations are respectively going up to 9% and 15% in sulphide droplets. Due to the small size of the various sulphide minerals it is impossible to analyze only one phase because of the droplets' size. But we can differentiate if pentlandite, pyrrhotite or chalcopyrite is the dominant phase. Droplets also contain Zn, Co, Cd, Sn, Se, Pb, As, Bi, Te, Ag (table 1). In most differentiated droplets all these elements seem to be associated with chalcopyrite except for Co which is coupled with Ni. Barnes et al. (2006) explain that this association is specific to pentlandite, with these two elements migrating into it during its exsolution from the monosulphide solution. This is in agreement with previous sulphide droplets observations.

For the noble metals there are traces of Pt, Re and Au. Their concentrations were determined in sulphide droplets in the sample from the South Atlantic Ridge. Pt are 100 to 200 ppb, Re 300-600 ppb and Au about 700 ppb. Signal strength does not vary as laser drilling proceeds, implying that there are no inclusions. The absence of Os, Ir, Ru and Rh signals could be linked to the very low concentration of these elements in MORB magma; according to Bézos et al. (2005), their concentrations in MORB glass are ranging around 0.01 ppb.

Table 1. Chalcophile elements concentration in sulphide droplets in ppm.

Co	Se	Zn	Pb	Te	Ag	As	Cd	Sn	Bi	Pt (ppb)	Re (ppb)	Au (ppb)
2020	740	320	100	65	20	15	12	12	3	100-200	300-600	700

5 REFERENCES

- Barnes, S.-J., Prichard, H.M., Cox, R.A., Fisher, P.C., and Godel, B., 2008. The location of the chalcophile and siderophile elements in platinum-group element ore deposits (a textural, microbeam and whole rock geochemical study): Implications for the formation of the deposits: *Chemical Geology*, v. 248, p. 295-317.
- Barnes, S.-J., Cox, R.A., Zientek, M., 2006. Platinum-group element, gold, silver and base metal distribution in compositionally zoned sulphide droplets from the Medvezky Creek Mine, Noril'sk, Russia. *Contributions to Mineralogy and Petrology*, v. 152, 187–200.
- Bézos, A., Lorand, J.P., Humler, E., and Gros, M., 2005. Platinum-group element systematics in Mid-Oceanic Ridge basaltic glasses from the Pacific, Atlantic, and Indian Oceans: *Geochimica et Cosmochimica Acta*, v. 69, p. 2613-2627.
- Kelly, D.P., Vaughan, D.J., 1983. Pyrrhotine-pentlandite ore textures: a mechanistic approach: *Mineralogical Magazine*, v. 47, 453–463.
- Makovicky E., Makovicky M., and Rose-Hansen J. 2002. The System Fe-Rh-S at 900° and 500°C, *Canadian Mineralogist*, v. 40, pp. 519-26.
- Mathez, E. A., 1976. Sulphur Solubility and Magmatic Sulphides in Submarine Basalt Glass: *Journal of Geophysical Research*. v. 81.
- Peregoedova, A., Barnes, S.J., and Baker, D.R., 2004. The formation of Pt-Ir alloys and Cu-Pd-rich sulfide melts by partial desulfurization of Fe-Ni-Cu sulfides: results of experiments and implications for natural systems: *Chemical Geology*, v. 208, p. 247-264.

Annexe D: Conférence au Ottawa 2011 Joint GAC-MAC-SEG-SGA meeting.

Présentation orale en Mai 2011 au 2011 Joint GAC-MAC-SEG-SGA meeting à Ottawa, Ontario, Canada.

Résumé soumis:

CHALCOPHILE AND SIDEROPHILE ELEMENT CONCENTRATIONS IN MORB SULPHIDE DROPLETS

C. Patten, S.-J. Barnes.*Sciences de la Terre, Université du Québec à Chicoutimi**clifford.patten@uqac.ca**Sarah-Jane_Barnes@uqac.ca***E. A. Mathez.***Department of Earth and Planetary Sciences, American Museum of Natural History, New York**mathez@amnh.org*

We have determined the concentrations of chalcophile and siderophile elements by LA-ICP-MS from sulphide droplets and fresh glass in contact with them from MORB pillow rims. The aim of the study is twofold. Firstly, MORBs play an important role in the understanding of mantle petrogenesis and differentiation of the Earth, providing information on chemical fractionation of elements in the mantle. However, chalcophile and siderophile element behaviour is not completely understood, partly due to the lack of data for partition coefficients between sulphide and silicate liquids. Secondly, mass balance work on ore deposits indicates that most platinum-group elements (PGE) are present in base metal sulphides in solid solution. However, Pt and Au tend to be present as discrete minerals in association with sulphides. The origin of the Pt and Au minerals may be that they crystallised directly from a sulphide liquid, that they exsolve from base

metal sulphides or precipitate from a deuteritic fluid. Examination of the MORB droplets allows us to investigate how these elements behave in unaltered, quickly-cooled systems.

Some droplets have homogenous textures and some have portions rich in monosulphide solid solution (Mss) and intermediate solid solution (Iss) indicating that they have undergone crystal fractionation. For the droplets with homogenous textures, concentrations of Ni and Cu are 10 to 1%; Co and Zn 1000 to 100 ppm; Se, Te, Ag and Pb 100 to 10 ppm; Cd, Sn, Pd, Bi and Pt 10 to 1 ppm; Au, Ru and Re 1 to 0.1 ppm. For some of these elements it was also possible to obtain data in fresh glass allowing the calculation of partition coefficients. These were calculated for Ni (giving a range of 440 ± 221), Cu (giving a range of 727 ± 336), Co (giving a range of 25 ± 9), Zn (giving a range of 3.2 ± 0.8), Sn (giving a range of 8.2 ± 2.2) and Pb (giving a range of 33.4 ± 12). Values for Ni, Cu and Co are in agreement with literature, suggesting that values for Zn, Sn and Pb are realistic.

In both the homogenous and fractionated droplets analysed, all elements have continuous profiles like S, Fe, Ni and Cu, suggesting that there are no discrete platinum group minerals (PGM) or Au grains present. This is also confirmed by SEM analyses. All elements are, therefore, integrated inside sulphide structures. This implies that no PGMs crystallise directly from sulphide liquid before quenching.

Annexe E: Conférence au Goldschmidt 2011

Présentation orale en Août 2011 au Goldschmidt à Prague, République Tchèque.

Résumé soumis:

CONCENTRATION OF CHALCOPHILE AND SIDEROPHILE ELEMENTS IN MORB SULPHIDE DROPLETS: NEW SULPHIDE MELT-SILICATE MELT PARTITION COEFFICIENTS.

PATTEN, C., BARNES, S.-J., MATHEZ, E. A.^{1,2,3}

¹ Sciences de la Terre, Université du Québec à Chicoutimi clifford.patten@uqac.ca

² Sciences de la Terre, Université du Québec à Chicoutimi Sarah-Jane Barnes@uqac.ca

³ Department of Earth and Planetary Sciences, American Museum of Natural History, New York mathez@amnh.org

We have determined the concentrations of chalcophile and siderophile elements by LA-ICP-MS from sulphide droplets and fresh glass in contact with them from MORB pillow rims. MORBs play an important role in the understanding of mantle petrogenesis, providing information on chemical fractionation of elements in the mantle. However, chalcophile element behaviour is not completely understood, partly due to the lack of data for partition coefficients between sulphide and silicate melts.

Some droplets present homogenous textures and others portions rich in monosulphide solid solution (Mss) and intermediate solid solution (Iss) indicating that they have undergone crystal fractionation. For homogenous droplets, concentrations of Ni and Cu are 10 to 1%; Co and Zn 1000 to 100 ppm; Se, Te, Ag and Pb 100 to 10 ppm; Cd, Sn, Pd, Bi and Pt 10 to 1 ppm; Au, Ru and Re 1 to 0.1 ppm. For some of these elements it was also possible to obtain data in fresh glass allowing the calculation of partition coefficients. These were calculated for Ni (745 ± 252), Cu (1219 ± 381), Co (42 ± 5.5),

Zn (3.4 ± 0.9), Sn (10.4 ± 1.8) and Pb (55.6 ± 9.3). Values for Ni, Cu and Co are in agreement with literature [1], suggesting that values for Zn, Sn and Pb are realistic.

[1] Sulfide melt-silicate melt distribution coefficients for noble metals and other chalcophile elements as deduced from MORB: Implications for partial melting, Peach et al. (1990), Geochimica et Cosmochimica Acta 54, pp. 3379-3389.